SLAC-PUB-13564
May 2009

3 GEV SPEAR INJECTOR DESIGN HANDBOOK

Stanford Synchrotron Radiation Laboratory

Work supported in part by US Department of Energy contract DE-AC02-76SF00515

3 GeV SPEAR Injector Design Handbook

Issue to : ____________________

Stanford Synchrotron Radiation Laboratory
Stanford University

Table of Contents

ISSUE DATE

PREFACE

Preface

This Design Handbook is intended to be the main reference book for the specifications of the 3 GeV SPEAR booster synchrotron project.

It is intended to be a consistent description of the project including design criteria, key technical specifications as well as current design approaches.

Since a project is not complete till it's complete changes and modifications of early conceptual designs must be expected during the duration of the construction. Therefore, this Design Handbook is issued as a loose leaf binder so that individual sections can be replaced as needed. Each page will be dated to ease identification with respect to latest revisions. At the end of the project this Design Handbook will have become the "as built" reference book of the injector for operations and maintenance personnel.

The task of keeping a large number of widely dispersed copies up to date would be prohibitively difficult. Consequently, we are forced to limit the distribution to a few libraries and group offices and to individuals with a bonafide use for it. We will attempt to maintain a list of all recipients and to provide them with updated sections as they become available. To avoid further delays and to get this book into the hands of those who might find it useful, we have decided to proceed with the first printing and distribution before all sections have been written.

The content of this book is the result of the efforts of many contributors from SSRL, SLAC and elsewhere. Grouped by systems we will try to recognize as many contributors as we know.

The content is ultimately the responsibility of the project Director, H. Wiedemann. He is aided in the management and administration of the project by the Project Manager/Engineer, J. Voss, the Electrical Systems Manager, R. Hettel, and the Budget and Planning Office for this project headed by Bessie Lo.

INTRODUCTION

1 Introduction

Chapter 1

Introduction

1 Introduction

1.1 Overview

Synchrotron light can be produced from a relativistic particle beam circulating in a storage ring at extremely high intensity and brilliance over a large spectral region reaching from the far infrared regime to hard x-rays. The particles, either electrons or positrons, radiate as they are deflected in the fields of the storage ring bending magnets or of magnets specially optimized for the production of synchrotron light. The synchrotron light being very intense and well collimated in the forward direction has become a major tool in a large variety of research fields in physics, chemistry, material sciences, biology and medicine.

The first SLAC storage ring enhanced for synchrotron radiation research was the SPEAR ring. This development began in 1972, with the first beam line becoming operational in mid-1974. SPEAR has a 234 meter circumference and operates at energies up to 3.5 GeV with currents up to 100 milliamps. The storage ring can accomodate 16 beam lines (not including all bending magnet beam line possibilities) without interference with a high physics energy experiment operating in the ring's West Pit. Additional beam lines can be implemented upon the completion of the high energy physics program.

Although SPEAR's emittance, 460 nm-rad at 3 GeV, for the regular mode of operation is larger than those of the most modern synchrotron radiation source, a low emittance configuration, with a design emittance of 130 nm-rad, was tested in 1984. The existing SPEAR injection system, however, makes its utilization on a day-to-day basis difficult because of limitations in the present injection configuration. Modifications to the injection system are described in this Design Handbook.

At present, SSRL operates 22 experimental stations on beam lines on the SPEAR storage ring. A layout of the SPEAR facilities is shown in Figure 1-1. The experimental stations of SSRL are used by more than 500 scientists from 99 different institutions in 32 states and 11 foreign countries.

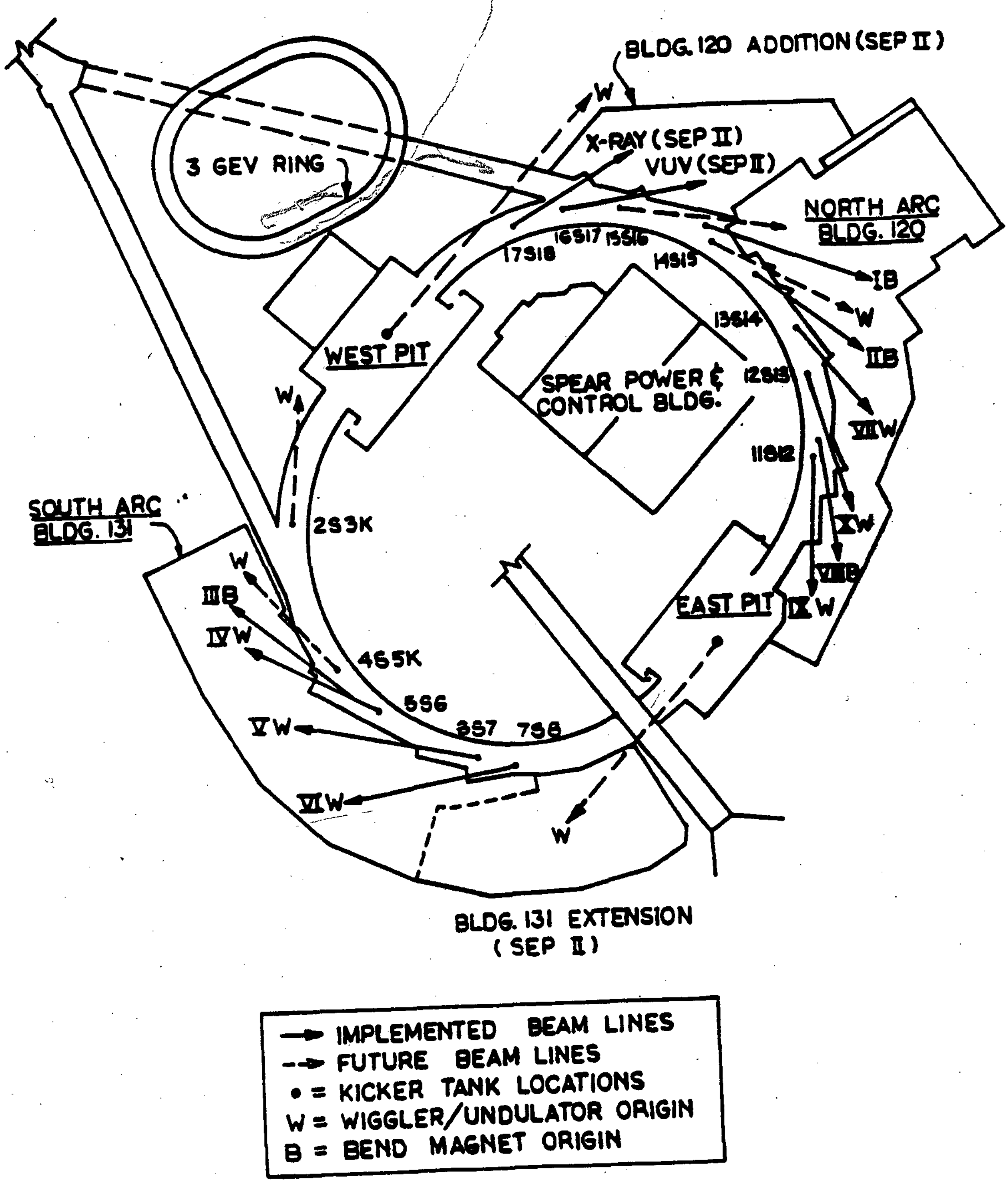

Fig. 1-1: Layout of the SSRL Facilities at SPEAR

These institutions include 51 universities, 15 private corporations and 12 government laboratories.

Particle beams usually circulate in the ultra high vacuum environment of a storage ring for several hours. After the beam current has decayed to a low value new particles are injected from a separate accelerator referred to as the injection system.

Injection of particles into the SPEAR storage ring has been traditionally performed from the existing 2 mile linear accelerator at the SLAC. This injector has been specified and designed for very high particle energies and is obviously too big an injector for a 3 GeV storage ring. To obtain reasonable injection efficiencies it is necessary to accelerate the particles in the linear accelerator to about 10 to 15 GeV and then decelerate them again to the low injection energy. This sequence of acceleration and deceleration is necessary to assure that a significant amount of particles survive the electromagnetic interaction with the accelerator sections while traveling over 2 miles during acceleration. As a result of this complicated acceleration process it has been difficult to run the injector in a reproducible way and injection into SPEAR has been reliable than is desirable or readily achievable.

Moreover the injection energy to SPEAR is limited at this time to 2.3 GeV due to limitations in components of the beam transport line from the linac to SPEAR. This makes it necessary to ramp the energy of the beam in SPEAR to the operating energy of 3 GeV for every fill.

This situation is expected to get aggravated in the SLC phase of operation which started in fall of 1986. In this mode of operation intense bunches of positrons and electrons are accelerated in the SLAC linear accelerator to energies up to about 50 GeV. After acceleration they are guided through two transport lines, one for the positron bunch and one for the electron bunch, which after 1400 m aim at each other. At that point both the electron and the positron bunches collide and produce the high energetic reactions to be studied by the high energy physics community. During this mode of operation of the linear accelerator low energy injection into SPEAR is highly interruptive for the high energy physics program and as a consequence only two SPEAR fills per day are planned to be available. With this schedule still the high energy physics program is interrupted for 2 hours every 12 hours. The running costs of the linac during these two hours are very high for SSRL since the linac must be kept operating at full power so as not to change the delicate thermal balance in the accelerating sections for SLC operation.

This schedule greatly limits the synchrotron radiation experimental program at SSRL. To keep SPEAR operating at a high performance level and develop improvements machine physics shifts must be available. For such machine developments it is crucial that on-demand injection is available. In the SLC era, however, this is not the case and if the beam is lost during machine physics the efforts are stopped till the next 12 hourly scheduled injection. This makes machine physics experimentation and scheduling extremely inefficient.

The nature of this interruption comes from the required precision control of the SLC beams at 50 GeV. To accelerate the very high intensity beams during SLC operation many strong quadrupoles are required along the linear accelerator to prevent a beam break up. These quadrupoles are much too strong to allow the passage of a 2 to 3 GeV beam for SPEAR and therefore must be turned off. While this is not a problem to do for SPEAR injection, it takes considerable time to recover from SPEAR injection back to SLC operation. This is because it generally is difficult to reproduce exact beam conditions after magnet strengths have been changed. Recovery from machine physics runs at PEP as well as at SPEAR traditionally have been difficult because of this reason. A change in the injection energy at SPEAR and at PEP is therefore done very rarely. A change in the injection energy requires at least several hours to be set up. For the SLC to obtain beam collision again after a SPEAR injection, the position of the electron as well as the positron beam must be reproduced at the end of the 2 mile linac to 0.1 mm and an angle of 1 microradian.

Consequently, dedicated injector for SPEAR appears to be the proper facility to both preserve the goals of the high energy physics community with the SLC and to assure the availability of photons for the synchrotron radiation user community. In addition such a dedicated injector can be optimized for SPEAR injection alone and therefore can provide greatly improved injection conditions. Since the operating costs of this injector will be much less than those for the 2 mile SLAC accelerator, SSRL should be able to provide synchrotron radiation for a much larger fraction of the year than it can now.

In this Design Handbook, an injection system which would allow the accumulation of electrons into a SPEAR at an operating energy of up to 3.0 GeV. To obtain optimum performance of a storage ring dedicated to the production of synchrotron radiation a full energy particle injector where the particles are injected into the storage ring at the operating energy is highly desirable. The feature of full energy injection provides several advantages. All storage ring components are left in their running conditions during injection since it is not necessary to change the storage ring energy from the operating energy to the injection energy. If the injection energy were different from the operating energy the excitation of the ring magnets would have to be changed for injection and a special magnet training routine must be followed to establish the desired magnetic fields again in the presence of hysteretic effects. For a large number of experiments it is very critical, however, to keep the photon beam as stable as possible over a long period of time which is very difficult to achieve when magnetic fields in the storage ring must be changed. In case of a full energy injection the photon beam steering is done once and will stay adjusted over many shifts.

For economic reasons often an injection energy lower than the operating energy of the storage ring is chosen. In case of a full energy injector, however, higher beam currents can be stored in the storage ring than would be possible at lower energies. All known instabilities allow higher storage ring beam currents to be reached as the beam energy is increased. Moreover, since magnet field training is not necessary the remaining beam current from the previous fill is not lost, the time for beam injection is reduced and the efficiency of the storage ring for the production of synchrotron radiation is significantly enhanced.

1.2 Rational for a Dedicated Synchrontron Booster Injector

To obtain full energy injection different types of injectors can be utilized. In particular, a linear accelerator as well as a booster synchrotron can serve as such a full energy injector. In this proposal a booster synchrotron is proposed in order to take advantage of several favorable features with respect to a full energy linear accelerator. To achieve a beam energy of one GeV or higher a booster synchrotron can be constructed at a significantly lower cost than a linear accelerator.

With present day technology a 3 GeV linear accelerator would require at least 30 accelerating sections, each 10 feet long, and one 100 MW klystrons for each of these sections. This type of klystron has been developed at SLAC for the SLC project and is not available yet from industry. With 35 MW klystrons as available from industry the linac would require 51 stations to reach 3 GeV. The length of such linacs would be 120 m or 190 m respectively and thereby longer than the circumference of the proposed booster synchrotron. The space available next to SPEAR would not allow the placement of such linacs. The costs for such linacs has been estimated to be more than twice the cost of the equivalent components in a booster synchrotron. In addition the operating and maintenance costs are significantly higher for a linear accelerator than for a booster synchrotron. Assuming a 20,000 hour lifetime on average for each klystron and a running time of 5,000 hours per year, 7.5 klystrons must be replaced every year at a cost of more than $400K. In contrast the proposed booster involves only four klystrons, three lower power linac klystrons and one DC klystron for the synchrotron itself.

For these reasons it has been decided to propose a 3 GeV booster synchrotron as a dedicated injector into SPEAR. Such a booster fits well in the space available next to SPEAR (Figure 1-2).

The technology involved in the construction of a synchrotron is similar to that of the storage ring and therefore the operation and maintenance of both rings is simplified which enhances its reliability. Of course, in the case of a synchrotron, a preinjector in form of a small linear accelerator or microtron is needed. In this proposal a three section linac is assumed which is much easier to operate and maintain. The beam characteristics for a preinjector linac to inject into a booster synchrotron are very much

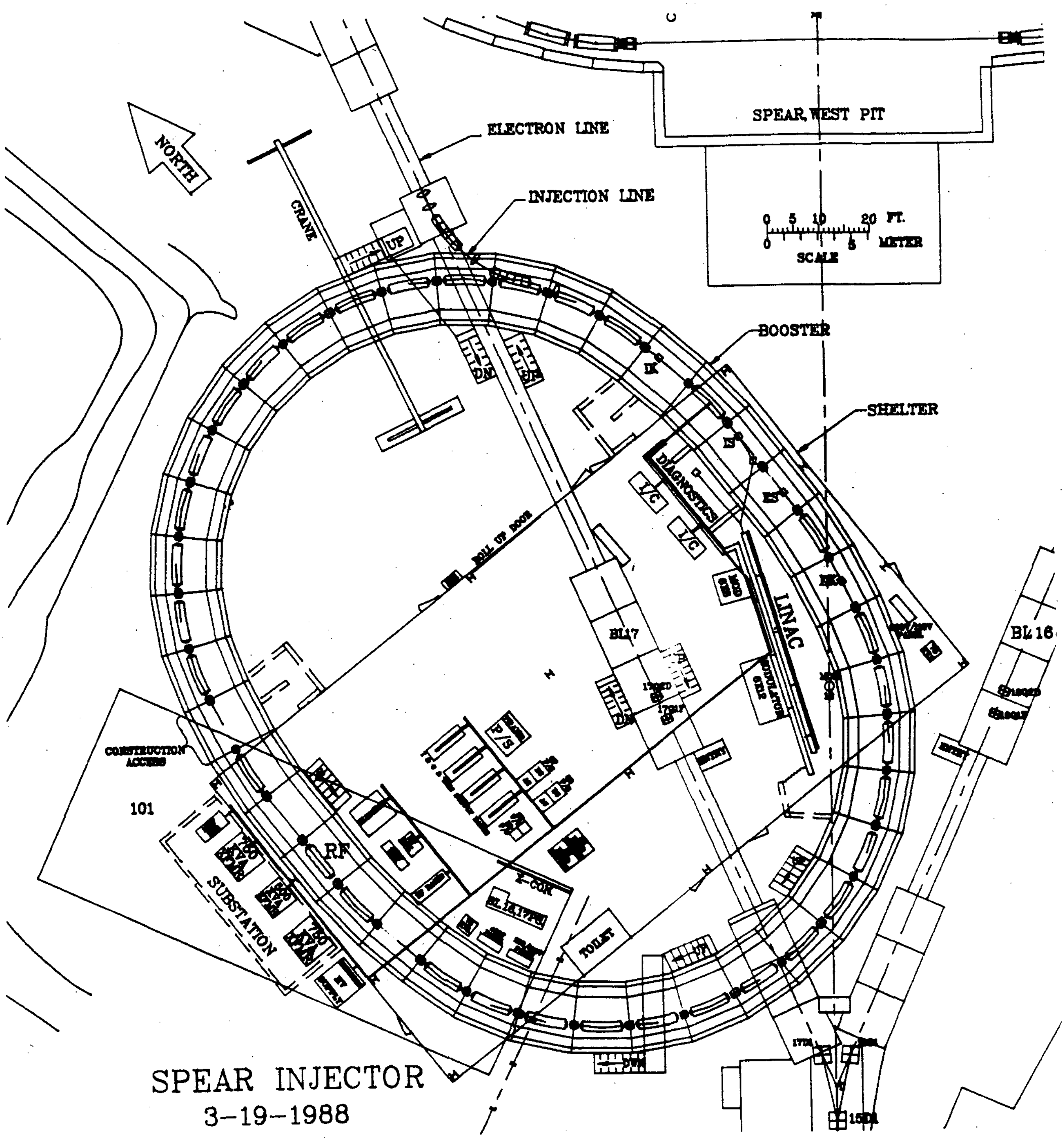

Fig. 1-2: General Layout of the Injector Complex

relaxed compared to injection into a low emittance storage ring.

In a linac/synchrotron injection system full energy injection is assured virtually at all times. If a full-energy linear accelerator is used, a loss of any klystron reduces the energy of the linac and therefore the injection energy into the storage ring is reduced until this klystron is replaced. In the proposed scheme the loss of one linac klystron would only reduce the injection energy into the synchrotron from the preinjector which, however, has no effect on the ultimate energy the synchrotron can reach. The only detrimental effect would be some increase in the storage ring injection time since the synchrotron probably would no longer be able any more the same beam current at the reduced preinjector energy. The operating parameters of the storage ring, however, need not be altered.

Of course, the loss of the synchrotron klystron would prohibit any further acceleration and injection. In this proposal we have therefore assumed that the RF system be the same as for the storage ring so that RF components and spares can be shared.

In addition to these operational and maintenance considerations it should be noted that the injection into a booster synchrotron from a linear accelerator is much easier than the direct injection from a linac into a low emittance storage ring. This is because a much simpler solution for the focusing lattice in the booster synchrotron can be chosen. The beam in such a lattice does not require the tight magnet field and alignment tolerances of a storage ring and allows for a larger physical and dynamic aperture. This significantly reduces the required beam quality from the linac preaccelerator and makes the operation of the short preinjector system relatively easy.

On the other hand, for injection into a high brilliance storage ring with limited aperture the injection system must provide a beam of high quality. Beam parameters like beam energy, beam size, and energy spread must be closely controlled for successful injection. This requires a powerful control system if direct injection from a high energy linac is desired. In a synchrotron the beam size and energy spread are determined by the design of the lattice and are therefore well known while the beam energy itself is well defined and controlled by the fact that the synchrotron acts like an energy defining spectrometer. In a linear accelerator these parameters can vary greatly if not closely controlled at all times.

Even in a well adjusted linear accelerator the beam parameters are ultimately determined by the source characteristics. Therefore, should it become desirable to use positrons in the storage ring it will be difficult to obtain a high injection efficiency in case of a linac injector because of the large positron beam emittance which is a consequence of the production process. The beam emittance and energy spread is well determined in a a synchrotron due to synchrotron radiation damping, and independent of the nature of the particles or their sources. Both quantities can be made equal and significantly smaller in a booster synchrotron than in a linear accelerator to facilitate injection into the low emittance storage ring.

In this proposal the synchrotron lattice has been designed for a relatively small beam emittance to provide easy injection into the storage ring. The general design concepts for the 3.0 GeV booster synchrotron are described in the following sections of this Design Handbook.

1.3 Review Process for the Injector

In late 1985 it became more and more obvious that the filling of the SPEAR storage ring would cause a major interference with the SLAC SLC program since it requires a reconfiguration of the SLAC linac. To recover from this linac reconfiguration is time consuming and therefore costly both from an economic and scientific point of view. With only two fills per day the interruption of the high energy physics program would be 2 hours for each fill or 16.7% of the time would not be available for high energy physics because of the filling of SPEAR. Moreover the linac cannot be operated for most of the year for fiscal reasons.

To protect SSRL's research program the SSRL directorate decided to propose a dedicated injector for SPEAR. After internal reviews the proposal was discussed with various committees and review panels. A list of these reviews in chronological order and other action relevant to the proposed SPEAR injector is given below:

1) March 11, 1987 : SLAC reviews injector proposal and in a preliminary statement agrees with technical plan, cost and schedule.
2) Stanford University administration authorized SSRL to submit a proposal for the SPEAR injector in the form of a Schedule 44.
3) April 15, 1986 : DOE/Headquarters review of SSRL's FY1988 Budget Call including SEP II and Injector Proposal.
4) April 25, 1987 : Formal submission of Schedule 44 to DOE
5) May 14, 1986 : SSRL users organization executive committee discussed injector proposal and stated in its report to the SSRL director "..support first priority for a new injector system....
6) May 27, 1987 : SLAC concludes its review of injector proposal.

7) May 28, 1986 : Director's Review of the whole SEP II proposal by outside 12 member committee chaired by Marvin Weber of LLNL. The report states "Of the various proposal elements, the 3 GeV SPEAR injector and the 12-m PEP undulator beam line were rated at the top or near-top by all panelists."
8) June 9, 1986 : SSRL Science Policy Board reviewed, among other SSRL plans, the injector proposal and supported it.
9) June 26, 1986 : DOE validation Review at DOE headquarters chaired by Mr.Ramsey (DOE). Submission of conceptual design report.
10) February 1987 : The SPEAR injector has been included in the President's budget for FY'1988 at $ 13.5 M over three years.
11) February 24, 1987 : Status report of injector project during annual DOE review of the SEP-I project at SSRL.
12) March 13, 1987 : Submit new CDR and bottoms-up cost estimate.
13) March 25, 1987 : SSRL program review at DOE headquarters.
14) April 21, 1987 : DOE validation review
15) August 13, 1987: DOE Construction Review
16) September 14, 1987: Technical Review
17) January 1988 : Congressional Approval at $ 14M.

1.4 R & D Effort for this Injector

The design of the SPEAR injector synchrotron is based on well known and well tested techniques as developed over more than 30 years. No specific Research and Development is, therefore, required. To test, however, materials and techniques applied to the design of some injector components prototypes have been built for the bending magnets and the vacuum chamber. A magnetic measurement system allowing the cycling of the prototype magnet will use to test the performance of various types of steel for the magnets. The test results will be included into this design handbook as they become available. Furthermore, the project schedule, however, has been adjusted to allow the fabrication of engineering models for some of the major components like magnets and a vacuum chamber to verify the technical solution before a large number of these components are fabricated.

Table of Contents

DESCRIPTION

2 General Description of Injector

Chapter 2

General Description of Injector

2 General Description of Injector

2.1 Performance Goals

The specifications of the injection system were determined to achieve the following objectives:

> The system must provide an electron beam to SPEAR at a maximum energy of at least 3.0 GeV.
>
> It must be an independent system that does not interfere with the operation of any other facility or experiment not associated with SPEAR.
>
> The actual SPEAR filling time should be less than 5 minutes to achieve a circulating current of 100 ma.
>
> The operation of the injector synchrotron should be reliable, easy to operate and of low maintenance so as to allow the integration of the injector operation with the SPEAR operation.

The dedicated SPEAR injector system consists of a short linear accelerator with a beam energy of at least 120 MeV as a preinjector, a 3 GeV slow cycling synchrotron and a beam transport line feeding the particles into the existing SPEAR injection lines. In the first stage the injector is limited to electrons and if positrons should be desirable later, at additional costs, a positron option could be exercised. The energy of the synchrotron has been chosen to match the usual operating energy of SPEAR for synchrotron light users and the injector therefore is a full energy injector allowing maximum use of the synchrotron light source. With a circumference of about 133 m it is possible to place the synchrotron just next to the SPEAR storage ring (Figure 2-1). At this location the high costs of tunnel construction can be avoided by constructing above-ground radiation shielding as for the SPEAR ring itself.

The preinjector linac is a slow cycling linac which can produce a string of S-band bunches in a single linac pulse. These bunches are stored around the booster synchrotron and then accelerated to the storage ring energy by slowly ramping the booster magnets to higher fields. At the final energy the bunches then are transferred from the booster to the desired buckets in the storage ring.

The total filling time for SPEAR to a circulating current of 100 ma is expected to take less than 5 minutes, assuming a storage efficiency of only 25%. This filling time is very short and is also compatible with our separate effort to increase the current capability of SPEAR to 150 or even 200 ma. Should it ever become necessary to use positrons, additional equipment must be installed. This positron option requires the extension of the electron linac to say 200 to 300 MeV, the addition of a positron converter, a positron focusing system and a 200 to 300 MeV positron linac. The need to use positrons in SPEAR for synchrotron light production has not been positively established yet and therefore, to minimize costs and construction time we propose to construct only an electron injector at this time.

After acceleration of the electrons to the operating energy of the storage ring the bunches are transferred to the storage ring into whatever bucket distribution is desired. At this point the question must be asked if it would be possible to inject, say, every five minutes so as to keep the storage ring current constant. Since this would be desirable, further studies are in order to demonstrate this feasibility. There is no problem from the injector point of view except for the continuous power consumption. In the storage ring, however, the already stored beam would be affected by the injection kickers which might be incompatible with experimentation. The scheme might work if the experiments can be interrupted for, say, 5 to 10 seconds every 5 to 10 minutes. In any case, having a dedicated injector, such schemes can be tried out and used if desirable.

2.2 General Design Concept of the Injector

The booster magnet lattice and ring dimensions are shown in Figure 2-1. The lattice is based on a simple FODO arrangement of the magnets with 20 equal FODO cells forming the total ring. A total of three bending-magnet-free FODO cells provide the space for injection and ejection components, a radio frequency cavity and other minor ring components. To minimize the occurrence of synchro-betatron instabilities the dispersion function is chosen to almost vanish in the straight sections where the rf cavities will be installed. This is accomplished by using a so-called dispersion suppressor lattice employing a missing bending magnet cell at the end of the arcs as shown in Figure 2-1.

Some general parameters of the injection system are compiled in Table 2-1.

Table 2-1

General Parameters of the Injection System

Design Energy	3.0	GeV
Circumference	133.64	m
Particles	electrons	
Cycling Rate	2 to 10.0	Hz
Intensity	$1.0 * 10^{11}$	e-/sec
Number of Bunches	≤ 8	
Preinjector	linac	
Linac Frequency	2856	MHz
Energy of preinjector	≥ 120	MeV
Storage Ring Filling Rate (for 25% filling efficiency)	≥ 20.0	mamp/min

The preinjector linac system is designed to cycle at up to 10 pps which is sufficient for all injection modes. Each linac pulse consists of one or more equidistant S-band bunches. These bunches are stored evenly around the booster synchrotron and then accelerated to the storage ring energy by ramping the booster magnets to higher fields. At the final energy the bunches are then transferred from the booster to the desired buckets in the storage ring.

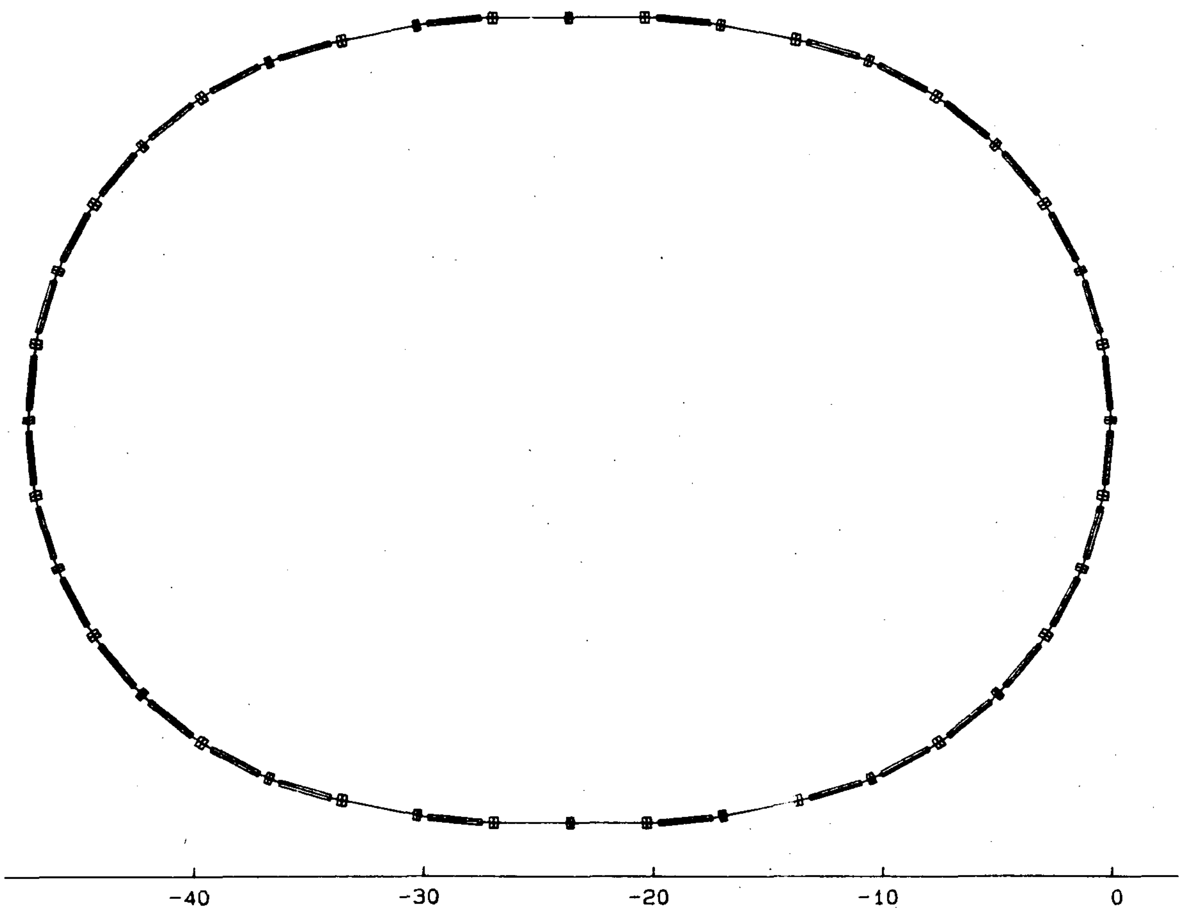

Fig. 2-1: SPEAR Injector Lattice

The electrons are generated from a special gun which is designed to deliver a high peak beam current thus avoiding the need for an elaborate prebunching and bunching section in the linac. The linac will consist of three standard S-band accelerating structures of the SLAC type. The linac sections will be fed by pulsed S-band klystrons tp produce a total beam energy of at least 120 MeV.

For a slow cycling rate of only 2.0 Hz in the synchrotron the total filling time to accumulate a circulating current of 100 ma in the storage ring is expected to take less than 5 minutes assuming a very conservative particle transfer efficiency of only 25%. Shorter filling times are possible when the booster is cycled at a higher rate up to 10 Hz. During operation in "top on" mode, when only part of the full beam current needs to be accumulated, the filling times are still shorter. This filling time is very short even if the storage ring current is increased to 200 ma or more since with time the injection efficiency is expected to increase operational experience and understanding of the machines.

2.3 Injection Process

The acceleration cycle starts with the injection at 120 MeV of one or more S-band bunches from the preinjector linac after which the magnetic fields of the booster are raised to the energy of the storage ring. At that point the beam is ejected from the booster and transferred to the storage ring. Subsequently the booster magnet current is reduced again to the preinjection value. The actual acceleration time takes about 0.25 seconds for a cycling rate of 2 Hz. Although the damping time at injection is more than 20 seconds long it is quickly reduced as the beam energy is increased and during the short acceleration time to 3.0 GeV the beam has gone through several damping times. At the end of the acceleration cycle the beam parameters therefore are fully determined by the synchrotron radiation in the booster synchrotron and not anymore by the preinjector beam characteristics. This is particular important for positron injection into the storage ring as mentioned previously.

RING LATTICE

3 Ring Lattice and Beam Parameters

Chapter 3

Ring Lattice and Beam Parameters

3 Ring Lattice and Beam Parameters

Basically the design of a synchrotron is similar to that of a storage ring, however, with much relaxed requirements.

For the design of a booster synchrotron a very simple lattice can be employed and special design efforts can be directed toward ease of operation and high reliability. After some special attention during commissioning, a synchrotron can eventually be operated remotely without the constant presence of an operator.

3.1 Lattice Design and Beam Characteristics

The design of the synchrotron in this proposal makes use of a simple FODO lattice which has been used for most synchrotrons constructed so far and has proven to be very reliable in its performance. The whole ring consists of 20 separated function FODO cells of which 14 are regular cells, 4 cells have missing bending magnets to provide matching of the dispersion function and 2 cells are totally free of bending magnets, providing the space needed for injection and ejection components, the RF-system and other machine components (Figure 3.1-1). The actual ring lattice deviates slightly from a fully regular FODO aray.

The detailed structure and geometrical dimensions of the synchrotron are compiled in Table 3.1-1 :

Table 3.1-1

Geometry of the Synchrotron

Circumference (m)	133.641
Diameter (m) long x short	47.239 x 35.293

The lattice structure for one quarter of the ring starting at the arc symmetry point of Figure 3.1-1 is given symbolically by:

The parameters of these lattice elements are:

DRIFT:	D0	DS	DB
length (m)	0.1625	0.1195	2.350
BEND MAGNET:	B		
length (m)	2.351		
bending radius (m)	11.975		
HALF QUADRUPOLES:	QFH	QDH	
length (m)	0.190	0.150	
SEXTUPOLES:*	SF	SD	
length (m)	0.086	0.086	

* In the lattice structure the sextupoles are treated as thin lens elements.

All FODO cells are 6.683 m long. To minimize the number of magnet power supplies only two quadrupole families are required in this lattice for focusing and control of the operating tunes. All bending magnets are powered by one single power supply and for chromaticity control, two families of sextupoles are sufficient. Finally a set of vertical and horizontal orbit correctors are placed around the ring to allow the control and correction of orbit distortions.

Some characteristic parameters of this lattice are compiled in Table 3-3. In Figure 3-4 the betatron functions are shown along the circumference of the ring displaying the uniform beating characteristic for regular FODO lattices. The horizontal betatron functions exhibits some variation of the maximum amplitude due to the lack of sector magnet focusing in the the bending magnet free cells. The dispersion function was chosen to reach minimum values in the straight sections for ease of injection and, particularly in the RF section, in order to minimize synchro-betatron oscillations and instabilities. A more even distribution of the dispersion function could be obtained if more than only two quadrupole families would be employed. The small gain in aperture, however, does not justify the increased cost and operating complexity to control additional magnet power supplies.

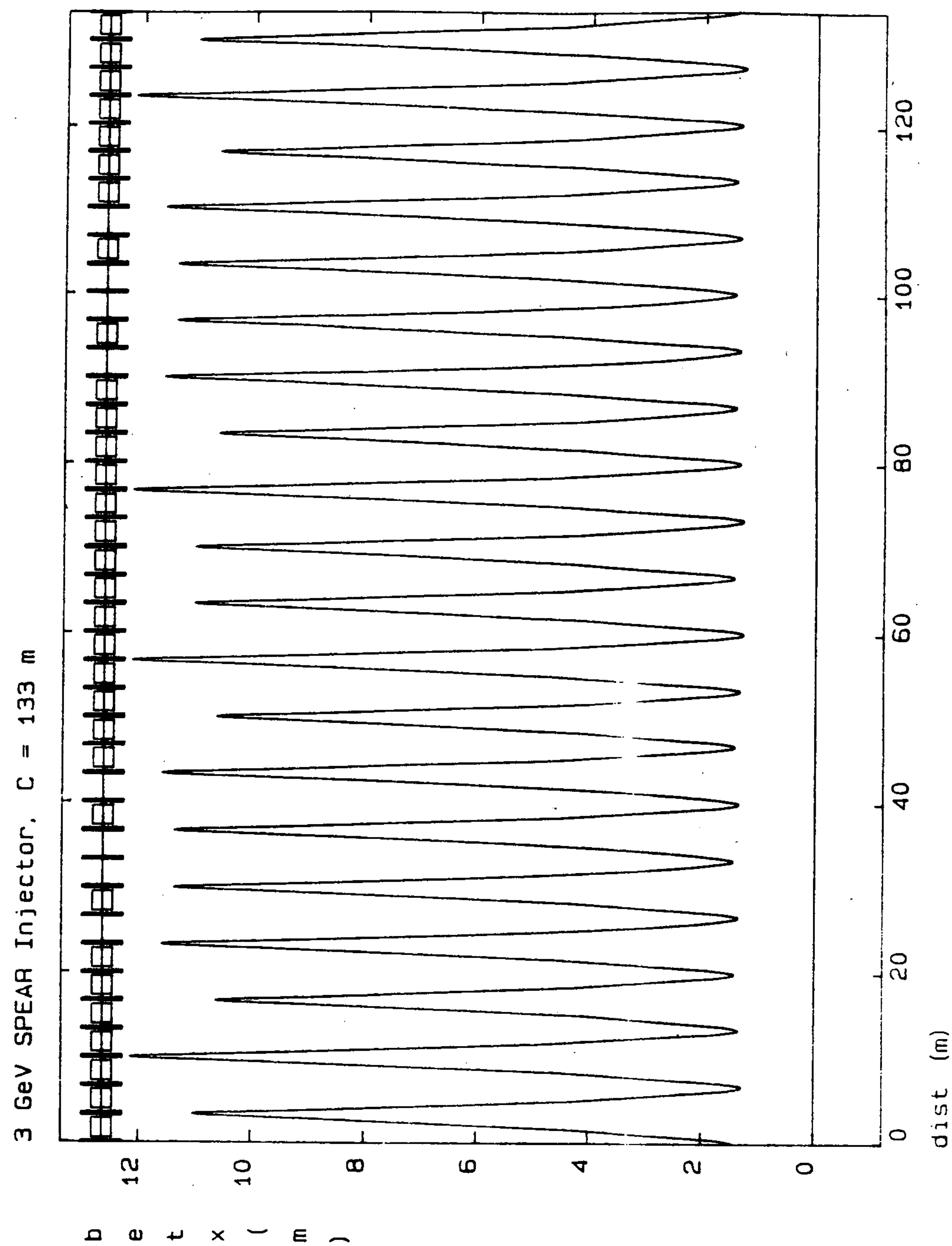

Fig. 3.1-2: Horizontal Betatron Function

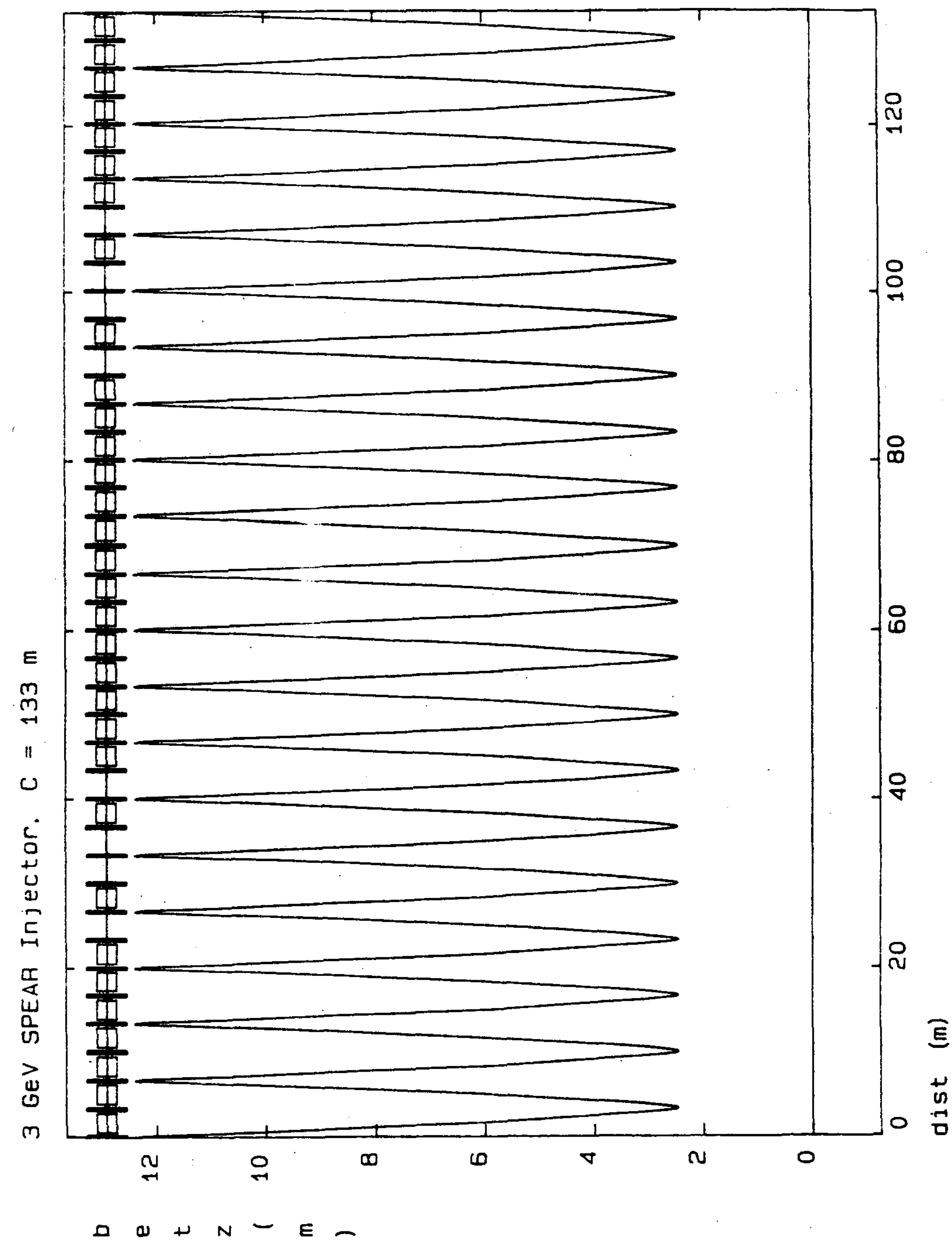

Fig. 3.1-3: Vertical Betatron Function

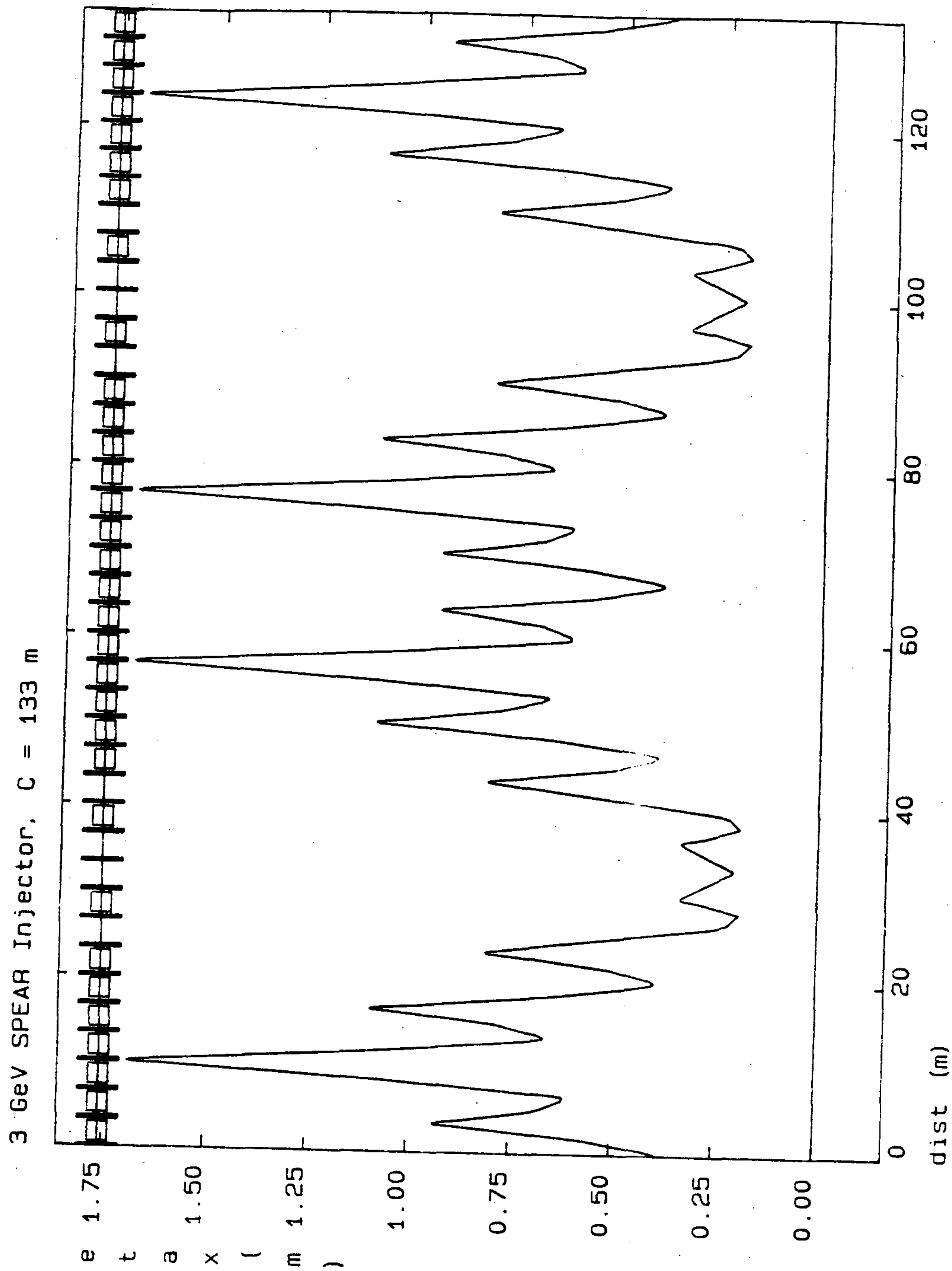

Fig. 3.1-4: Dispersion Function

Table 3.1-2

Lattice Parameters

Lattice Type	FODO
Magnet Structure	separated function
Cell Length (m)	6.683
Total Number of FODO cells	20
Max. Value of Betatron Functions(x/y) (m)	12.2 / 12.4
Max. value of Dispersion Function(m)	1.69
Tunes (x/y)	6.250 / 4.175
Momentum Compaction Factor	0.03349
Natural Chromaticities (x/y)	-7.51 /-5.70
Beam Emittance (mm * mrad) @ 3.0 GeV	0.190
Beam Energy Spread (%)	0.073
Beam Emittance (mm * mrad)	$0.021 * E^2(GeV^2)$
Beam Energy Spread	$0.000244 * E(GeV)$

3.2 Beam Stay Clear and Aperture

For ease of injection and specifically in preparation for possible positron injection at a later date a rather large vacuum chamber cross section has been chosen. In Figure 3.2-1 the beam stay clear region (BSC) is shown both for the horizontal and vertical plane. The BSC is the maximum cross section a beam may have before particles get lost on the physical aperture.

The minimum physical aperture or beam stay clear, as shown in Figure 3.2-1, is based on the assumption that eventually it will be desired to accelerate positrons injected at 250 MeV. This requires an acceptance in the storage ring of at least 18 mm*mrad horizontally and 10 mm*mrad vertically. During acceleration the beam reaches the equilibrium beam size as determined by the quantum excitation due to synchrotron radiation and radiation damping. The particle distribution becomes a gaussian distribution and scales linearly with the energy. The beam size is defined as one standard deviation of the gaussian distribution. The vacuum chamber aperture must accommodate at least 5 units of the standard beam size in addition to an allowance for orbit distortions to retain a useful beam lifetime. In this design the beam sizes are smaller than the aperture up to 3.50 GeV. In more detail the beam sizes under various assumptions (see Table 3.2-1) have been calculated and have been used to determine the BSC. Extreme beam sizes as required for positron injection or for a higher end energy of 3.5 GeV have been used to determine the required vacuum chamber aperture.

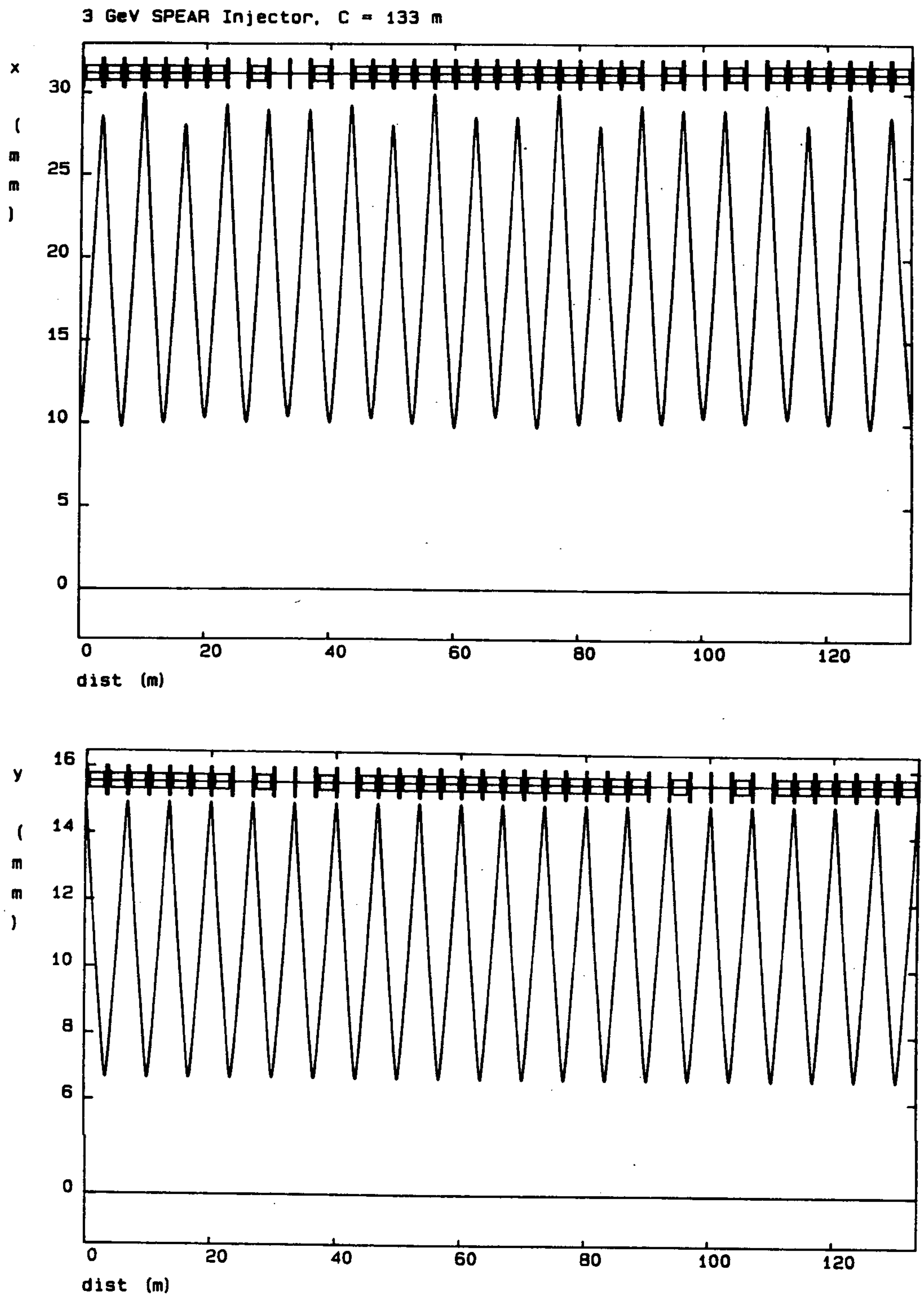

Fig. 3.2-1: Beam Stay Clear in the Booster Injector

Table 3.2-2

Beam Size under Different Conditions

Electron Beam:	
at injection (100 MeV):	
Beam Emittance (both planes)	0.10 $mm * mrad$
Energy Spread	1.0%
Max. Beam Width	14.5 mm
Max. Beam Height (quad)	1.1 mm
at 3.0 GeV:	
Beam Emittance (1 σ)	0.19 $mm * mrad$
Max. Beam Width ($\pm 5(\sigma_\beta + \sigma_\eta)$)	15.2 mm
Max. Beam Height ($\pm 5\sigma_\beta$)	10.7 mm
Max. Beam Height	10.0 mm
Positron Beam:	
at injection (250 MeV):	
Beam Emittance (Horizontal)	18.0 $mm * mrad$
Beam Emittance (Vertical)	10.0 $mm * mrad$
Energy Spread	1.0%
Max. Beam Width	45.0 mm
Max. Beam Height	22.3 mm
Max. Beam Height	20.8 mm

The maximum beam width for any beam considered is about 45 mm and the maximum beam height in the quadrupoles and in the bending magnets is 22 mm. A horizontal free aperture of 60 mm and a clear height of 30 mm is, therefore, assumed for the vacuum chamber in the quadrupoles and the bending magnets , leaving 15 mm and 8 mm for orbit distortions in the horizontal and vertical plane respectively. The dynamic aperture has been determined to be much larger than the physical aperture in both planes.

3.3 Aberrations

The focusing structure of the quadrupoles is perfectly correct only for a monochromatic beam at the design energy. A realistic beam from the linac preaccelerator, however, has a finite energy spread. Off energy particles will be focused somewhat differently and may get lost if the focusing lattice is specifically sensitive to energy error of particles. The deviations from the ideal focusing structure are called chromatic aberrations in analogy to light optics. One of the most obvious aberrations are the so-called chromaticities, which are the variations of the tunes with energy. These chromaticities must be compensated with the help of sextupole magnets to avoid beam loss due to the head tail instability.

The chromatic aberrations after chromaticity corrections are very small. The energy acceptance is at least 3.0% (Figure 3.3-1) based on lattice considerations only and not considering limitations due to too low a choice for the RF voltage. This acceptance is comfortably large and can easily accommodate the large energy spread of a future positron beam. The variation of the betatron function with energy is less than 10% everywhere around the ring for an energy deviation of 1%. Finally the second order momentum compaction factor is only 5% of the first order momentum compaction factor.

The inclusion of sextupole magnets not only compensates the chromatic aberrations but due to the nonlinear fields also introduces geometric aberrations which can lead to a limitation in the transverse area for stable betatron oscillations. This limit of stability is generally caused by a variation of the tunes with the betatron oscillation amplitude leading to a resonance. In this lattice the linear tune shift with amplitude is very small and reaches a value of only 0.0025 for the maximum possible betatron amplitude of 30 mm within the vacuum chamber.

In summary all chromatic and geometric aberrations are very small as is to be expected for such a lattice. As a result of these weak chromatic and geometric aberrations the dynamic aperture (Figure 3.3-2) is much larger than the physical aperture of the vacuum enclosure and provides, therefore, a large margin for the effects of orbit and field errors.

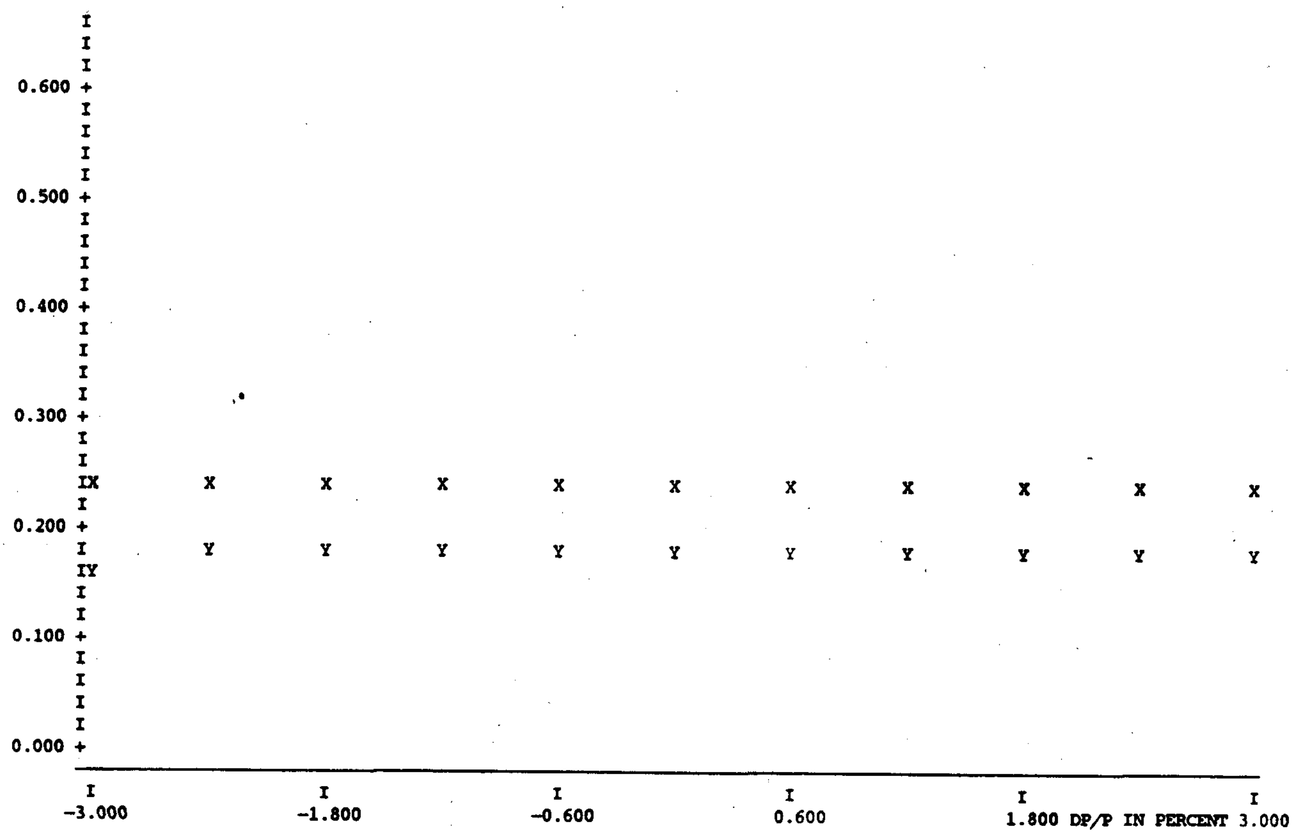

NUEX	0.2466	0.2477	0.2487	0.2495	0.2499	0.2500	0.2498	0.2491	0.2481	0.2462	0.2431
NUEY	0.1659	0.1704	0.1729	0.1743	0.1749	0.1750	0.1749	0.1747	0.1744	0.1740	0.1736

Fig. 3.3-1: Tune Variation with Energy

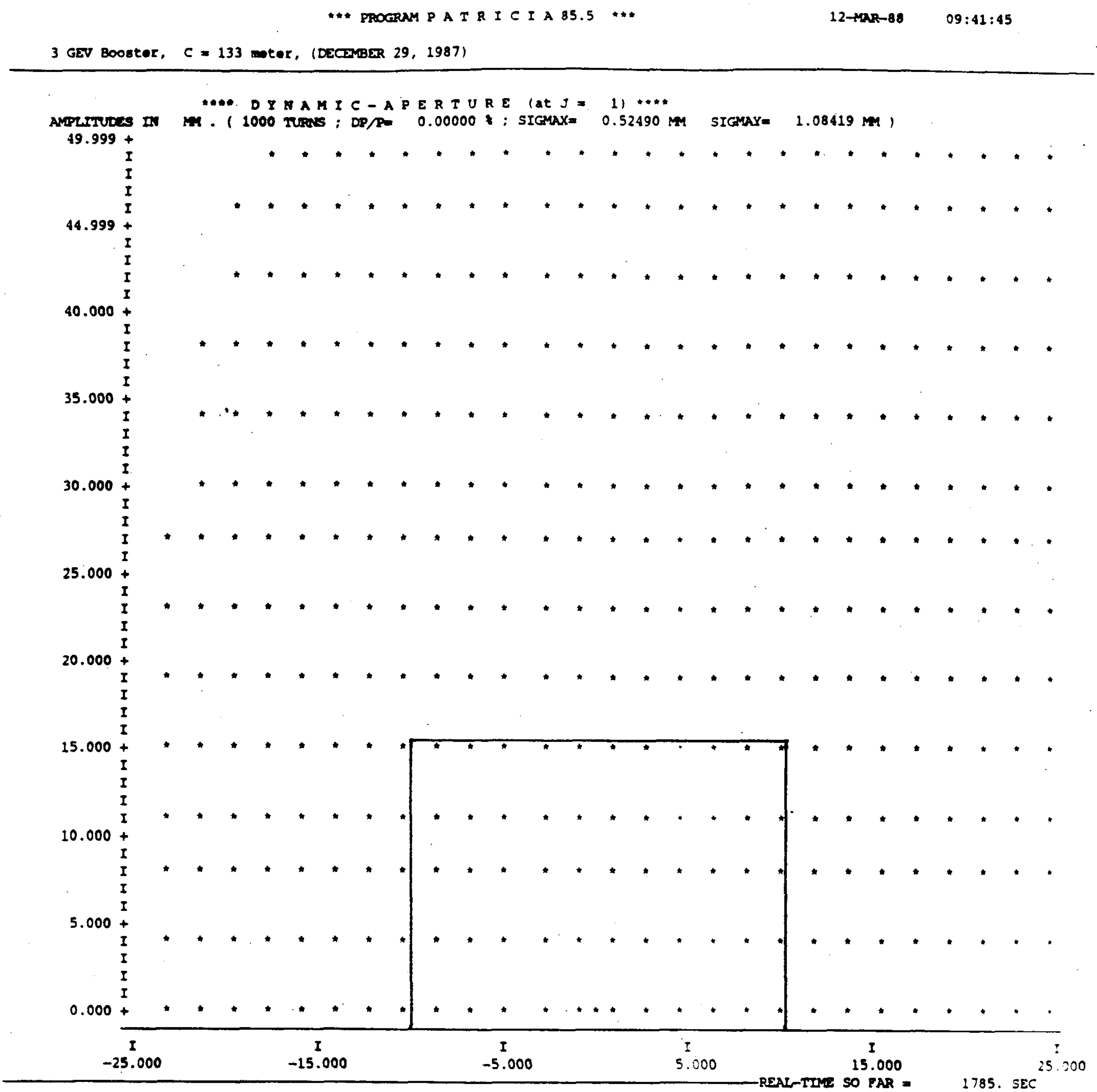

Fig. 3.3-2: Dynamic Aperture

PREINJECTOR

4 Preinjector Linear Accelerator

Chapter 4

Preinjector Linear Accelerator

4 Preinjector Linear Accelerator

The preaccelerator for injection into the booster synchrotron consists of a linac composed of three accelerating sections of the SLAC type and a microwave gun similar to those used in microtrons to produce the electron beam. Each of the three accelerating sections is powered by a separate 30 MW klystron.

4.1 Microwave Gun

The electrons are generated in the microwave gun from a LaB_6 cathode which, when heated to 1600 K^0, can deliver current densities in excess of 100 A/cm^2. This type of gun is used in microtrons as well as in linear accelerators.[1][2] The cathode reaches directly into the high field of a microwave cavity where the electrons are quickly accelerated to relativistic energies. After focusing and energy definition the beam is injected into the linear accelerator sections for acceleration to more than 100 MeV. This type of a gun can produce an instantaneous electron current of more than 10 amp. The advantage of such a gun compared to the often used thermionic gun is that the electrons are accelerated by an RF field to relativistic energies in the very short distance of about 3 cm, the length of one S-band cavity. This fast acceleration efficiently overcomes the electrical space charge forces which cause a significant increase in beam emittance and beam size. For optimum injection efficiency into the booster we plan to take advantage of this greatly reduced beam blow up in a microwave gun. One further advantage of this type of gun is that no other equipment, like prebuncher or buncher section, is required in the linac since the beam is automatically bunched through the field of the microwave gun cavity. This greatly reduces the complexity of the preinjector and allows easy operation.

With a peak current of 10 amp from the microwave gun we expect a population of 4.2 10^8 electrons in each 2 mm S-band bunch. For a much longer bunch length the energy spread in the beam becomes large. Some of the gun parameters are summarized in Table 4.1-1:

[1] G.A. Westenkow et. al., Laser and Particle Beams, Vol. 2, part 2, (1984), pp.233.

[2] S.V. Benson et. al., Proc. of 1985 FEL Conference Granlibakken.

Table 4.1-1

Microwave Gun Parameter

Gun Cavity Frequency (MHz)	2856
Particle Energy (keV)	> 500
Cathode Peak Current (amp)	≥ 10.0
Bunch Length (mm)	2.0
Particles/S-Band Bunch	$4.2\ 10^8$
Particles per 3 S-Band Bunches	$12.5\ 10^8$

4.2 Momentum Filter

The energy spread of the electron beam from the microwave gun is very large due to the varying RF field in the cavity. A magnetic momentum filter will be used to eliminate all particles with energies outside the acceptable energy bin. This momentum filter makes use of the momentum dispersion caused by the deflecting field of a dipole field. Placement of a slitted absorber at the position of maximum momentum dispersion allows selection of a narrow momentum bin from the beam for further acceleration.

4.3 Beam Chopper

Without any further devices a long string of electron bunches, separated by the linac RF wavelength of 10 cm, would enter the linac sections (see Figure 4.3-1). Not all of these bunches can be accepted by the booster synchrotron or by the storage ring. To reduce the level of radiation caused by these partially accelerated and eventually lost particles, it is prudent to eliminate these particle bunches at very low energies. This is performed by a device called a chopper located between the momentum filter and the linear accelerator. The string of S-band bunches emerging from the microwave gun will be modified by the chopper in such a way as to fit special requirements of the booster synchrotron and storage ring.

Since the booster RF frequency is much lower than the linac RF frequency, it is possible to accept three or even more consecutive linac bunches into one booster RF bucket, where they eventually merge into one bunch by radiation damping. Therefore, a chopper composed of a fast deflector with a slit will be used to generate, from the continuous stream of S-band bunches, a particle beam made up of a string of equidistant triplet bunches. Each triplet consists of three consecutive S-band bunches and the distance between the triplets is equal to the desired bunch distance in the booster synchrotron (Figure 4.3-1).

The conceptual layout of the chopper is shown in Figure 4.3-2. Here a DC magnetic field deflects the beam from the gun into an absorber. Superimposed is an electrical pulsed field which deflects the beam against the magnetic field toward the slit and allows the beam, during a short time period, to emerge through the slit to be accelerated in the linac. This way a string of S-band triplets can be produced for multibunch injection into the booster and SPEAR.

While this multibunch mode of operation is the prevailing mode of operation in SPEAR, there are occasions when a single or few bunches are desired.

For timing experiments it is desirable to make use of the very short storage ring bunch to excite atomic or molecular states with an extremely short burst of photons. To observe the decay of these states a "long" radiation free time must follow. In the extreme case only one bunch would be filled

At the e^- gun:

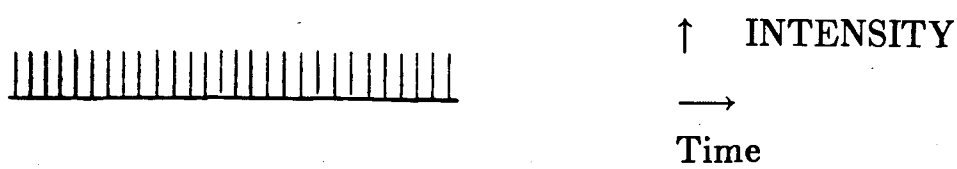

After beam chopper:

Fig. 4.3-1: Bunch Patterns in the Injection System

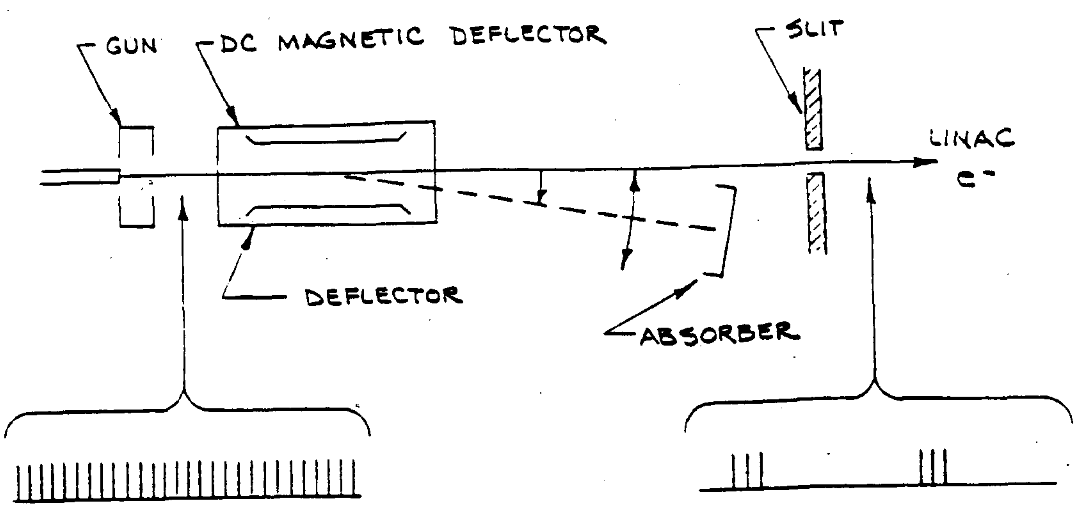

Fig. 4.3-2: Beam Chopper System

in the SPEAR storage ring providing a radiation free time equal to one full revolution time. For this case also only one bunch is being accelerated per accelerating cycle in the booster. This booster bunch consists of 3 linac buckets and therefore 12.5 10^8 electrons are accelerated per cycle giving an injection rate for a single bunch in the SPEAR storage ring of at least 5.0 mamp/min assuming a 25% overall transfer efficiency and a booster cycle rate of 2.0 Hz. Since the single bunch current in the storage ring will not be larger than 10 to 20 mamp because of instabilities or Touschek lifetime limitations, a single bunch filling time of less than five minute can be expected from this injector.

When many bunches are desired in the storage ring, strings of bunches can be accelerated and transferred to the storage ring in a single pulse. In this mode of operation the fastest storage ring filling rate of more than 50 ma/min can be achieved assuming eight bunches to be accelerated per booster cycle and a 25% injection efficiency into the storage ring. This will also be the most efficient mode of operation for beam cleaning the vacuum chamber in SPEAR to achieve long beam lifetime.

For further planning we will assume the preinjector beam characteristics as compiled in Table 4.3-1:

With these preinjector beam parameters we expect to achieve the SPEAR injection parameters as summarized in Table 4.3-2. For the multi-bunch made we assume 8 bunches to be accelerated in the booster while only a single bunch in accelerated for single bunch mode in SPEAR.

Table 4.3-1

Preinjector Beam Parameter

Energy from Preinjector (MeV)	≥ 100
Number of Booster Bunches	8
Number of Particles per Pulse	10^{10}
Pulse Repetition Rate (Hz)	10
Total Energy Spread at full Linac Energy	0.010
Normalized Beam Emittance ($\epsilon\,\gamma$)	
Horizontal (m)	$20 \cdot 10^{-6}$
Vertical (m)	$10 \cdot 10^{-6}$
Beam Emittance	
Horizontal (m)	$0.085 \cdot 10^{-6}$
Vertical (m)	$0.043 \cdot 10^{-6}$

Table 4.3-2

SPEAR Injection Parameters

Storage Ring Bunch Mode	Single Bunch	Multi Bunch
Storage Ring Beam Current (ma)	20.0	100.0
Circumference (m)	234.0	234.0
Total Number of Particles (10^8)	975	4875
Injection Efficiency (%)	25.0	25.0
Number of Booster Cycles needed	312	195
Booster Cycles per Second	2	2
Storage Ring Filling Time (sec)	31	20
Storage Ring Filling Rate (ma/min)	> 35	> 300

4.4 Linear Accelerator

For the acceleration of the electrons coming from the gun to high energies, three 10 foot accelerating sections of the SLAC type will be used. The energy gain per linear accelerator sections is determined by the RF power from the klystrons and is given by:

$$E_0(MeV) = 10 * (P(MW))^{1/2} = 54.8\,MeV$$

This energy gain per section can be obtained straightforward without relying on any RF-pulse compression scheme like the SLED scheme. In the three accelerating sections, therefore, a total "no load" energy of about 164.4 MeV can be reached if three 30 MW klystrons are used. In reality, however, this "no load" energy gain is reduced by beam loading leading actually to a somewhat lower beam energy of at least 100 MeV depending on the intensity of the beam accelerated. The performance of the booster synchrotron basically improves with increasing injection energy from the preinjector. However, this dependence is rather weak and the additional complexity of a SLED'ed accelerating scheme is not advisable. From a technical view point a SLED'ed mode of operation is also not desirable since it would not allow the acceleration of a long string of bunches.

The proposed mode of operation of the linac sections is straightforward and most components are expected to be, and perform similar to those used at the Stanford Linear Accelerator.

Some of the main parameters of the linear accelerator are compiled in Table 4.4-1.

Because of the low repetition rate of no more than 10 Hz, the RF power requirements for the linac are very modest. This allows a reduced cost and complexity compared to high power klystron modulators required for high pulse repetition rates. In Table 4.4-2 the klystron and modulator specifications are summarized.

Table 4.4-1

Linac Parameter

Accelerating Sections	three
Length/Section (m)	3.0
Frequency (MHz)	2856
Type	constant impedance
RF Filling time (sec)	$0.75 * 10^{-6}$
Klystron/Modulators	three
Pulse Power (MW)	$\geq$ 30.0
Pulse Length (sec)	1.5 to $2 * 10^{-6}$
Pulse Rep. Rate (Hz)	$\leq$ 10
Preinjector Energy (MeV) (no load)	164.4
Pulse Length (nsec)	> 330

Table 4.4-2

SLAC Klystron Parameter

Klystron Peak Output Power	35	MW
Frequency	2856	MHz
Peak Beam Voltage	265	kV
Peak Beam Current	286	A
Peak Beam Power	75.8	MW
Repetition Rate	10	Hz
RF Pulse Length (max)	1.5	$\mu - sec$
Modulator Pulse Length (max)	3.35	$\mu - sec$
Klystron Efficiency	47	%
AC Power	3.32	kW
Focusing Magnet	permanent	
Cathode Type	oxide	

4.5 Beam Transport to the Booster Synchrotron

A beam transport system will guide the electron beam from the preinjector linac to the booster synchrotron where it will be injected "on axis" through a full aperture kicker magnet. Bending and focusing magnets will match the beam to the optical parameters of the synchrotron at the injection point. A septum magnet close to the synchrotron will align the beam direction so as to let the incoming beam cross the booster beam orbit in the middle of the full-aperture kicker magnet. This kicker magnet then will be turned on for not more than one revolution time of 330 nsec to align the injected beam exactly with the ideal booster beam orbit. The kicker magnet must be turned off before the first particles injected arrive again at the kicker location after one turn in the booster,

Along the transport line and in a special beam diagnostics branch the beam characteristics like beam intensity, energy and energy spread will be measured and controlled. For this purpose intensity monitors are installed in the transport line. A dispersive section of the transport line will make measurements and determinations of the exact beam energy and energy spread. This analyzing station will be helpful in setting up the preinjector beam while the SPEAR storage ring is used for experiments. For this purpose a downstream bending magnet will be turned off to guide the beam into a separate beam dump. A Faraday cup in front of this beam dump can be inserted into the beam for a precise beam intensity measurement.

Beam position monitors and scintillators with TV cameras will be installed to observe the beam position and quality. Orthogonal steering magnets at the end of the transport line are designed to allow the independent adjustment of the beam position and angle at the injection point.

Because of the low beam energy rather small magnets are required and the power supplies therefore are chosen to be the same as those for the beam steering magnets in the booster.

MAGNET

5 Ring Magnet System

Chapter 5

Ring Magnet System

5 Ring Magnet System

The magnets for the booster synchrotron must be constructed in such a way as to minimize the occurrence of eddy currents during energy ramping. Therefore, the magnet cores are constructed from laminations of silicon steel stock. All magnets can be split in the horizontal midplane to allow the installation of the vacuum chamber.

The aperture of the magnets is determined by the larger of both the injected beams size and the beam size at high energies plus an additional allowance required for orbit distortion in the vacuum chamber. The space required for the beam, called the "beam stay clear" region or BSC, is shown in Figure 3.2-1 and was determined mostly by the size of a possible future positron beam during injection at a minimum energy of at least 250 MeV. The requirements for the electron beam both at injection and at 3 GeV are smaller.

The magnetic field properties are modeled with the help of a computer program MAGNET which has been used extensively for the design of synchrotron and storage ring magnets at CERN and elsewhere. Finally the magnet quality will be determined by magnetic measurement which allows expansion of the magnetic field into the fundamental field and the higher harmonics. The magnet pole shapes will be determined such as not to cause beam instability by higher harmonic field errors.

Special trim coils and orbit correction magnets in connection with beam position monitors will be used to control the beam orbit during acceleration.

Three different types of magnets are required for the booster synchrotron:

* bending magnets to bend the electrons onto a circular path,
* quadrupole magnets to hold the particles in the vicinity of the ideal design orbit within the vacuum chamber, and,
* sextupole magnets to correct chromatic aberrations which can cause beam instabilities.

The construction of these magnets as well as the alignment follows well established procedure since the simplicity of the lattice does not require high construction and alignment tolerances.

5.1 Magnets

5.1.1 Bending Magnets

The main bending magnet system consists of a total of 32 H type magnets. All bending magnets have the same cross section as shown in Figure 5.1-1 , the same lengths and the same field strengths. The main parameters of the bending magnets are compiled in Table 5.1-1.

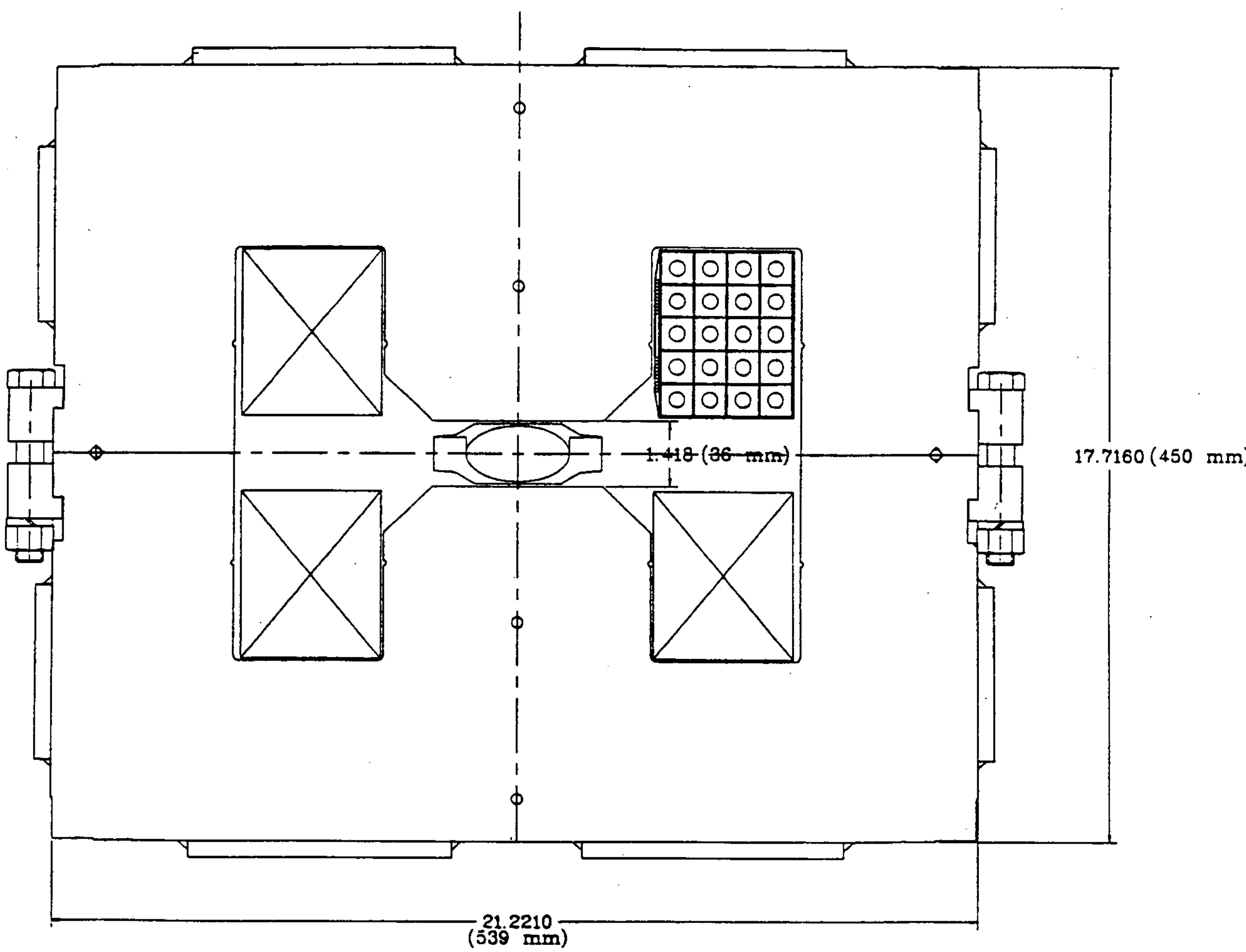

Fig. 5.1-1: Bending Magnet Cross Section

The sagitta of the beam orbit in the longer magnets is quite significant at 58 mm. If one would build a straight magnet the pole width would have to be 58 mm wider and the total magnet would be 116 mm wider than required for the beam alone. To minimize the width of the magnets it is planned to "bend" the magnet by splitting the iron core into straight blocks with wedge-shaped spacers in between (Figure 5.1-2). Still the whole magnet will be powered by two long excitation coils.

The maximum required strength of all magnets is 8.35 kGauss for 3.0 GeV leaving a comfortable margin for higher energy operation if so desired.

Table 5.1-1: Bending Magnet Specifications @ 3 GeV

Magnet Name in Lattice	B
Magnet Designation	36 B 2315
Beam Energy (GeV)	3.0
Field Strength at 3.0 GeV (kG)	8.35
Field Strength at Injection (120 MeV) (kG)	334
Maximum Strength (kG)	15.7
Magnetic Length (mm)	2351.27
Bending Radius (mm)	11974.90
Bending Angle (degrees)	11.25
Sagitta (mm)	57.66
Overall Length (m)	2.48
Overall Width (m)	.813
Overall Height (m)	.562
Overall Weight (m)	3240
Gap Height (mm)	36
Good Field Region (mm)	32 high x 60 wide
Max. Beam Width (mm)	31
Max. Beam Height (mm)	22
Magnet Efficiency at 8.35 kG (%)	> 98
Current (Amps)	600
Ampere Turns	24,000

Table 11: Bending Magnet Specifications (con't)

Max. Induced Voltage at 10 Hz. (V)	441
Magnet Resistance at 37° C (m ohm)	24.0
Magnet Inductance (mH)	23.4
Magnet Time Constant L/R (sec)	0.98
Total Power Loss at 10 Hz (kW)	7.4
Driving Current Loss (kW)	6.5
Coil Eddy Loss at 10 Hz (kW)	0.6
Core Loss (Eddy & Hyst) at 10 Hz. (kW)	0.3
Stored Energy (kJ)	4.2
No. Turns/Coil	20
No. Coils/Magnet	2
Current Density (A/mm^2)	2.24
Conductor Dimensions (mm)	18.2 x 18.2 w/8.9 D Hole
Conductor Material	Aluminum
Conductor X-Section Area (mm^2)	269.03
Length/Coil (m)	107
Weight/Coil (kg)	107
Cooling Circuits/Coil	1
Water Flowrate (GPM)	2.0
Pressure Drop/Magnet (psi)	100
Temperature Rise in Coil (deg. C°)	20
No. Blocks in Bend	5
Core Material (kg)	Silicon Steel (M-36)
Steel Core Weight (kg)	2937
Fabrication Technique	Laminated H Type
Lamination Thickness (mm)	.625 (.0246")
Laminations/Magnet (Figure 5.1-3)	7410
Laminations/Block	1482
Magnet Steel Length (mm)	2315.27
Magnet Block Length (mm)	453.4
Gap Between Blocks at Center (mm)	12
Interlaminate Pressure (psi)	60

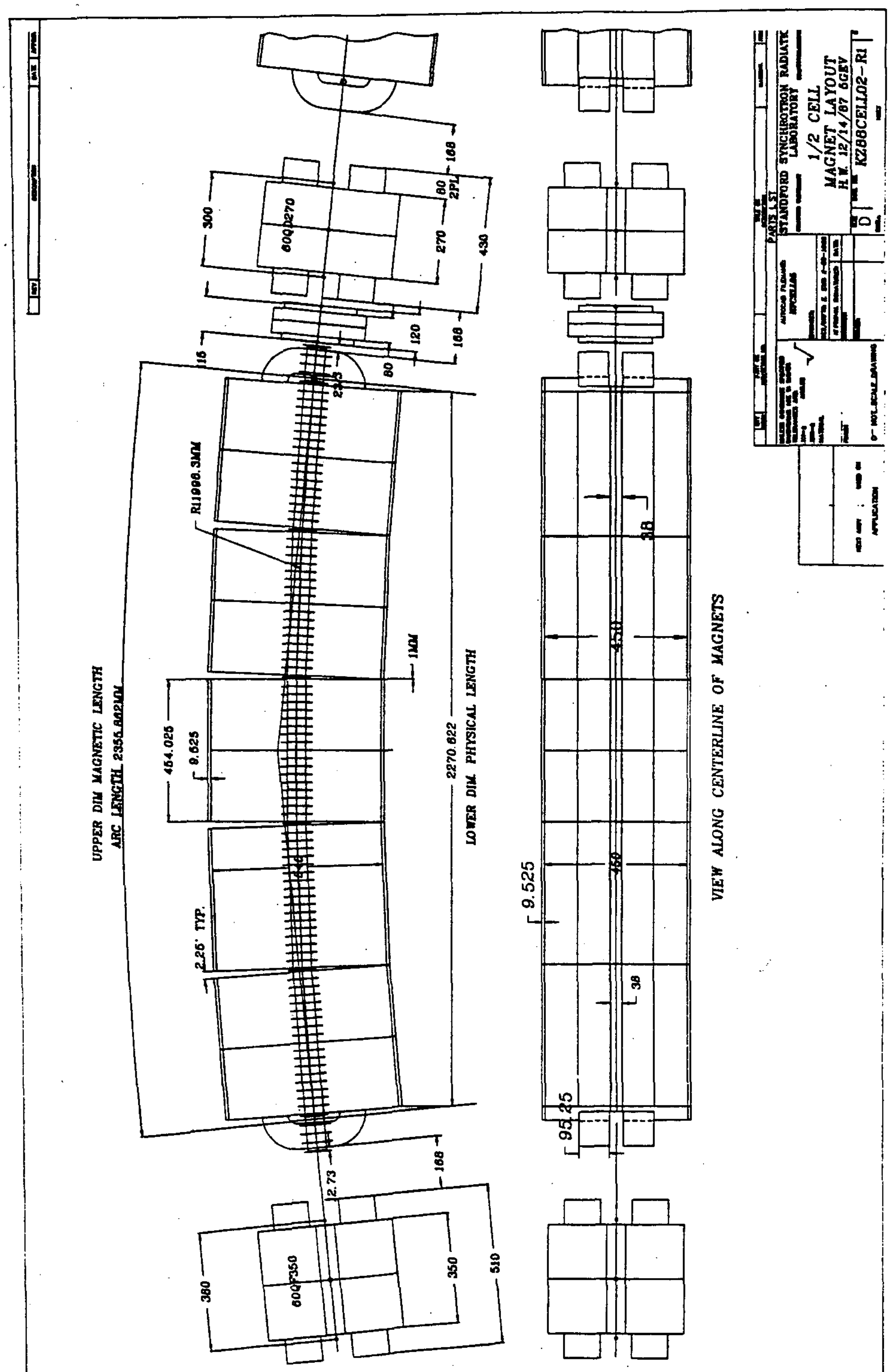

Fig. 5.1-2: Construction of the Bending Magnets

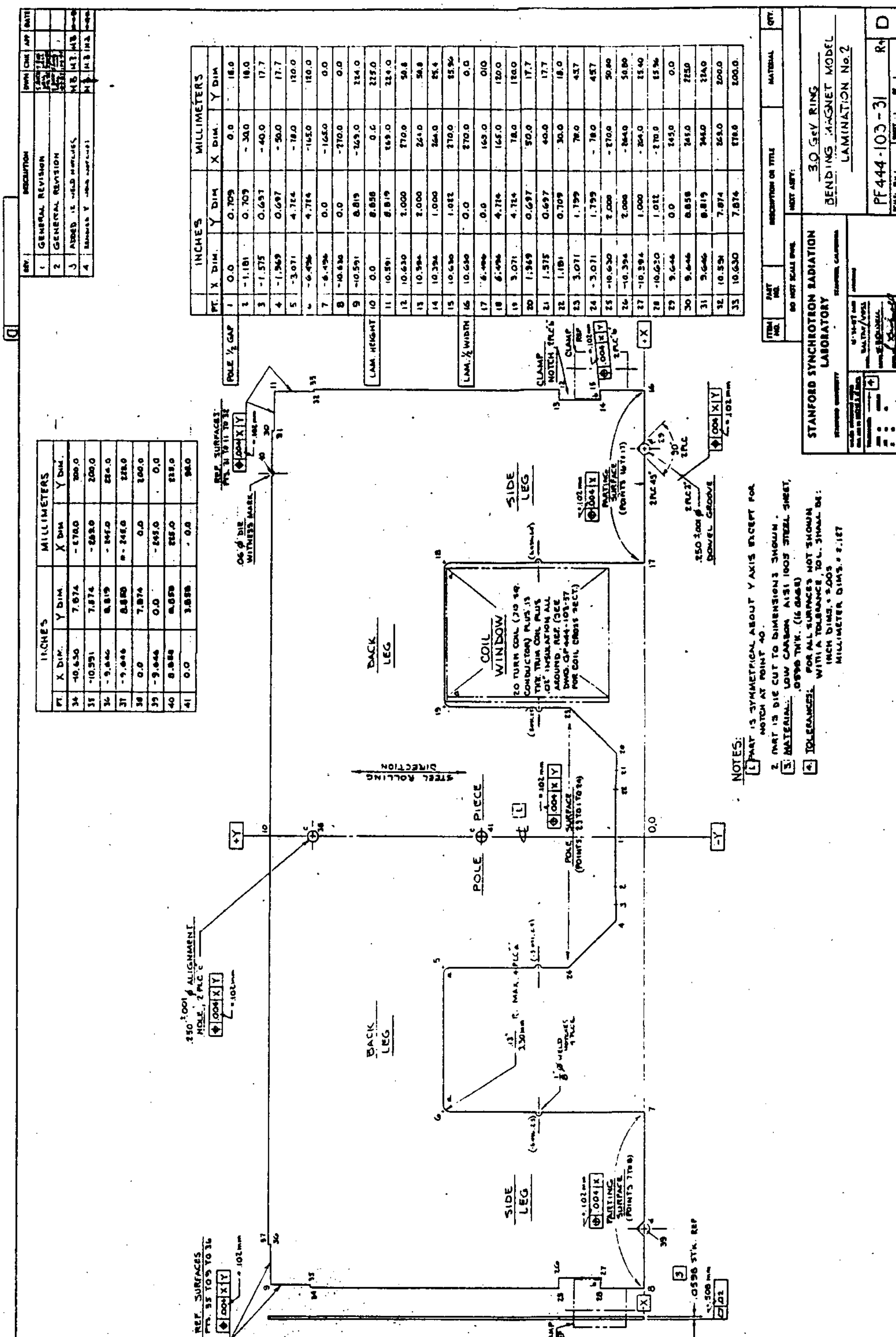

Fig. 5.1-3: Bending Magnet Lamination

PERMEABILITY MAP.

DISTANCE BETWEEN COLUMNS = 20.00MM (= 2 TIMES H)
DISTANCE BETWEEN ROWS = 10.00MM (= 1 TIMES H)

2000	2810	3160	2840	2114	1472	1292	1304	1426	1769	2503	3160	2899	2000
2155	2996	3160	2815	2101	1465	1289	1303	1423	1757	2484	3160	3151	2226
2589	3160	3160	2754	2061	1444	1280	1298	1414	1723	2426	3158	3160	2917
3159	3160	3160	2670	1995	1408	1266	1291	1399	1662	2332	2971	3160	3160
3160	3160	3098	2563	1906	1357	1248	1282	1380	1577	2210	2710	3132	3160
3160	3160	2866	2429	1799	1282	1224	1272	1354	1446	1990	2404	2595	2677
3089	2905	2636	2274	1680	1195	1198	1261	1327	1299	1745	1963	2011	2017
2660	2568	2372	2060	1524	1055	1166	1249	1291	1031	1338	1280	1212	1189
2331	2262	2075	1772	1374	937	1138	1240	1264	844	899	863	855	854
1984	1901	1720	1445	1088	701	1098	1229	1223	439	612	656	680	688
1694	1634	1481	1210	825	0	0	0	0	0	427	512	554	566
1550	1514	1431	1305	1131	0	0	0	0	0	458	478	494	499
1491	1469	1419	1347	1268	0	0	0	0	0	422	440	453	458
1483	1469	1439	1399	1356	0	0	0	0	0	399	419	432	437
1505	1497	1480	1458	1433	0	0	0	0	0	390	414	430	439
1546	1542	1535	1525	1514	0	0	0	0	0	404	431	449	456
1596	1597	1599	1603	1608	0	0	0	0	0	441	471	495	504
1648	1653	1665	1688	1724	0	0	0	0	0	223	453	557	592
1692	1700	1722	1763	1834	0	0	0	0	0	65	426	761	835
1719	1728	1753	1799	1892	0	0	0	0	0	0	0	0	0
1728	1735	1753	1771	1752	0	0	0	0	0	0	0	0	0

Fig. 5.1-4: Saturation of the Bending Magnet at 13 kGauss

No serious saturation effects occur as can be seen from Figure 5.1-4 where the permeability is plotted across one quarter of the otherwise symmetric magnet for 13 kGauss.

All magnets are equipped with trim coils to provide orbit correction capabilities. The maximum strength of the trim coils will be specified to allow the correction of any reasonable orbit distortion expected in the synchrotron.

The peak power at 3 GeV for the bending magnets is expected to be about 9.4 kWatt while the average power is 33% of that.

The assembly of the bending magnets consists of five magnet blocks, Figure 5.1.-5, energized by one common coil. This way it is possible to use the straightforward and precise technique of assembling linear magnets instead of having to "curve" them. A three block prototype of such a magnet, shown in Figure 5.1-6, has been built and is being evaluated mechanically as well as magnetically.

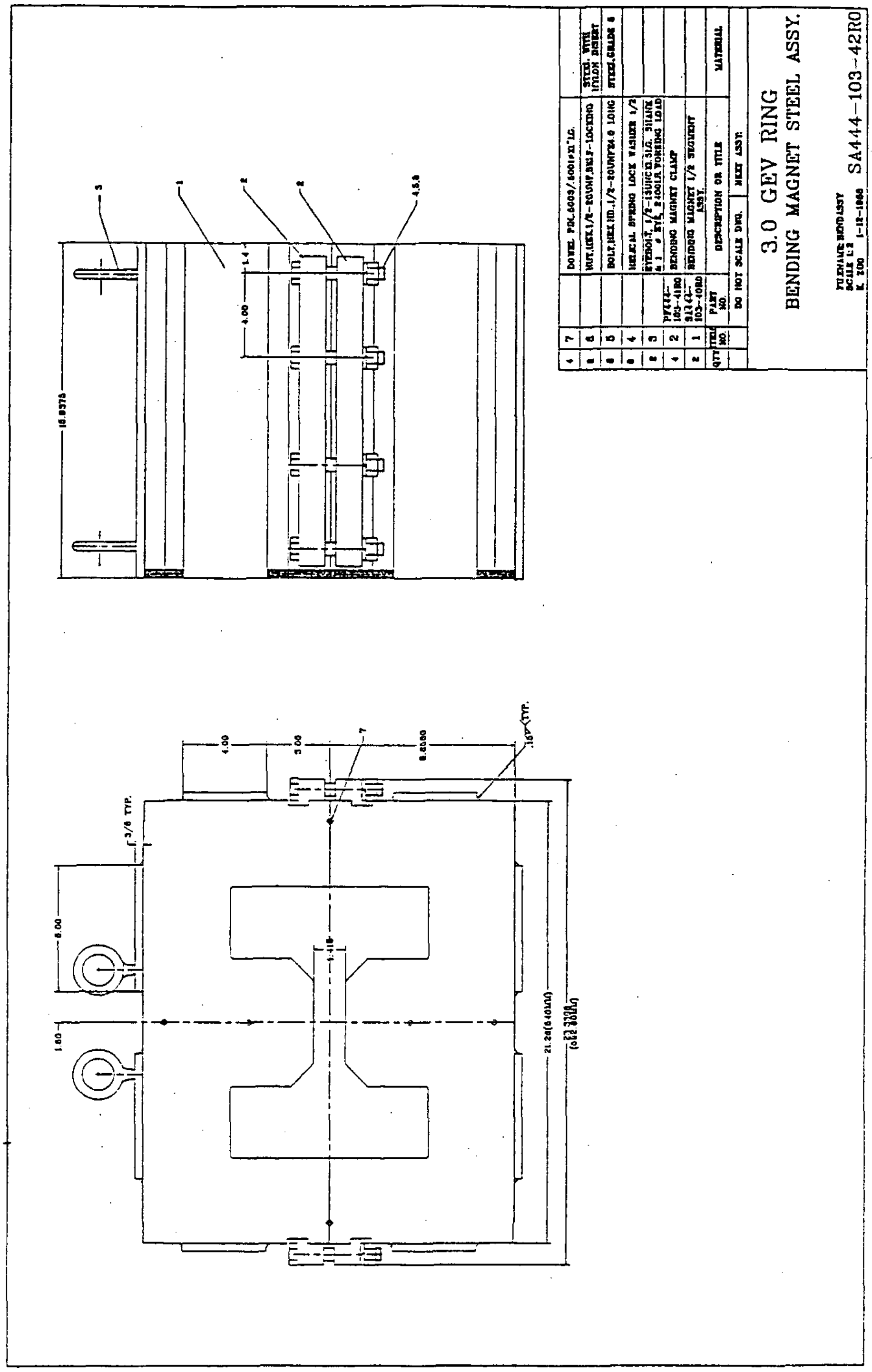

Fig. 5.1-5: Bending Magnet Block Assembly

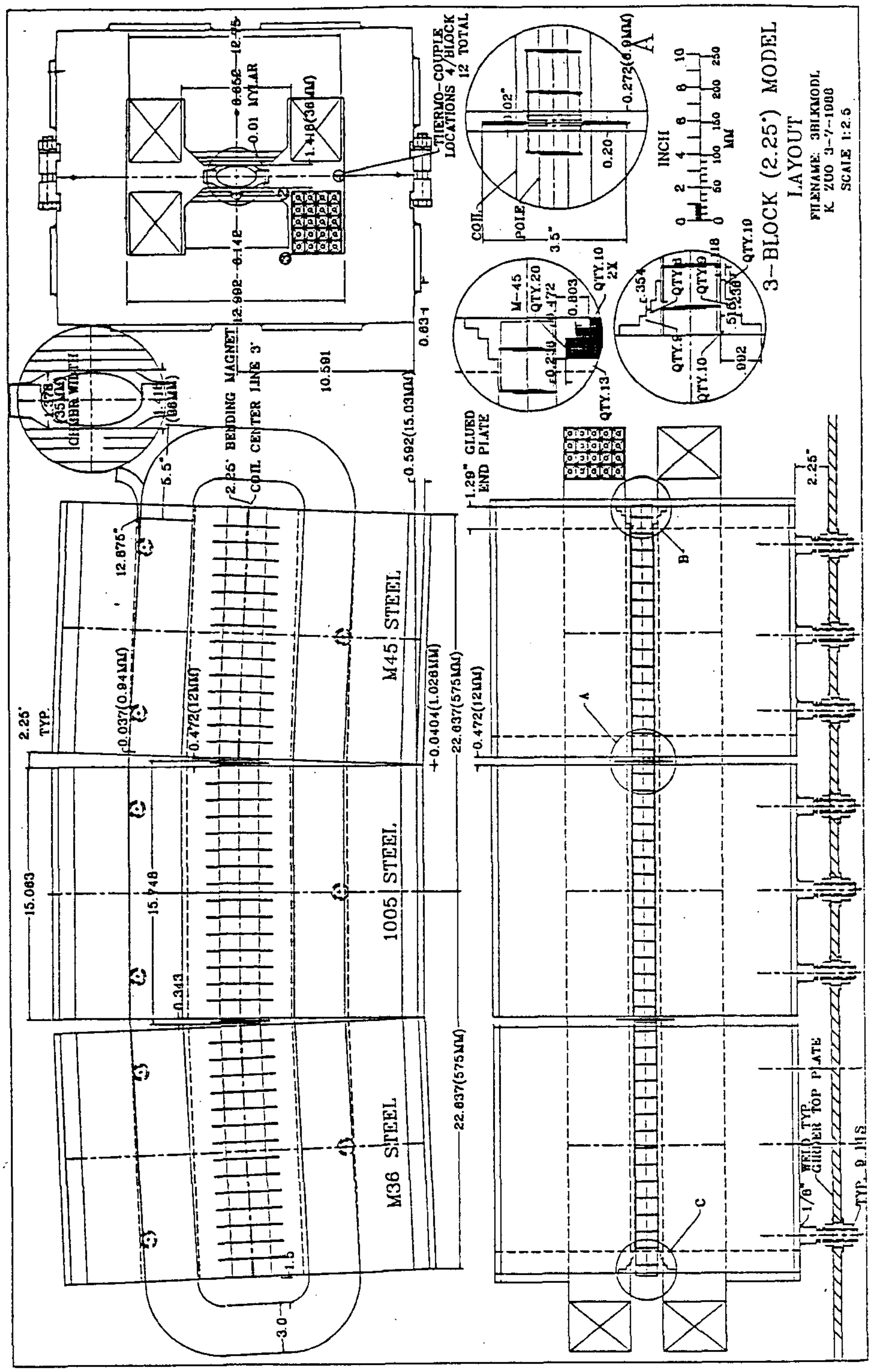

Fig. 5.1-6: Bending Magnet 3-Block Model

5.1.2 Quadrupole Magnets

The focusing is performed by 40 quadrupoles, 20 each QF and QD. While their cross section is the same, Figure 5.1-7, they have different mechanical length with the QF and the QD being 0.35 m and 0.27 m long respectively. To avoid eddy currents these magnets also are constructed from silicon steel laminations like the bending magnets. The two families of quadrupoles, the QF's and the QD's, form one electrical circuit. The strength of the two quadrupole types are:

$$QF : k = -1.33060\ m^{-2} \quad \text{or for } 3.0GeV : \quad g = 1.3315\ kGauss/cm$$
$$QD : k = 1.30595\ m^{-2} \quad \text{or for } 3.0GeV : \quad g = 1.3068\ kGauss/cm$$

The specifications of the quadrupoles is compiled in Table 5.1-2.

Table 5.1-2: Quadrupole Specifications @ 3 GeV

Magnet Name in Lattice	QD	QF
Magnet Designation	60 QD270	30 QF350
Beam Energy (GeV)	3.0	3.0
Field Gradient at 3.0 GeV (kG/cm)	1.3068	1.3315
Field Gradient @ Injection (120 MeV)(kG/cm)	.0523	.05328
Field Gradient (kG/cm)	2.4	2.4
Field at Pole Tip 3 GeV (kG)	3.92	4.0
Magnetic Length (mm)	300	380
Core Length (mm)	270	350
Overall Length (mm)	430	510
Overall Width (mm)	490	490
Overall Height (mm)	490	490
Overall Weight (mm)	130	162
Good Field Region (mm)	32 high x 60 wide	
Max. Beam Width (mm)	11	31
Max. Beam Height (mm)	22	7
Magnet Efficiency at 8.35 kG (%)	> 95	> 95
Current (Amps)	600	600

Table 5.1-2: Quadrupole Specifications @ 3 GeV (con't)

Magnet Name in Lattice	QD	QF
Ampere Turns	4800/Pole	4800/Pole
Max. Voltage Drop/Coil @ 10Hz (V)	14.7	18.6
Magnet Resistance @ 37° C (m ohm)	3.4	3.9
Magnet Inductance/Coil (mH)	0.8	1.0
Magnet Time Constant L/R (sec)	0.23	0.25
Total Power Loss @ 10Hz (kW)	0.86	0.97
Driving Current Loss (kW)	0.45	0.53
Coil Eddy Loss at 10 Hz (kW)	0.05	0.054
Core Loss (Eddy&Hyst) @10Hz. (kW)	0.007	0.008
Stored Energy (kJ)	0.14	0.18
No. Turns/Coil	8	8
No. Coils/Magnet	4	4
Current Density (A/mm^2)	2.24	2.24
Conductor Dimensions (mm)	18.2x18.2 w/8.9 D Hole	
Conductor Material	Aluminum	Aluminum
Conductor X-Section Area (mm^2)	269.03	269.03
Length/Coil (m)	7.518	8.788
Weight/Coil (kg)	6.43	7.65
Cooling Circuits/Coil	2	2
Water Flowrate (GPM)	1.0	1.0
Pressure Drop/Magnet (psi)	60	60
Temperature Rise in Coil (deg. C°)	20	20
Core Material (kg)	Silicon Steel (M-36)	
Steel Core Weight (kg)	94.2	122
Fabrication Technique	Laminated 4 pieces	
Lamination Thickness (mm)	.625 (.0246")	.625 (.0246")
Laminations/Magnet	436 x 4	565 x 4
Magnet Steel Length (mm)	270	350
Interlaminate Pressure (psi)	60	60

The calculated saturation characteristics for the quadrupoles are shown in Figure 5.1-8 where the permeability is plotted across the magnet for a field gradient of 2.0 kGauss/cm. Obviously there is little saturation for beam energies up to 3.0 GeV.

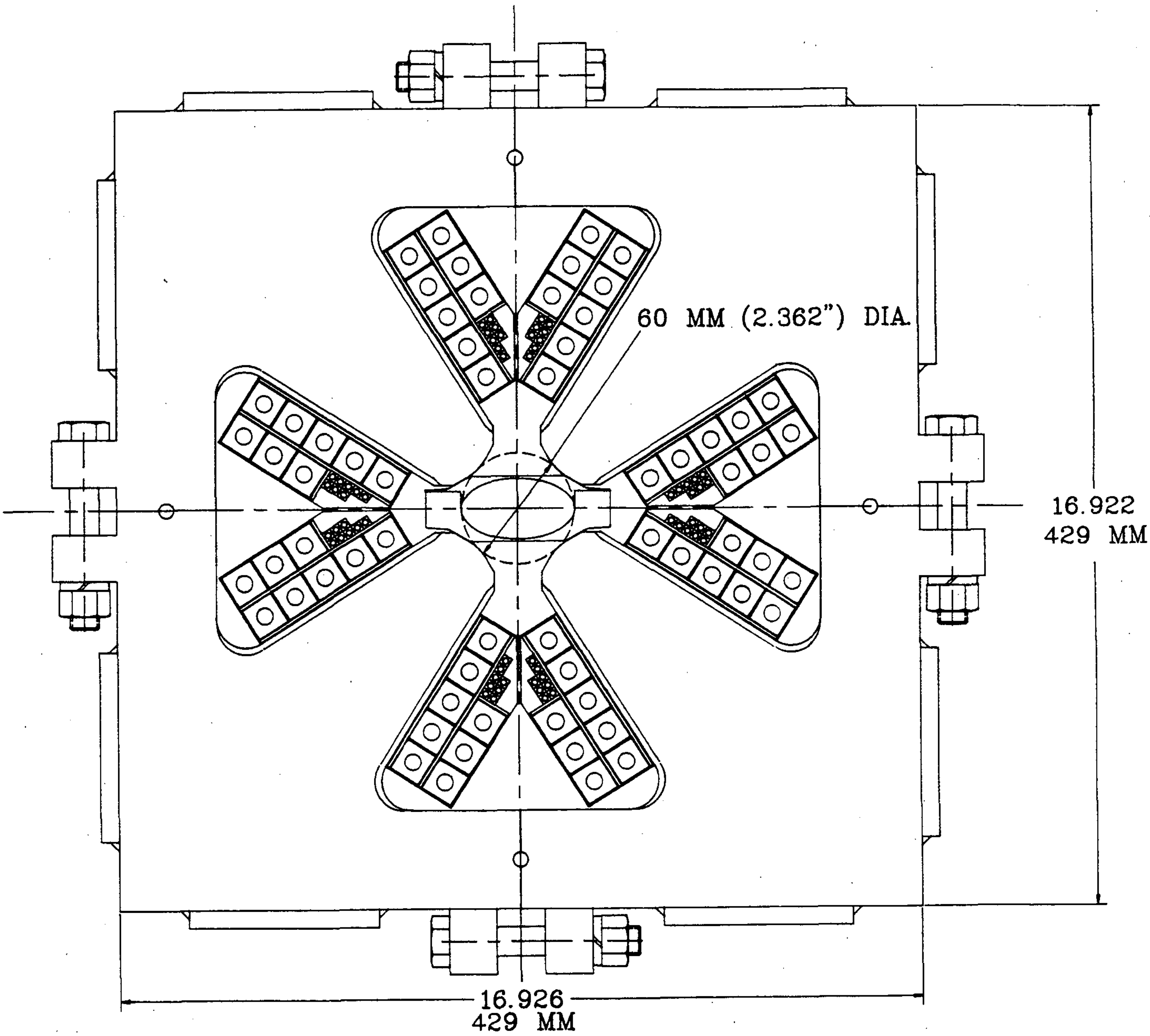

Fig. 5.1-7: Quadrupole Magnet

PERMEABILITY MAP.

DISTANCE BETWEEN COLUMNS = 10.00MM
DISTANCE BETWEEN ROWS = 5.00MM

0	0	0	0	0	0	0	0	0	0	0	0	0	0	0	0	0	0	0
0	0	0	0	0	2000	2000	0	0	0	0	0	0	0	0	0	0	0	0
0	0	0	0	0	2000	2002	0	0	0	0	0	0	0	0	0	0	0	0
0	0	0	0	2099	2041	2063	2166	0	0	0	0	0	0	0	0	0	0	0
0	0	0	0	2178	2131	2152	2245	0	0	0	0	0	0	0	0	0	0	0
0	0	0	0	2267	2230	2257	2346	2502	0	0	0	0	0	0	0	0	0	0
0	0	0	2437	2369	2348	2381	2465	2619	0	0	0	0	0	0	0	0	0	0
0	0	0	2534	2462	2481	2527	2619	2759	2978	0	0	0	0	0	0	0	0	0
0	0	2691	2637	2621	2646	2710	2804	2932	3077	0	0	0	0	0	0	0	0	0
0	0	2758	2751	2793	2851	2931	3018	3078	3078	3078	0	0	0	0	0	0	0	0
0	0	2828	2889	2977	3071	3078	3078	3078	3078	3078	0	0	0	0	0	0	0	0
0	2797	2910	3040	3078	3078	3078	3078	3078	3078	3078	3078	0	0	0	0	0	0	0
0	2791	3006	3078	3078	3078	3078	3078	3078	3078	3078	3078	0	0	0	0	0	0	0
2462	2825	3078	3078	3078	3078	3078	3078	3078	3078	3078	3078	3078	0	0	0	0	0	0
2540	2914	3078	3079	3078	3078	3078	3078	3078	3078	3078	3078	3078	0	0	0	0	0	0
2742	3034	3078	3078	3078	3078	3078	3078	3078	3078	3078	3078	3078	3078	0	0	0	0	0
2945	3078	3078	3078	3078	2663	0	0	3077	3078	3078	3078	3078	3078	0	0	0	0	0
3077	3078	3078	3078	3078	0	0	0	0	3078	3078	3078	3078	3078	3078	0	0	0	0
3078	3078	3078	3078	2961	0	0	0	0	0	3078	3078	3078	3078	3078	0	0	0	0
3078	3078	3078	3078	3078	0	0	0	0	0	3078	3078	3078	3078	3078	3078	0	0	0
3078	3078	3078	3078	3078	0	0	0	0	0	0	3078	3078	3078	3078	3078	0	0	0
3078	3078	3078	3078	3078	0	0	0	0	0	0	0	3078	3078	3078	3078	3078	0	0
3078	3078	3078	3078	3078	0	0	0	0	0	0	0	0	3078	3078	3078	3078	0	0
3078	3078	3078	3078	3078	0	0	0	0	0	0	0	0	3078	3078	3078	3078	3078	0
3078	3078	3078	3078	3078	0	0	0	0	0	0	0	0	0	3078	3078	3078	3077	0
3078	3078	3078	3078	3078	0	0	0	0	0	0	0	0	0	0	3078	3078	3078	2363
3078	3078	3078	3078	3078	0	0	0	0	0	0	0	0	0	0	3078	3078	3078	2336
3078	3078	3078	3078	3078	0	0	0	0	0	0	0	0	0	0	0	3078	3078	0
3078	3078	3078	3078	3078	0	0	0	0	0	0	0	0	0	0	0	0	0	0
3078	3078	3078	3078	3078	0	0	0	0	0	0	0	0	0	0	0	0	0	0
3078	3078	3078	3078	3078	0	0	0	0	0	0	0	0	0	0	0	0	0	0

Fig. 5.1-8: Saturation Characteristics for the Quadrupoles

5.1.3 Sextupole Magnets

Chromatic correction requires 12 each SF and SD sextupoles with a magnetic length of 0.0858 m. To avoid eddy currents these magnets are constructed from silicon steel lamination. The specifications of the sextupoles are compiled in Table 5.1-3. The sextupole cross section is shown in Figure 5.1-9 and the saturation characteristics in Figure 5.1-10.

Table 5.1-3: Sextupole Specifications

Magnet Name in Lattice	S
Magnet Designation	70 S 50.8
Beam Energy (GeV)	3.0
Field Gradient at 3.0 GeV (kG/cm^2)	.24
Field Gradient at Injection (120 MeV) (kG/cm^2)	.004
Field Gradient (kG/cm^2)	0.4
Field at Pole Tip 3 GeV (kG)	1.47
Magnetic Length (mm)	85.8
Overall Length (mm)	90
Overall Width (mm)	320
Overall Height (mm)	370
Overall Weight (mm)	22.5
Good Field Region (mm)	32 high x 60 wide
Max. Beam Width (mm)	31
Max. Beam Height (mm)	22
Magnet Efficiency at 8.35 kG (%)	> 98
Current (Amps)	160.8
Ampere Turns	1447/Pole
Max. Voltage Drop/Coil at 10 Hz. (V)	4.2
Magnet Resistance at 37° C (m ohm)	0.8
Magnet Inductance/Coil (mH)	0.41
Coil Time Constant L/R per Coil (sec)	0.5

Table 5.1-3: Sextupole Specifications (con't)

Total Power Loss at 10 Hz (kW)	6.0
Driving Current Loss (kW)	4.0
Coil Eddy Loss at 10 Hz (kW)	1.0
Core Loss (Eddy & Hyst) at 10 Hz. (kW)	1.0
Stored Energy (J)	52
No. Turns/Coil	9
No. Coils/Magnet	6
Current Density (A/mm^2)	5.33
Conductor Dimensions (mm)	6.48 x 6.48 w/.318 D Hole
Conductor Material	Copper
Conductor X-Section Area (mm^2)	30
Length/Coil (m)	2.0
Weight/Coil (kg)	.945
Cooling Circuits/Coil	1
Water Flowrate (GPM)	0.51
Pressure Drop/Magnet (psi)	50
Temperature Rise in Coil (deg. C)	20
Core Material (kg)	Silicon Steel (M-36)
Steel Core Weight (kg)	20
Fabrication Technique	Laminated 2 pieces
Lamination Thickness (mm)	.625 (.0246")
Laminations/Magnet	82 x 2
Magnet Steel Length (mm)	50.8
Interlaminate Pressure (psi)	60

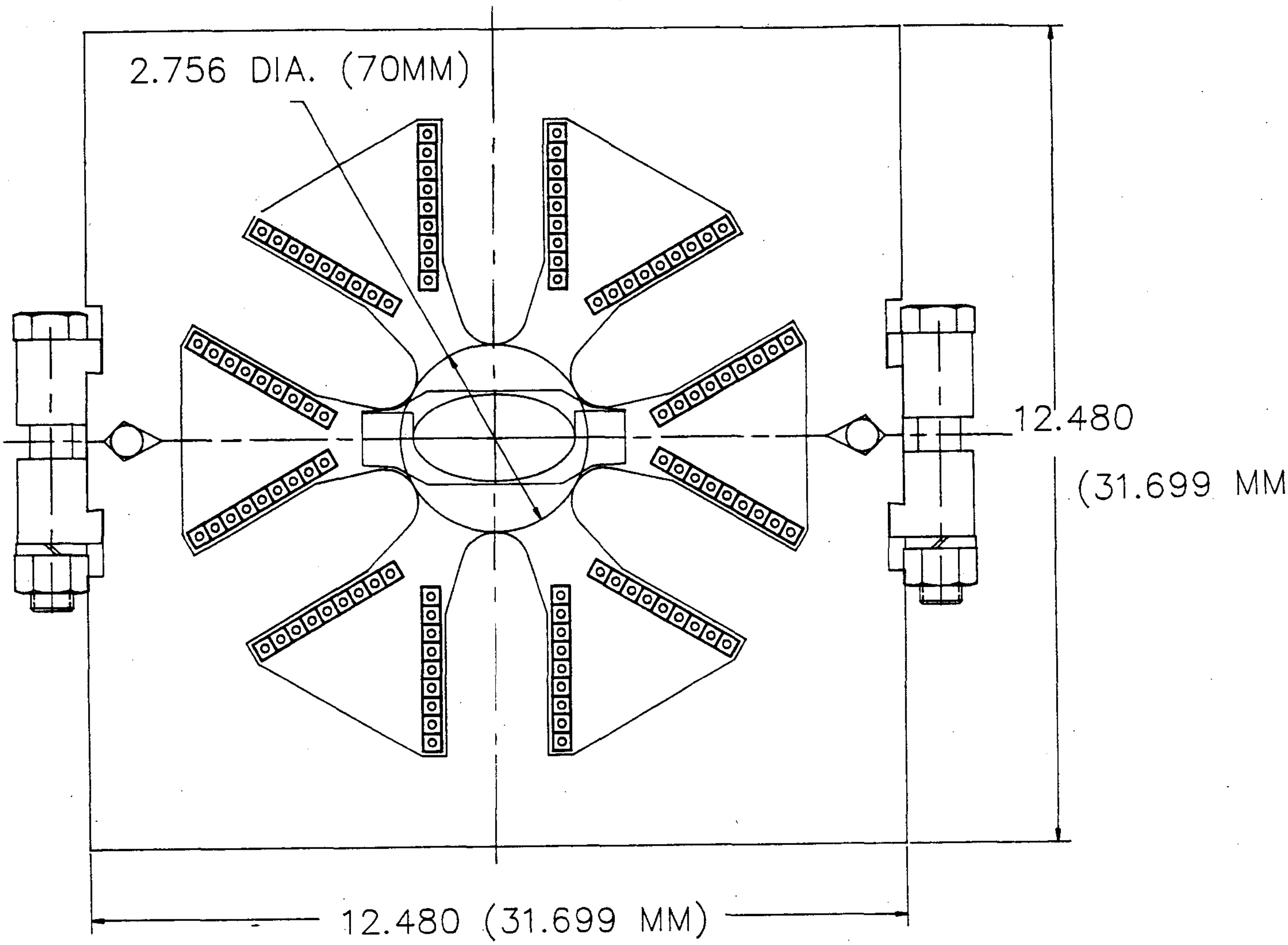

Fig. 5.1-9: Sextupole Magnet

PERMEABILITY MAP.

DISTANCE BETWEEN COLUMNS = 10.00MM (= 2 TIMES H)
DISTANCE BETWEEN ROWS = 5.00MM (= 1 TIMES H)

1903	1910	1918	1926	1934	1943	1952	1972	2010	2045	2073	2087	2075	2021	1949	1918
1905	1911	1918	1926	1934	1943	1952	1973	2012	2047	2076	2093	2085	2036	1954	1928
1909	1913	1919	1927	1935	1944	1953	1977	2015	2052	2083	2106	2108	2073	1988	1944
1912	1915	1921	1928	1936	1945	1954	1982	2021	2059	2094	2125	2145	2134	2063	1985
1915	1918	1923	1930	1938	1947	1956	1989	2029	2068	2107	2149	2192	2206	2161	2089
1918	1920	1925	1932	1940	1949	1959	1999	2039	2078	2122	2174	2184	2119	2153	2199
1921	1923	1928	1934	1942	1951	1970	2010	2049	2089	2135	2198	2142	2058	2113	2098
1923	1926	1930	1937	1945	1954	1984	2024	2061	2100	2147	2205	2107	2693	2929	2130
1925	1928	1933	1940	1948	1959	2001	2040	2075	2110	2156	2198	2087	2910	3144	2742
1927	1930	1935	1943	1952	1977	2022	2059	2089	2119	2160	2199	2082	0	3047	2885
1928	1931	1937	1946	1956	2002	2049	2082	2105	2126	2158	2203	0	0	3009	2926
1929	1932	1939	1949	1973	2033	2083	2110	2121	2130	2153	0	0	0	2998	2949
1928	1933	1941	1953	2001	2073	2128	2142	2137	2131	0	0	0	0	2997	2960
1927	1932	1943	1958	2036	2127	2187	2181	2152	0	0	0	0	0	2992	2962
1924	1931	1944	1976	2080	2201	2163	2198	2162	0	0	0	0	0	2985	2958
1920	1930	1946	2001	2136	2135	2031	2164	0	0	0	0	0	0	2976	2948
1915	1929	1948	2029	2195	2043	2813	0	0	0	0	0	0	0	2964	2932
1910	1928	1951	2060	2178	2961	0	0	0	0	0	0	0	0	2951	2911
1910	1930	1957	2096	2141	2832	3072	0	0	0	0	0	0	0	2935	2882
1918	1936	1982	2144	2101	2618	2993	2981	0	0	0	0	0	0	2917	2843
1930	1946	2030	2200	2050	2581	2932	2968	2984	0	0	0	0	0	2899	2669
1943	1962	2094	2141	2255	2754	2913	2952	2967	2974	0	0	0	0	2874	2345
1962	2024	2170	2031	2870	2878	2919	2943	2949	2952	0	0	0	0	2778	2025
2023	2094	2183	2619	3072	2952	2938	2940	2934	2923	2920	0	0	0	2005	2063
2087	2160	2129	3026	3188	3002	2957	2941	2922	2895	2873	2863	0	0	2099	2131
2146	2205	2104	2815	0	3016	2972	2946	2915	2869	2800	2627	2222	0	0	2199
2196	2179	2094	2283	0	0	2981	2954	2915	2852	2543	2208	2043	0	0	0
2190	2158	2093	2004	0	0	0	2964	2924	2851	2379	2015	2105	0	0	0
2167	2143	2097	2048	0	0	0	0	2943	2867	2334	2046	2159	0	0	0
2150	2133	2101	2071	0	0	0	0	0	2898	2403	2071	2207	0	0	0
2139	2126	2104	2083	0	0	0	0	0	2934	2596	2091	2201	0	0	0
2132	2122	2106	2090	0	0	0	0	0	0	2824	2097	0	0	0	0
2128	2120	2107	2095	0	0	0	0	0	0	0	0	0	0	0	0
2127	2120	2108	2101	0	0	0	0	0	0	0	0	0	0	0	0

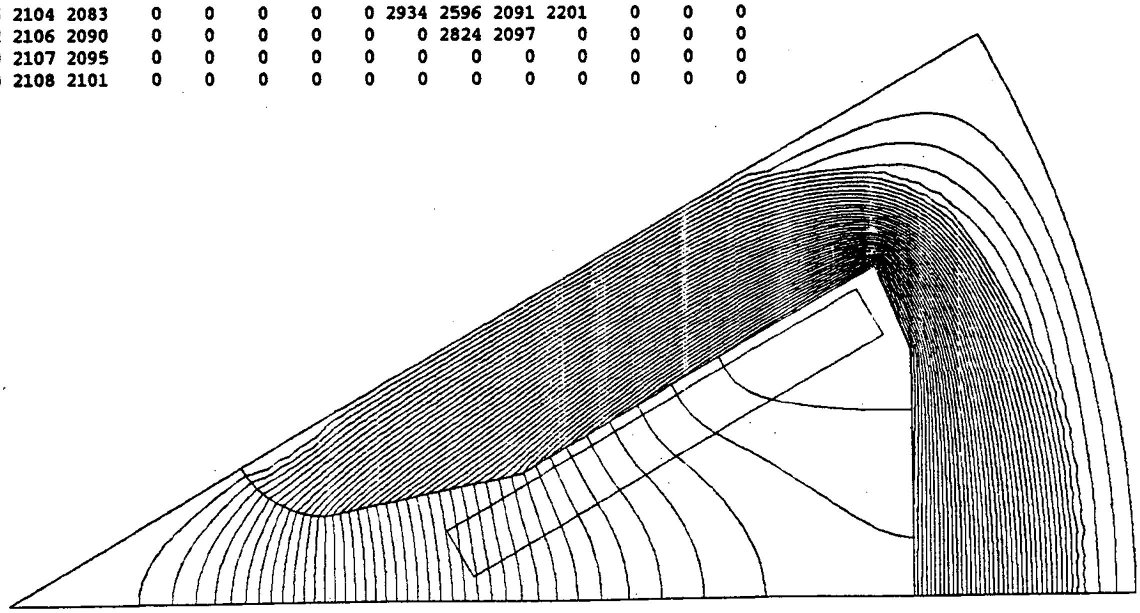

Fig. 5.1-10: Saturation Characteristics in 1/12 Sextupole

5.1.4 Special Magnets

Most magnetic fields used for orbit correction will be generated by trim coils in bending magnets and quadrupoles. They will be powered by independent, DC power supplies With trim coils in time-varying fields, like for the bending and quadrupole magnets, a significant voltage is induced in each trim coil which is too large for the small power supplies. Hence the alternating voltage must be removed from each correction circuit. To accomplish this a special arrangement of corrector trim coils is employed to allow the compensation of the induced currents. This scheme is described in more detail in the power supply section 5.5.

5.1.5 Summary of Ring Magnet System

Table 5.1-4: Ring Magnet Parameters

Ring Circumference (m)			133.64	
Magnet Name	Bend	QD/QF	SD/SF	Total
Cycling Frequency	10	10	10	10
No. Magnets in Ring (133m)	32	20/20	12/12	96
Weight/magnet (kg)	3240	2600/3240	540	7020
Electrical Circuit	White	White	Series	5
Current (Amps)	600	600	161	
Total Resistance (m ohm)	845	74/87	14.4/14.4	
Total Inductance (mH)	749	15.6/19.8	4.9/4.9	
Power Loss @ 10 Hz (kW)	129	11/13	0.1/0.1	
Magnetic Ring Packing Fraction (%)				68.36

5.2 Supports

Each girder is supported at both ends by pedestals which are shared between girders and the magnets are fixed to the girder. Specific attention is given to vibrational problems in connection with the alternating excitation of the magnets up to 10 or 15 Hz. The construction of the girders will therefore be done in such a way as to avoid eigenfrequencies below the excitation frequency of the magnets. A girder assembly is shown is Figure 5.2-1 and the girder specifications are compiled in Table 5.2-1.

Table 5.2-1: Support Specifications

No. Girders in Ring	40
No. Pedestals in Ring	40
No. Water Manifolds	80
Earthquake Design	0.75 g All directions

Weight Girder	=	1,060 lbs.
Weight 5-Block Core (1340 × 5)	=	6,525 lbs.
Weight 5-Block Coil (222 × 2)	=	444 lbs.
Weight Quad. (Core + Coil) 280 + 15(4)	=	340 lbs.
Weight Sext. (Core + Coil)	=	80 lbs.
Magnet Support Hardware	=	100 lbs.
Vacuum Chamber and Pump	=	300 lbs.
Water Manifold	=	100 lbs.
Buss Bars	=	120 lbs.
Subtotal	=	9,069 lbs.
Pedestal x 2	=	600 lbs.
Weight Distribution: Total Girder + Pedestals	=	9,669 lbs.

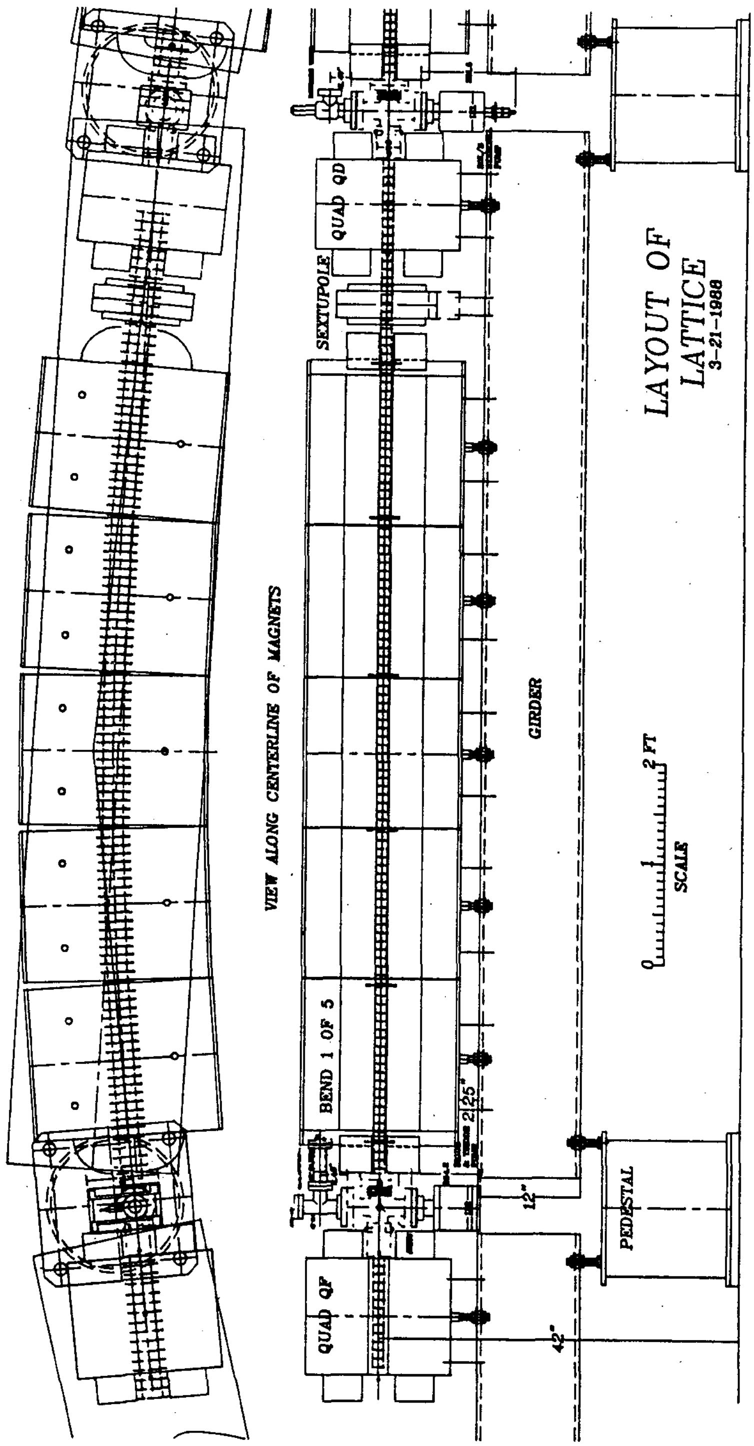

Fig. 5.2-1: Magnet Girder Assembly

Vibration Analysis

It is important that the cycling of the magnets does not mechanically disturb the support structure. For this reason the natural frequency of the support structure must be higher than the magnet cycling rate or less than 1 Hz. Two prototypes of magnet girders have been constructed to study these and other features. Specifically the vibrational behavior has been measured and the results are given in Table 5.2-2:

Table 5.2-2: Mechanical Specifications

Girder Natural Frequency	23 Hz
Magnet Natural Frequency	TBD
System Natural Frequency	TBD

5.3 Magnet Cooling System

Two-high (200 psig) pressure 2 inch diameter supply and return headers will incircle the ring providing Magnet Cooling Water. These headers will be in the housing with valves every 20 feet to connect to hoses. The headers will be made of copper. The differential pressure between the supply and return header will be less than or equal to 130 psi. The total flow in this subsystem will be 80 gpm. Temperature will be held within 12 degrees F of setpoint. Setpoint is assumed to be at least 85 degrees F. Some of the relevant Cooling system parameters are compiled in Table 5.3-1:

Table 5.3-1: Cooling System Parameters

Total Flow Water (GPM)	80
Magnet System Pressure Drop (Psi)	130
Magnet Supply Pressure (Psi)	200
System Return Pressure (Psi)	70
Power to Remove (kW)	288
Temperature Rise Max. (deg. C)	20
Temperature Variation (± deg C)	12
Water Supply	LCW
No. Cooling Circuits in Ring	2
No. Cooling Circuits per magnet	one for all magnets

5.4 Alignment System

The magnets are preassembled and prealigned to the girder with a precision of better than ± 0.3 mm before installation of the whole girder assembly in the ring shielding enclosure. A girder/magnet assembly is then installed on the pre-positioned pedestal and the girder is aligned to the final tolerance with the quadrupoles as reference. The alignment tolerances are summarized in Table 5.4-1

Table 5.4-1: Alignment System Specifications

Pedestal Alignment Tolerance	6 mm
Girder Ring Alignment	2 mm
Girder Final Alignment	.3 mm
Magnet Alignment	.3 mm
Pedestal Movement	fixed
Girder Movement	± 30 mm (x,y,z)

5.5 Magnet Power Supply System

To accelerate particles from an injection energy of 120 MeV to an extraction energy of 3 GeV, the field strengths of the booster lattice magnets and their driving currents be ramped in magnitude by a factor of 30. The inductances of the magnets convert this current surge to a reactive power load proportional to ramp frequency for power sources connected directly to them. For example, the reactive power load generated by ramping 32 dipole magnets, 23.4 mH per magnet, at a 2 Hz rate to their 3 GeV level is 1.7 MVAr. The consequent current surging on the 12.47 kV booster mains system would cause a degree of voltage fluctuation on the feeder lines (¿0.5%) that could adversely affect the performance of accelerator and storage ring electrical systems at SLAC.[1]

A resonant network power system (White circuit,[2]) will be implemented for the dipole magnets to achieve a high level of power load isolation during booster operation. Even though the reactive power load for the quadrupole QD and QF circuits is an order of magnitude lower than that for the dipole circuit, White circuits will also be configured for each of them to minimize the effects of booster ramping on other powered systems. The principal advantages of the White circuit are that

1) the resonant network transforms the impedance seen by the power supply to a purely real (resistive) one and the supply simply acts to restore real power dissipated by the circuit elements; and
2) the energizing current has the biased sine waveform that has been repeatedly demonstrated to be highly suitable for booster synchrotron operation.[3],[4]

The power requirements and inductances of the sextupole magnets are low enough to permit them to be driven directly from programmable power supplies.

5.5.1 Bending Magnet Power Circuit

The White circuit configuration planned for the dipole magnets is shown in Fig 5.5-1 and its electrical parameters are listed in Table 5.5-1. A 16 cell configuration was chosen to limit the maximum DC plus induced AC voltage level to less than 1 kV during 10 Hz, 3 GeV operation. The number of cells can be reduced to 8 if twice the maximum voltage level can be tolerated or if the dipole coil design is altered to reduce the magnet inductance. The current, voltage, and energy storage waveforms for each cell are shown in Fig. 5.5-2.

A distributed choke system, where the individual choke for each resonant cell is located underneath an appropriate magnet girder in the ring, was chosen over a centrally located choke system to reduce the amount of high current bussing required and to avoid having to situate and house a large and massive (tens of tons) choke structure. The dimensions of the distributed choke can be optimized to fit in the space available under the magnet girders (1.3 ft X 2.4 ft X 7 ft.[5]). The value of choke inductance is 1.7 times that of two series-connected dipoles so that the costs and volumes of the choke and its resonating capacitor are approximately equalized.[5]

The capacitor bank for each cell is composed of many individual capacitor units connected in series and/or parallel to achieve the capcitance and energy storage requirements for each cell. To minimize the fluctuation of capacitance with temperature change, polypropylene capacitors or capacitors with an equivalent temperature coefficient will be used. Trimmer capacitors can be remotely switched in and out to compensate for drifts in cell frequency. Groups of capacitors within each cell bank will be fused in a way that prevents a cascading fuse-burn throughout the bank should one fuse fail. Each bank is housed in a weather-proof box (2 ft X 3 ft X 6 ft) located on top of the ring tunnel shielding directly over its respective cell magnets.

A DC bias current is applied to the circuit from a highly regulated DC power supply (0.05% or better regulation to avoid excessive current ripple at injection fields). It is expected that 12-phase SCR firing circuits for the supply will be needed to reduce the 60 Hz harmonic and subharmonic content in the current waveform to within tolerable limits.[7] A transductor unit monitors the DC current level provides feedback information for the supply regulator. The DC current level is remotely controlled and monitored by the Injector computer control system.

AC excitation of the circuit is provided via primary windings on each choke. The primary windings are all connected in parallel and coupled to the AC supply. The network coupling the supply to the choke primary coils must provide an adequate level of drive frequency and line frequency harmonic suppression.[7] It may be possible to reduce the choke size by superposing a DC current on the AC primary coil excitation current that effectively nullifies the DC component of the choke magnetic field generated by the DC secondary current. Possible candidates for AC supply configuration include a pulsed supply,[3] an inverter,[4] a cycloconverter,[7] and a pulse width modulated (PWM) chopper supply.[8]

The level of AC excitation in the magnet circuit is monitored with a transductor. The transductor and/or a calibrated field probe situated in the gap of one of the ramping dipoles will provide information for regulating the supply. The frequency of excitation is locked to the 60 Hz line frequency, and its magnitude is remotely controlled and monitored by the Injector computer control system. It is possible to use a peaking strip situated within the gap of one of the dipoles to produce a synchronizing pulse for the Injector timing system at the moment the magnetic field reaches a prescribed value.

The parallel-connected choke primary windings serve to couple and equalize the individual resonant cells,[2] thus ensuring their uniform excitation around the ring. The coupled resonator circuit warrants thorough modeling and analysis to optimize its efficiency and performance.[2],[9]

The grounding point for the DC circuit is chosen to be half way around the ring from the power feeder points so as to symmetrize the DC voltage drop from coil to ground around the ring and thereby reduce its maximum value to one half the supply voltage. The grounding point for the AC secondary system is chosen to be at the common connection point between the two series capacitors bypassing the DC supply/choke cell (Figure 5.5-1). This connection symmetrizes the AC voltage induced across the two series-connected dipoles in each cell with respect to ground, with the result that the common point of connection between the magnets remains and at ground potential and the maximum voltage to ground is one half of the induced voltage.

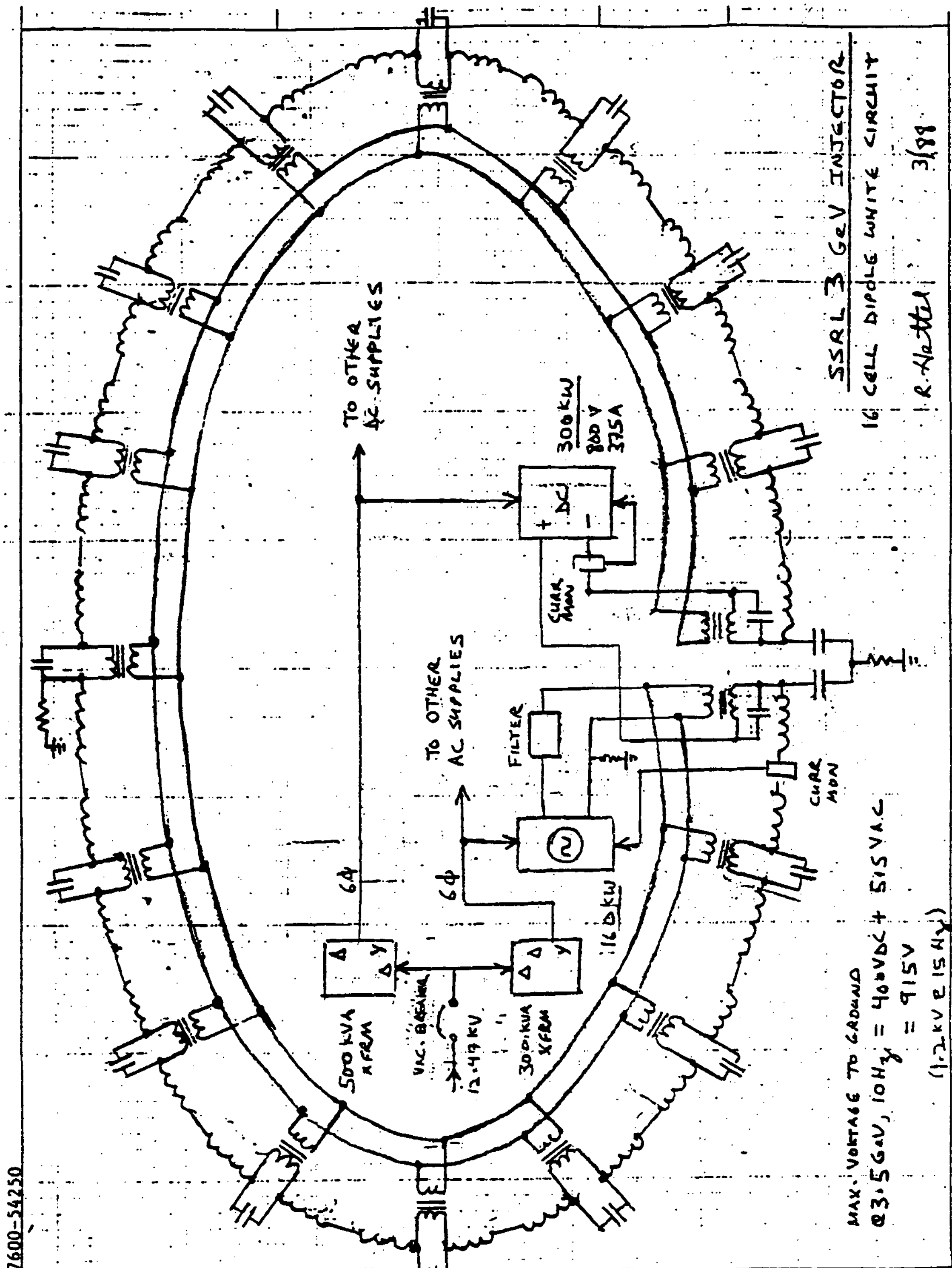

Figure 5.5-1: 16 Cell Dipole White Circuit

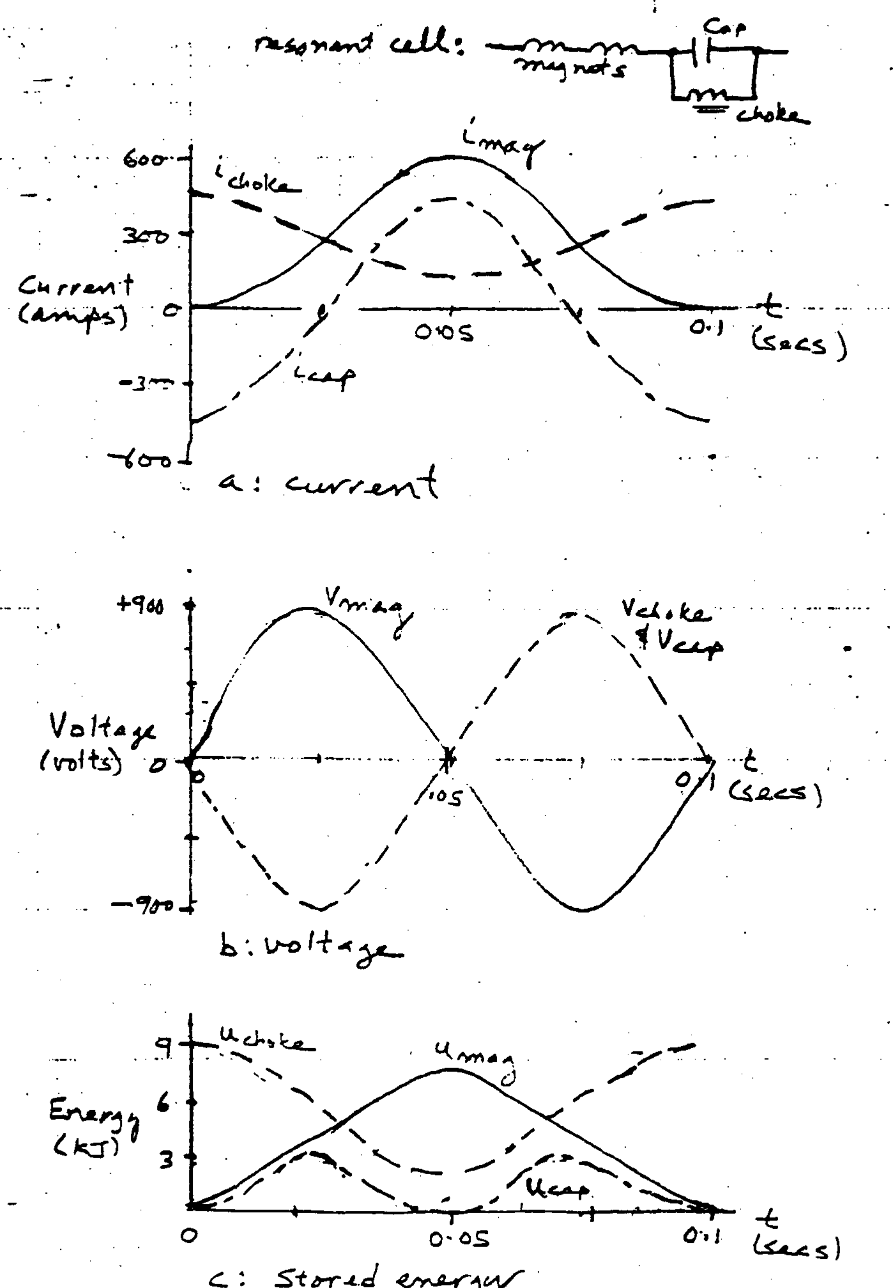

current, voltage, and energy waveforms for dipole resonant cell – 3 GeV, 10Hz

Figure 5.5-2: Waveforms of White Circuit Parameters

Table 5.5-1: Bending Magnet Power System Parameters, 3 GeV

Resonant Cell Parameters	
No. of cells	16
No. of bending magnets/cell	2
Resonant frequency	10 Hz
Inductance/cell	
Magnet	46.8 mH
Choke	79.6 mH
Resistance/cell	
Magnet	48 mohm
Choke	85 mohm
Total	133 m ohm
Capacitance/cell	8600 uF
DC current/cell	
Magnet	300 A
Choke	300 A
AC current/cell	
Magnet	± 300 A
Choke	± 176 A
Capacitor	± 476 A
DC voltage drop/cell	38 V
AC induced voltage/cell	880 V
Peak stored energy/cell	
Magnet	8.4 kJ
Choke	9.0 kJ
Capacitor	3.5 kJ
DC power dissipation/cell	
Magnet	4.3 kW
Choke	7.7 kW
Total	12.0 kW
AC power dissipation/cell	
Magnet	3.0 kW
Choke	1.5 kW
Capacitor	0.5 kW
Total	5.0 kW

Table 5.5-1: Bending Magnet Power System Parameters, 3 GeV (con't)

Total System Parameters	
DC resistance	2.34 ohm
DC voltage drop	702 V
Maximum voltage to ground	800 V
Peak current in magnets	600 A
Stored energy in circuit	145 kJ
DC power dissipation	212 kW
AC power dissipation	90 kW

The magnet current buss system in the ring is configured in conjunction with the quadrupole busses to minimize the stray magnetic fields emanating from them that could influence the accelerating beam. This is best accomplished by situating parallel busses carrying equal and opposite currents close to each other so that their induced fields effectively cancel each other.

Two separate transformers are used to supply power to the magnet power system, one for the DC supplies (dipole, quadrupole, and sextupole) and one for the AC supplies (dipole and quadrupole). The transformers are rectifier types having 3-phase primary windings and 6-phase secondary windings. The transformers have different taps that can be used to optimally match the secondary output voltages to the requirements of the supplies for a given operating energy and thus reduce the supply ripple level.

The power supplies and circuit elements are equipped with safety interlocks that prevent the accidental exposure of personnel to dangerous voltage levels. High voltage suppression and magnet discharge circuits are provided to safely dissipate the stored energy in circuit elements in the event of system failure.

5.5.2 Quadrupole Magnet Power Circuits

The inductances of the two quadrupole magnet circuits (QD and QF) permit the implementation of single cell White circuits for them as depicted in Figure 5.5-3. Technical details concerning these circuits are discussed in the previous section. Power system parameters are listed in Table 5.5.2.

The excitation current waveform for each quadrupole circuit must track the bending magnet waveform with a precision of better than 0.5% .[10] In addition it is desirable to be able to modify the quadrupole current waveforms with respect to that of the dipole to optimally tune lattice parameters as a function of ring energy. This capability enables the equalization of any mismatch in magnetic field properties between the magnet circuits that might occur as a function of ramping current level. Trimming the quadrupole field strength at any point along its excitation curve by a factor of $\pm$ 10% of the full energy value is accomplished either by modifying the choke primary drive current or by driving an auxiliary series-connected trim coil circuit for each magnet string with a lower power (10% of the main coil AC supply) current source. In either case the quadrupole excitation will be programmed within the trimming limits from the Injector control computer.

Table 5.5-2: Quadrupole Magnet Power System Parameters, 3 GeV

Resonant Cell Parameters	QD	QF
No. of Cells	1	1
No. of quad magnets/cell	20	20
Resonant frequency	10 Hz	10 Hz
Inductance/cell		
Magnet	15.6 mH	20.0 mH
Choke	26.5 mH	34.0 mH
Resistance/cell		
Magnet	73.9 mohm	86.5 mohm
Choke	65 mohm	65 mohm
Total	139 mohm	152 mohm
Capacitance/Cell	25900 uF	20200 uF
DC current/cell		
Magnet	300 A	300 A
Choke	300 A	300 A
AC current/cell		
Magnet	$\pm 300A$	$\pm 300A$
Choke	$\pm 176A$	$\pm 176A$
Capacitor	$\pm 467A$	$\pm 467A$
DC voltage drop/cell	42.0 V	45.6 V
AC induced voltage/cell	294 V	377 V
Peak Stored Energy/cell		
Magnet	2.8 kJ	3.6 kJ
Choke	3.0 kJ	3.9 kJ
Capacitor	1.1 kJ	1.4 kJ
DC Power dissipation/cell		
Magnet	6.7 kW	7.8 kW
Choke	5.9 kW	5.9 kW
Total	12.6 kW	13.7 kW
AC Power dissipation/cell		
Magnet	4.4 kW	5.3 kW
Choke	2.4 kW	2.4 kW
Capacitor	0.1 kW	0.4 kW
Total	6.9 kW	7.8 kW

Table 5.5-2: **Quadrupole Magnet Power System Parameters, 3 GeV (con't)**

Resonant Cell Parameters	**QD**	**QF**
Total System Parameters		
DC Resistance	153 mohm	167 mohm
CD voltage drop	46 V	50 V
Maximum voltage to ground	170 V	213 V
Peak current in magnets	600 A	600 A
Stored energy in circuit	3.0 kJ	3.9 kJ
DC power dissipation	13.8 kW	15.0 kW
AC power dissipation	7.6 kW	8.6 kW

Table 5.5-2: Quadrupole Magnet Power System Parameters, 3 GeV

Resonant Cell Parameters	QD	QF
No. of Cells	1	1
No. of quad magnets/cell	20	20
Resonant frequency	10 Hz	10 Hz
Inductance/cell		
Magnet	15.6 mH	20.0 mH
Choke	26.5 mH	34.0 mH
Resistance/cell		
Magnet	73.9 mohm	86.5 mohm
Choke	65 mohm	65 mohm
Total	139 mohm	152 mohm
Capacitance/cell	25900 uF	20200 uF
DC current/cell		
Magnet	300 A	300 A
Choke	300 A	300 A
AC current/cell		
Magnet	+/- 300 A	+/- 300 A
Choke	+/- 176 A	+/- 176 A
Capacitor	+/- 476 A	+/- 476 A
DC voltage drop/cell	42.0 V	45.6 V
AC induced voltage/cell	294 V	377 V
Peak stored energy/cell		
Magnet	2.8 kJ	3.6 kJ
Choke	3.0 kJ	3.9 kJ
Capacitor	1.1 kJ	1.4 kJ
DC power dissipation/cell		
Magnet	6.7 kW	7.8 kW
Choke	5.9 kW	5.9 kW
Total	12.6 kW	13.7 kW
AC power dissipation/cell		
Magnet	4.4 kW	5.3 kW
Choke	2.4 kw	2.4 kW
Capacitor	0.1 kW	0.1 kW
Total	6.9 kW	7.8 kW
Total System Parameters		
DC resistance	153 mohm	167 mohm
DC voltage drop	46 V	50 V
Maximum voltage to ground	170 V	213 V
Peak current in magnets	600 A	600 A
Stored energy in circuit	3.0 kJ	3.9 kJ
DC power dissipation	13.8 kW	15.0 kW
AC power dissipation	7.6 kW	8.6 kW

5.5.3 Sextupole Magnet Power Circuits

The power requirements and other electrical parameters for the SD and SF sextupole circuits are listed in Table 5.5-3. The circuits will be driven directly from programmable transistor trim supplies similar to those used for steering magnets. Sextupole current is remotely controlled and monitored by the Injector control computer.

Table 5.5-3: Sextupole Power Supply Parameters

	SD	SF
No. of magnets/circuit	12	12
Drive frequency	10 Hz	10 Hz
Inductance/circuit	4.9 mH	4.9 mH
Resistance/circuit	15 mohm	15 mohm
DC current	80 A	80 A
AC current	$\pm 80A$	$\pm 80A$
Peak current in magnets	160 A	160 A
DC voltage drop/circuit	1.3 V	1.3 V
AC voltage drop/circuit	$+1.5/-1.0V$	$+1.5/-1.0V$
Maximum voltage to ground	3 V	3 V
Peak stored energy/circuit	63 J	63 J
Power dissipation/circuit	150 W	150 W

5.5.4 Corrector Magnets

Horizontal orbit correction in the booster is accomplished using trim coils wound on the bending magnet cores. Following a technique employed at DESY's Doris II, each bending magnet is supplied with two sets of trim coils having an equal number of windings that can be connected in series but with opposite magnetic senses so that no net voltage is induced across them by the main coils. The common connection point between the two trim coils is then connected together with the common points of all other horizontal trim coils as shown in Figure 5.5-4. Each trim set is driven by an independent programmable power supply, controlled and monitored by the Injector control computer. The net effect of energizing a single trim set is to cause a global horizontal orbit shift without altering the beam orbit path length and beam energy. Twelve active horizontal corrector circuits are planned for the ring.

Vertical orbit correction is accomplished using separate corrector magnets situated at specific points in the ring lattice. The vertical correctors are driven with programmable supplies similar to those used for horizontal correction. Twelve vertical corrector circuits are planned for the ring.

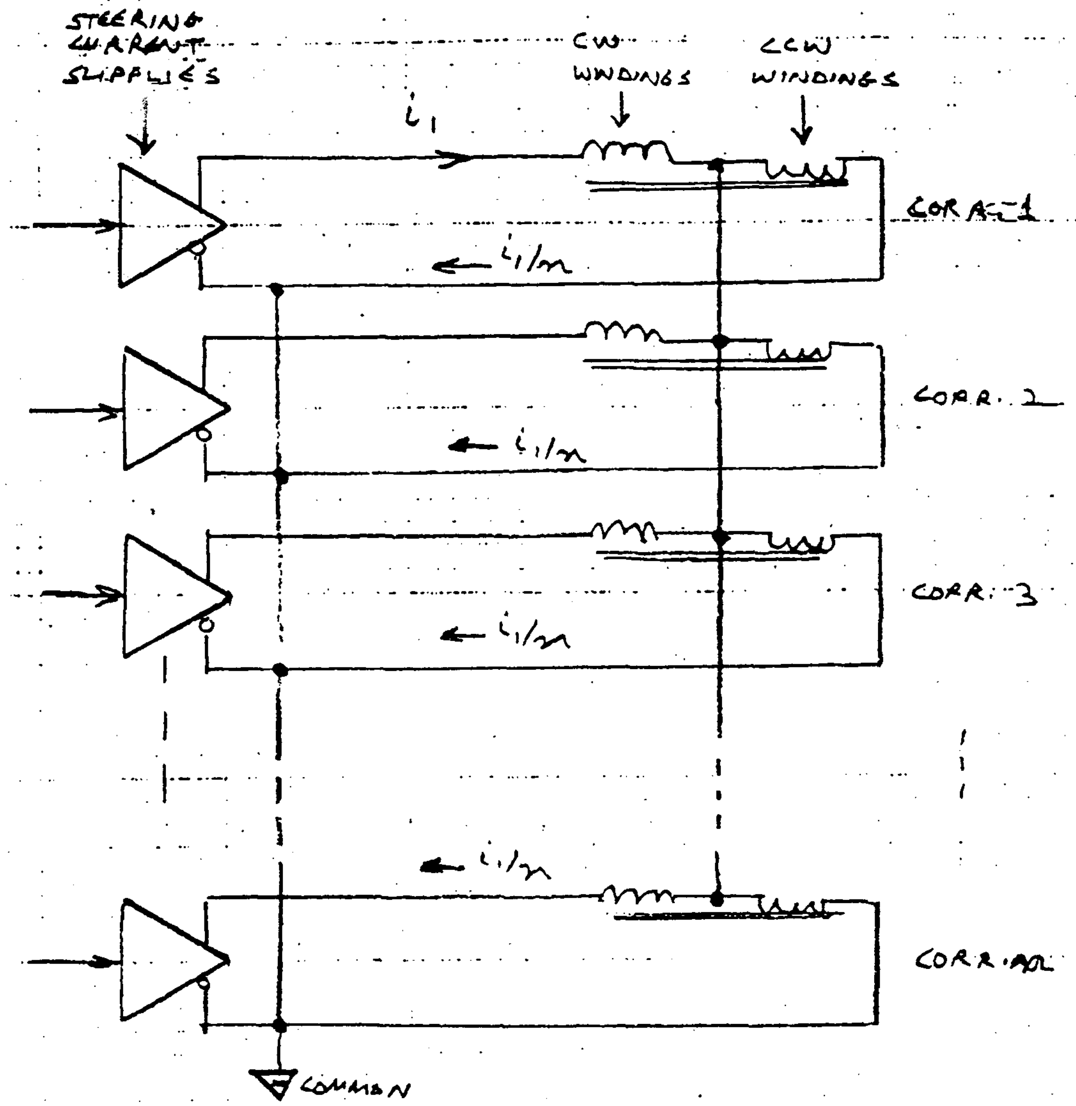

: Counterwound horizontal corrector coils on bending magnet cores nullify induced voltages from main windings. Connecting all of their center taps together results in orbit corrections that do not affect orbit path length.

Figure 5.5-4: Induced Voltage Compensation in Trim Coils

5.5.5 References

1. R. Hettel, "SSRL 3 GeV Injector - 2 Hz Power Requirements", tech. note, 2/16/88; and M. Machicao, "SSRL 2 Hz Filter", tech. note, 2/88.
2. S. Waaben, "Synchrotron Magnet Power Circuit with a Distributed Capacitor Bank", Nucl. Instr. and Meth. 9 (1960) 78-86.
3. "Cambridge Electron Accelerator: A Comprehensive Account", CEAL-1000, 3/1/1964.
4. J. Lyall, "Daresbury SRS Booster Magnet Power Supply", Proc. 6th Intl. Conf. on Magnet Technology, Bratislava 1977, p. 934-937.
5. R. Hettel, tech. note choke design, 3/88.
6. N. Marks, "Examination of Dipole Magnet Power Supplies for the ESRF Booster Synchrotron, Part I", ESRF-SYN-86-04, Aug. 5, 1985.
7. W. Bothe and P. Pillat, "Magnet Excitation Circuits for DESY II", IEEE Trans. Nucl. Sci, NS-32, No. 5, Oct. 1985.
8. L.T. Jackson and W. Flood, "Hardware Implementation and Test Results of PEP Chopper Magnet Power Supply System", IEEE Trans. Nucl. Sci., NS-26, No. 3, June 1979.
9. J. Dinkel, "Transmission Line Mode Damping in the Booster Magnet Supply", TM-201, 0323, Fermilab (FNAL), Jan. 9, 1970.
10. H. Wiedemann, private communication.

5.6 Magnetic Measurements

The magnet measurement program is divided into three phases:

Phase 1 consists of measurement of engineering model magnets to evaluate initial concepts and design parameters. Development of measurement techniques and evaluation of measurement equipment and software for later phases will also take place during this phase.

Phase 2 will consist of measurements on prototype magnets to validate design and establish performance criteria for production magnets.

Phase 3 will consist of making quality control measurements of production magnets prior to final assembly of the synchrotron.

Phase 1 activities are underway for the main bending magnets. Some design issues being evaluated are:

CORE MATERIAL SELECTION;

CORE LAMINATION THICKNESS;

CORE STACKING AND CLAMPING TECHNIQUES;

EFFECTS OF MANUFACTURING AND ALIGNMENT ERRORS;

POLE PROFILE;

MAGNET END SHAPE;

EDDY CURRENT LOSSES IN CORE, COIL, AND VACUUM CHAMBER;

HYSTERESIS EFFECTS AND LOW FIELD PERFORMANCE;

COIL DESIGN AND POWER SUPPLIES DESIGN CONCEPTS;

The graphs on the following pages show results of d.c. field measurements made on three bend magnet core blocks made from different materials and with differing pole end profiles. The measurements were made separately on the individual blocks. The data was taken using a F.W. Bell Model 640 gaussmeter attached to a model HTB-8-0608 Hall probe.

Figure 5.6-1 is a plot of the excitation curves of the three different block materials.

Figure 5.6-2 is a plot of the field in the gap of the M-45 block vs transverse position for different excitation levels. It illustrates the effect of shims which have been designed into the pole faces.

Figure 5.6-3 shows the longitudinal fringe field distribution for a rectangular as well as for an approximation of a Rogowski end pole profile. In the final magnet designs a Rogowski end pole configuration may be employed to minimize the eddy current heating effects there.

The three blocks have been assembled into an array with the same configuration as the completed five block ring magnet and with the capability of cycling the field sinusoidally.

Flux coils have been fabricated with which to measure the a.c. properties of the individual blocks as well as the field integral of the assembly and effects of vacuum chambers.

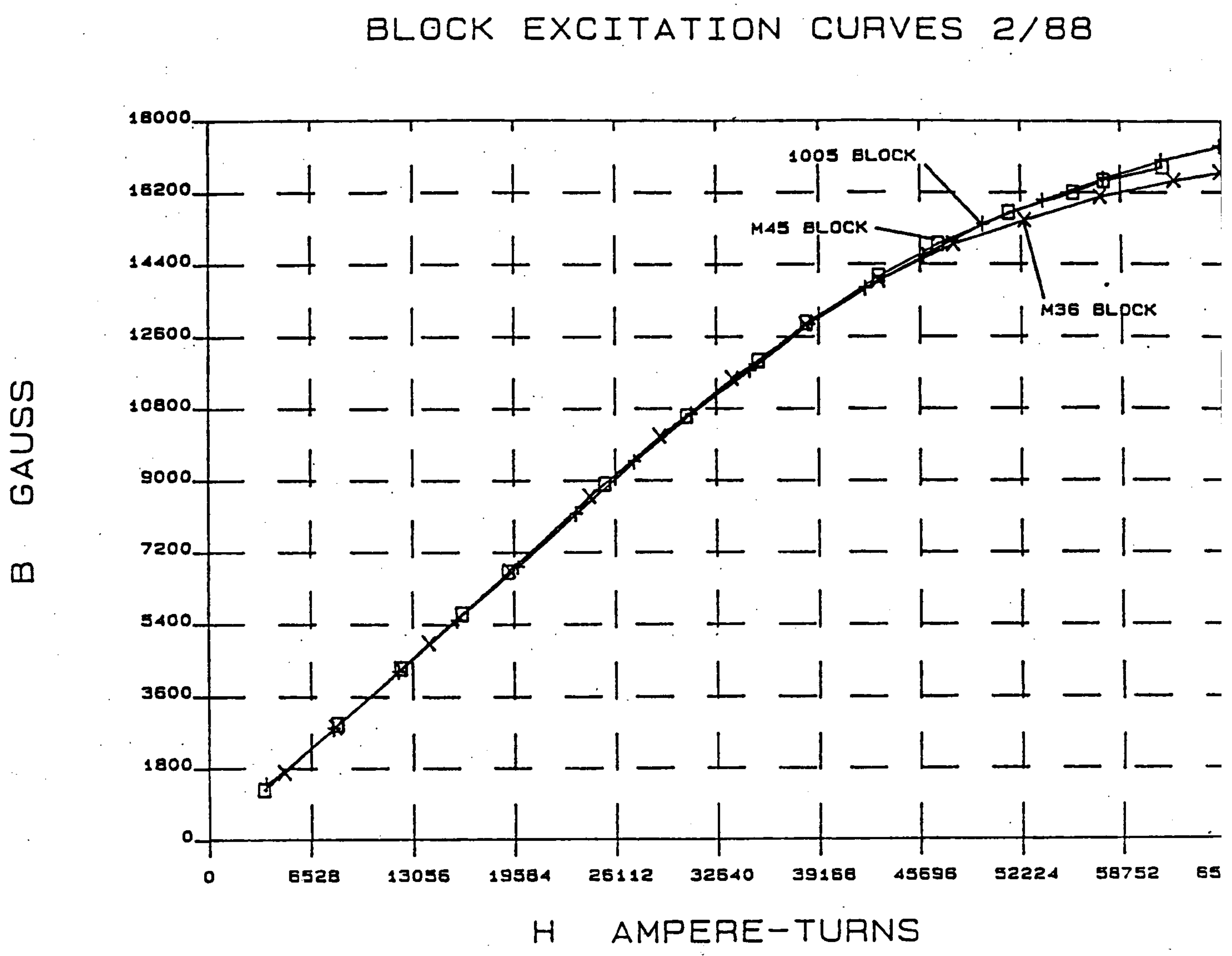

Figure 5.6-1: Excitation Curves for Single Bending Magnet Prototypes

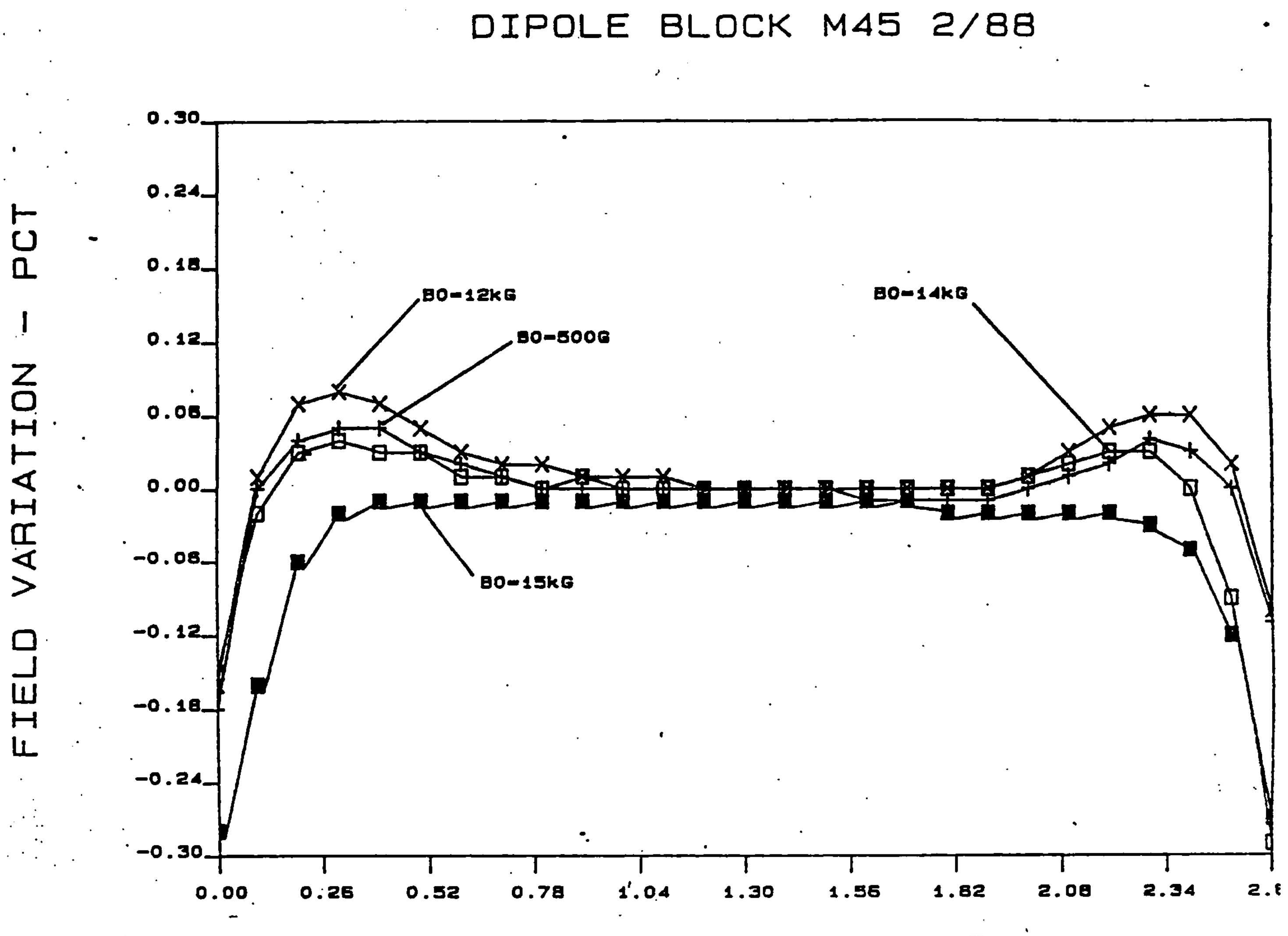

Figure 5.6-2: Transverse Field Distributions

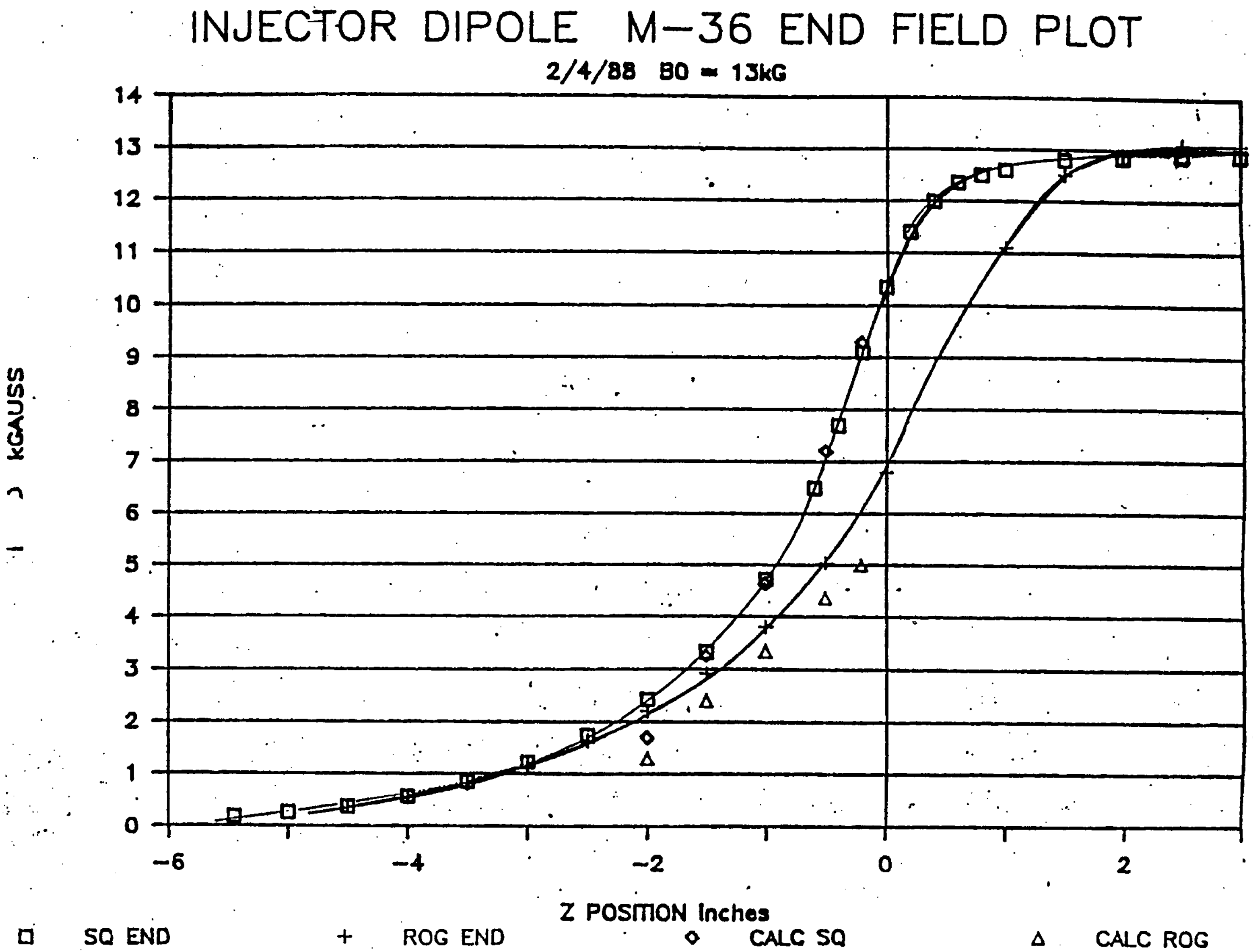

Figure 5.6-3: Longitudinal Fringe Field

5.7 Eddy Current in the Injection Magnet Coils

Introduction: This note describes calculations of eddy currents from the changing magnetic fields in the injector quadrupole and bending magnet coils. The power loss due to such eddy currents was calculated as well as the magnetic field that is generated by these eddy currents.

The first step in the analysis was to use the program Poisson to calculate the magnetic fields under the assumption that the driving currents do not vary with time. The next step was to assume that these calculated fields vary sinusoidally with time and to use Faraday's law to calculate the resulting eddy currents. The coils consist of several rectangular conductors, and in applying Faraday's law was assumed that the magnetic filed is uniform across each errors into the calculation. The power loss from these eddy currents was then calculated.

For an electron energy of 3.5 GeV was found that the power loss from eddy currents is 122 Watts per meter of quadrupole and 245 Watts per meter of bending magnet. This means that eddy currents account for 10.1% and 13.4% of the total power losses in the coils of the quadrupoles and bending magnetics respectively. (Total losses refers to the sum of the losses from driving currents and eddy currents).

The eddy currents in turn create their own magnetic field which is ninety degrees out of phase in time with the field from the driving currents. In order to calculate these fields, the eddy current distribution in each conductor was approximated by four current filaments. The strengths and locations of thes current filaments was calculated so that they produced the same far fields in vacuum as the true eddy current distribution. Poisson was again used to calculate the magnetic fields throughout the magnet from these current filaments. The plots of thes magnetic fields show that each conductor produces eddy current dipoles that counter the changing magnetic field produced by the driving current. This is as expected from Lenz's Law.

Continuing this process one could calculate the eddy currents from the magnetic fields from the eddy currents from the magnetic fields from the driving currents. Luckily, this is not necessary, because the peak to peak magnetic field swing in the coil from eddy currents is much smaller than that from the driving currents (less than 20%) for the bends and 15% for the quadrupoles).

The fields from the eddy currents at the electron orbit were analysed to determine their effects on the electron beam dynamics. The quadrupole strength is reduced by these fields at the most by 0.016%. Such a strength reduction in all quadrupoles in the injector results in a tune shift of 0.0013 in x and 0.0009 in y. This will have no appreciable effect on beam dynamics. The multipole fields in the quadrupoles from the eddy currents are also insignificant. The bend coil eddy currents reduce the dipole strength by 0.002% which translates into an rms closed-orbit distortion of only 0.02 mm. Bend multipole fields are also negligable.

Conclusion: Eddy currents increase the power losses in the quadrupole magnet coils by 10% and the losses in the bend coils by 13%. The field distortions from eddy currents have no significant effects on electron beam dynamics.

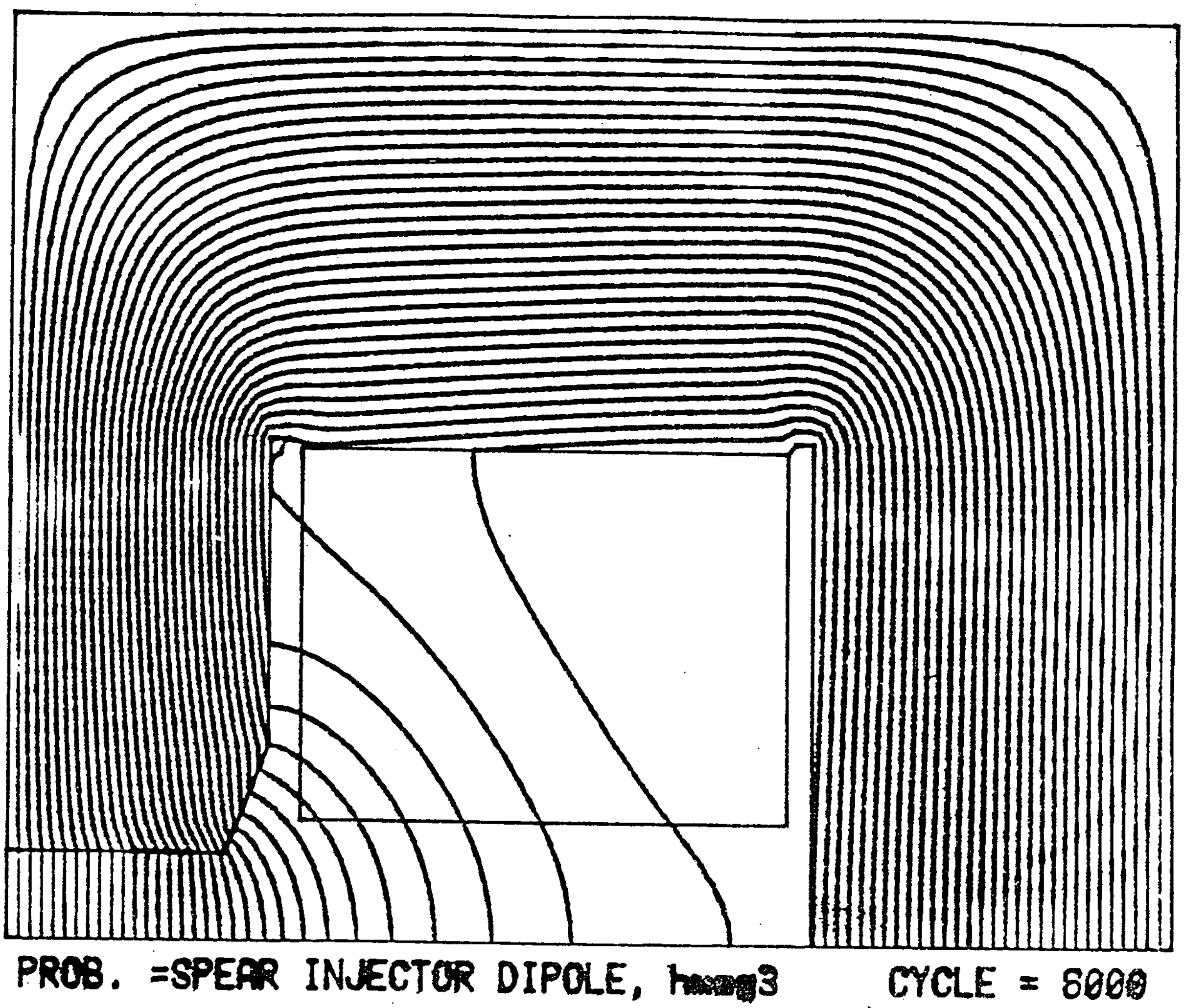

Figure 5.7-1: Magnetic Field induced by coil driving current

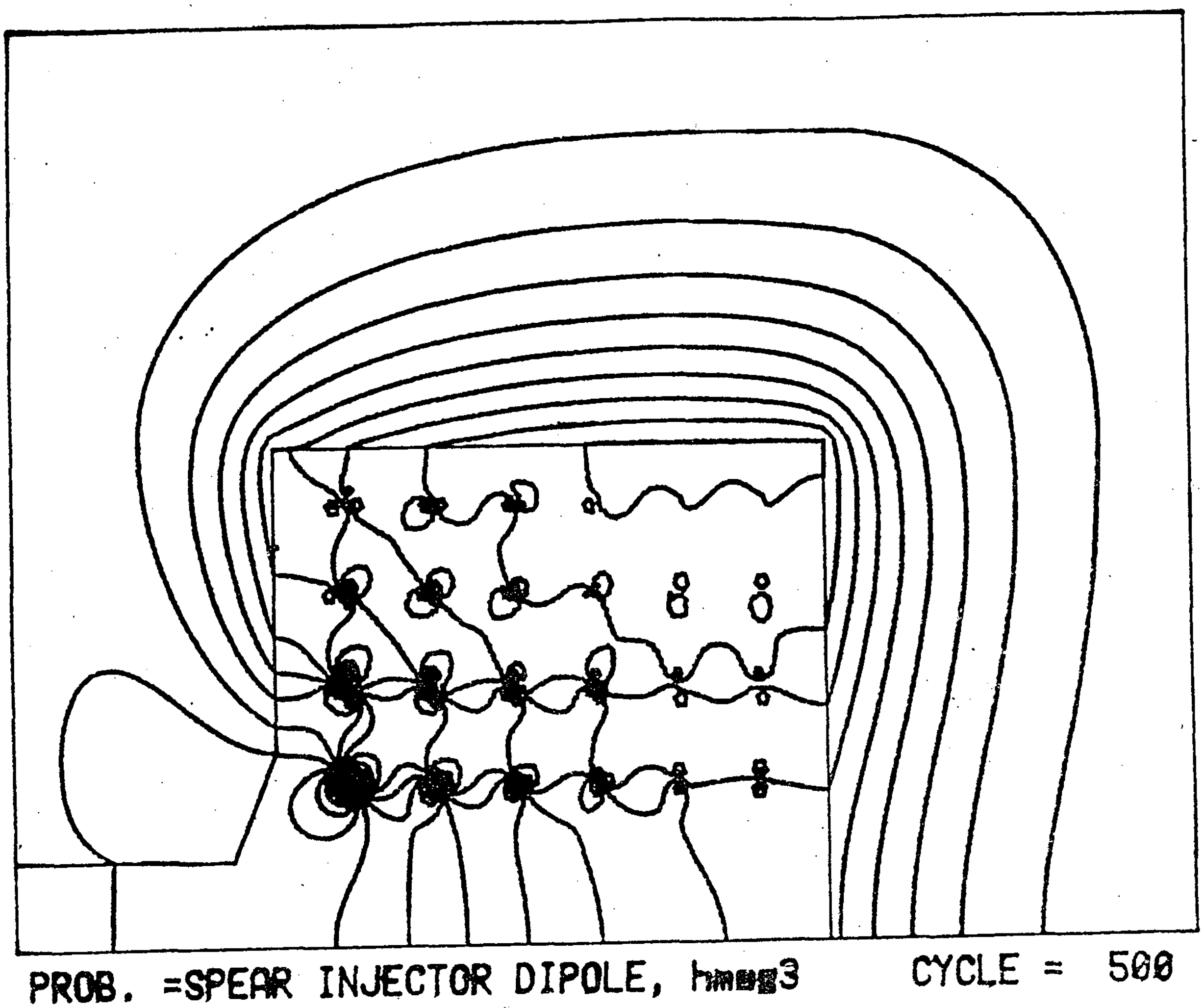

Figure 5.7-2: Magnetic Field induced by coil eddy currents

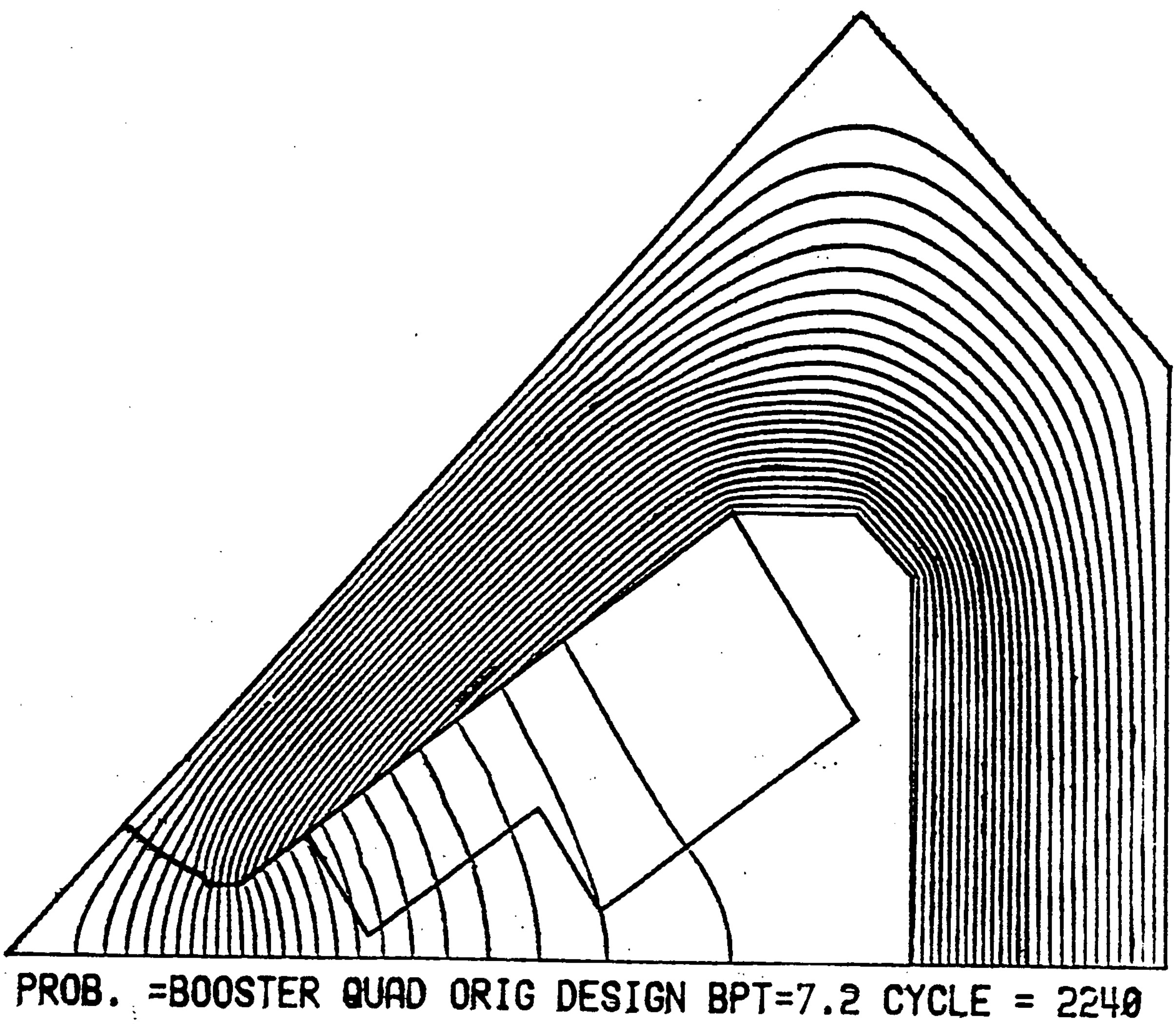

Figure 5.7-3: Magnetic Field induced by coil driving current

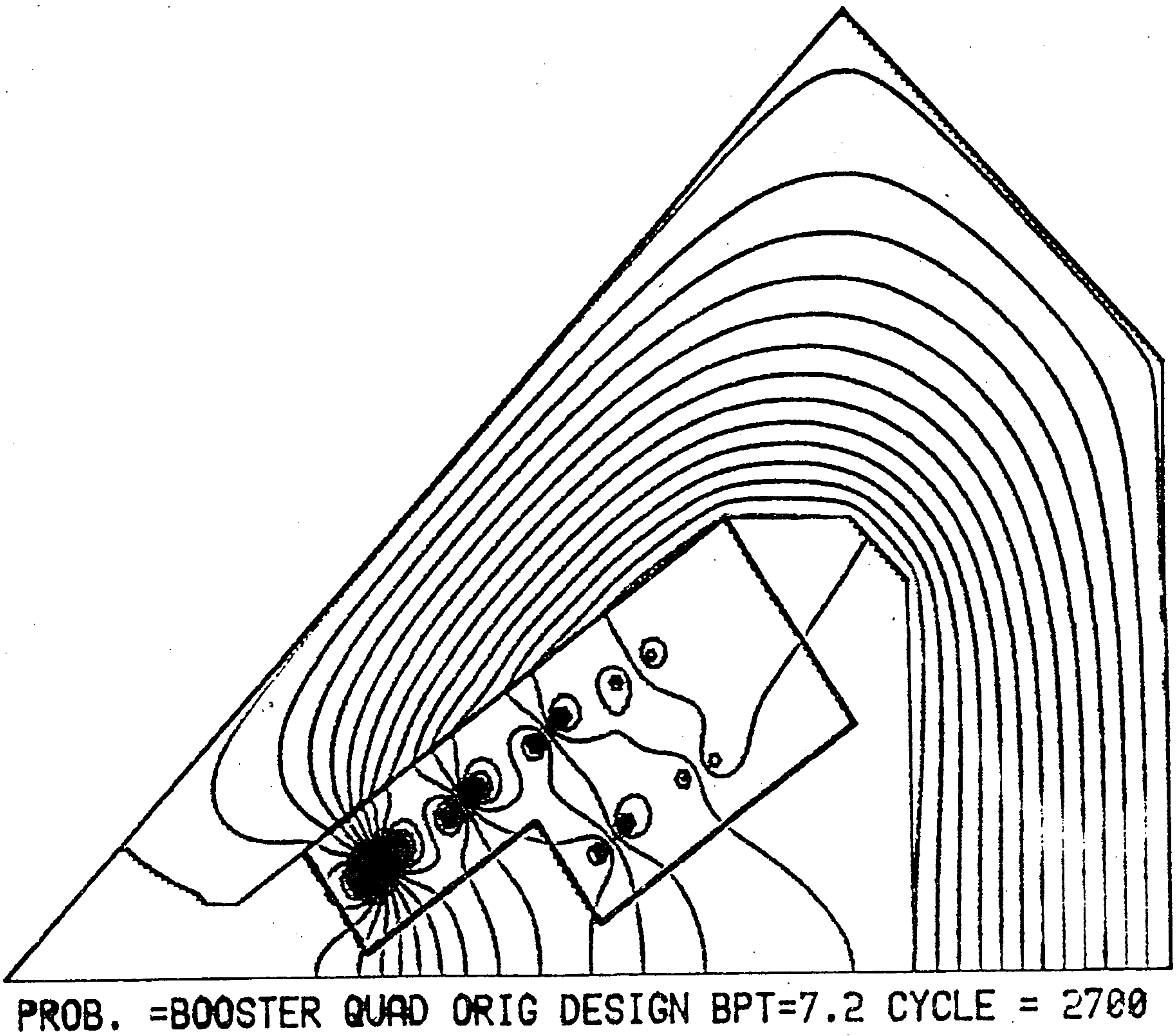

Figure 5.7-4: Magnetic Field induced by coil eddy currents

VACUUM

6 Ring Vacuum System

Chapter 6

Ring Vacuum System

6 Ring Vacuum System

In a booster synchrotron a special design of the vacuum chamber must be employed. Fortunately, since the particles remain in the synchrotron only a very short time, an operating pressure of only 10^{-6} Torr is sufficient and the high fabrication and maintenance costs of an ultra-high vacuum system can be avoided. Also the synchrotron radiation heating of the wall can be shown to be quite negligible due to the low average current and low duty cycle, so no special cooling of the vacuum chamber walls will be required. However, the changing magnetic fields during acceleration will induce eddy currents in the chamber material which can greatly affect the magnetic field quality inside the vacuum chamber. This effect can be avoided by using costly ceramic chambers, or for slow cycling synchrotrons such as proposed here, by using vacuum chambers made of very thin (0.3 mm) stainless steel pipes. In this proposal such a thin walled stainless steel chamber is used. To avoid the collapse of this chambers under atmospheric pressure external stiffening ribs will be attached to the outer surface at periodic longitudinal intervals. The ribs must be designed to fit within the various magnet pole gaps. Such a design has been successfully used at DESY in the recently constructed 12 GeV synchrotron, and allows the booster to be cycled at up to 12 times per second.

The pumping system design is dictated largely by the cross-sectional dimensions required for the vacuum chamber to fit inside the poles of the magnets. In the quadrupoles and sextupoles, a thin-walled round tube of approximately 50 mm diameter appears to be suitable. A number of round tubings can be partially flattened to an an approximately elliptical cross section of dimension 32 mm by 40 mm and used in the bending magnet regions. These dimensions allow the use of external ribs of sufficient thickness to provide the stability against atmospheric pressure within the specified quadrupole and sextupole bore diameters. In the bending magnets the stiffening rips would be only 1 mm in the pole gap but much wider in the horizontal plane (Figure 6-1).

An analysis has been made of the pressure distribution in a long tube of the above-mentioned dimensions with thermal outgassing rates assumed to be those of clean, degreased but unbaked stainless steel, and ignoring the very small gas desorption due to synchrotron radiation. It shows that an

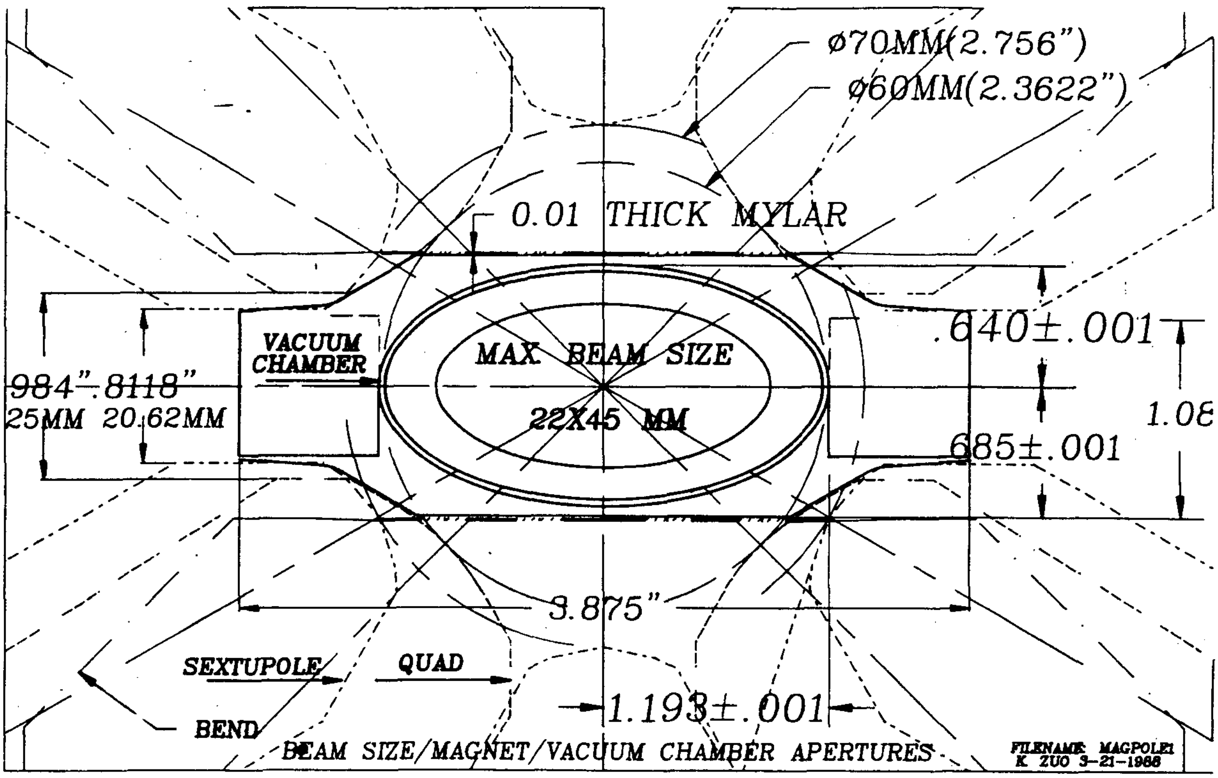

Fig. 6-1: Vacuum Chamber Cross-section

average pressure in the booster ring of about 700 n Torr can be achieved using only lumped ion pumps. In particular one 8 l/sec ion pump for each 2.8 meter long cell in the lattice is sufficient to reach that pressure. No distributed pumps in the bending magnets are required. Thus, for maintaining an adequately low and smooth pressure profile around the ring, 36 ion pumps with a pumping speed of 8 l/sec, approximately equally spaced, will be installed. To minimize cost several ion pumps at a time will be connected to one power supply. A set of vacuum gauges will be used to monitor the pressure around the ring.

To evacuate the ring from atmospheric pressure down to a pressure where ion pumps can safely be turned on, gate valves are used to segment the ring into sectors that the sectors can be evacuated separately. A mobile mechanical roughing pump together with liquid-nitrogen-cooled sorption pumps will be connected to the vacuum chamber at the center of a sector. Each sector is then evacuated separately until the ion pumps can be started.

When the vacuum pressure reaches a sufficiently low value in all sectors, the gate valves can be opened.

Taking advantage of the highly periodic magnet lattice only one basic type of vacuum chambers are needed to cover all of the ring. Each chamber reaches through one bending magnets, and one quadrupole/sextupole combination. All chambers are joined by conventional 4.5 inch Conflat flanges.

Each quadrupole/sextupole section consists of a straight round steel tubing with simple circular rings on the outside as stiffening ribs where necessary. The repetitive chambers will be connected by a conventional pump-out Tee with bellows. A single ion pump and the valve to the roughing system will be attached here. At one end, near the flange, an axi-symmetric beam position monitor (BPM) module will be installed, and at the other end, a short bellows section to accommodate small manufacturing tolerances. A thin ceramic ring will be incorporated at the end of each chamber to avoid induced current circulation in the ring. The layout of the arc vacuum chamber with pumping is shown in Figure 6-2.

Vacuum Chamber Tests Summary

Prototype ribbed elliptical sst vacuum chambers, (1.280" x 2.386" ellipse, 0.012" wall, 15.33" long, with 0.0355" thick ribs spaced approximately 1" apart) were designed, and tests performed to check the integrity of the design.

Initial chamber deflection tests were performed on a chamber which had the ribs merely tack welded on the ends to hold the elliptical contour of the chamber.

These initial tests were performed by evacuating the chamber and taking careful measurements of the exterior wall deflection. These tests showed a negative deflection of 0.027" at approximately 1 atmosphere.

Subsequent tests were performed on a brazed rib design technique. The brazed rib design produced a very rigid thin-walled vacuum chamber, and when tested as above, exhibited a negative deflection of only 0.004" at 1 atmosphere. Additional two-atmosphere tests showed a negative deflection of only 0.007".

Ultimately, collapse pressure tests were performed, which showed the

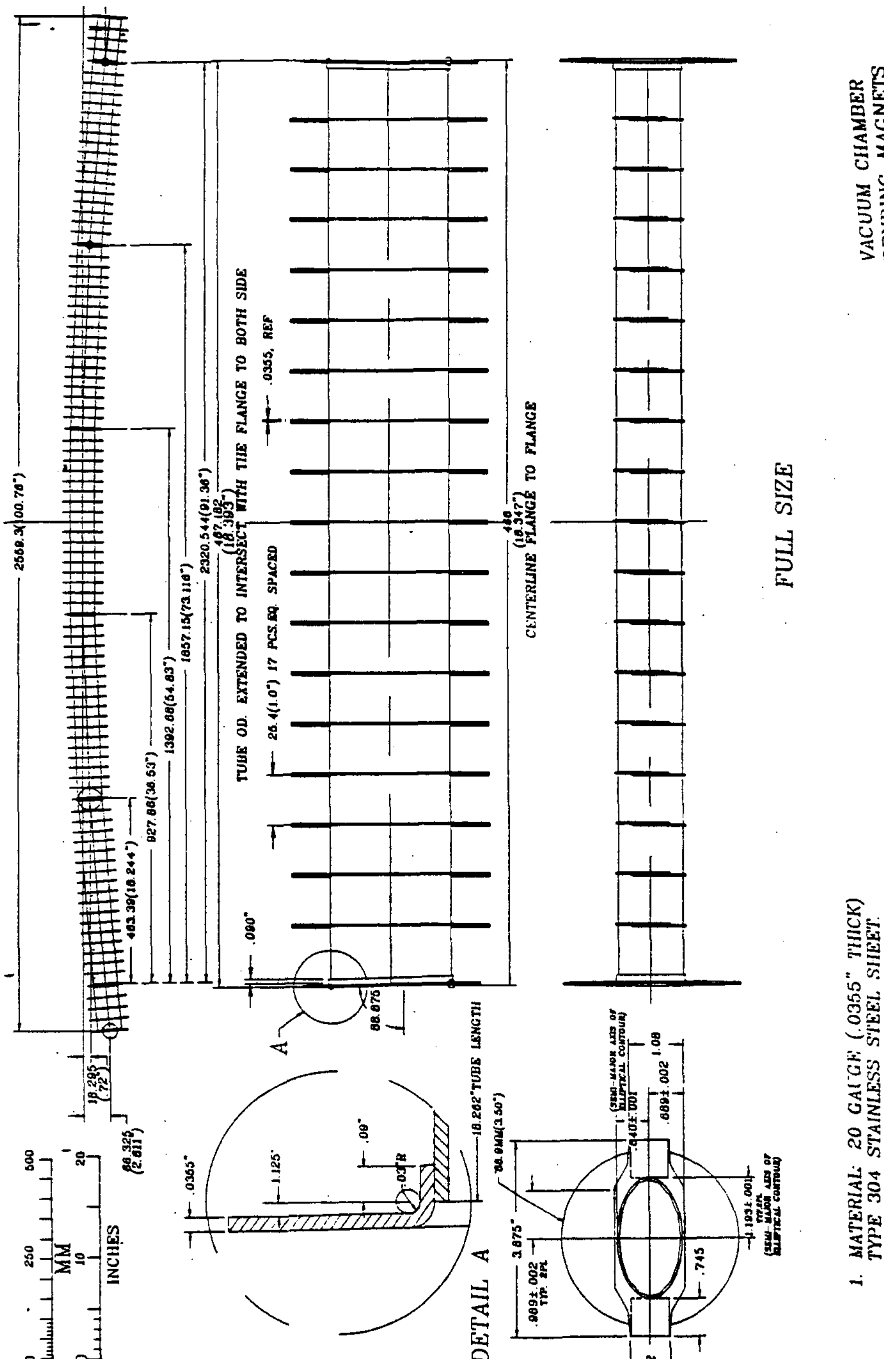

Fig. 6-2: Arc Vacuum Chambers

collapse pressure of the brazed rib design to be > 10 atmosphere (> 150 psi).

Vacuum Chamber Pressure Deflection Tests

I. Chamber Asembly

Requirements:

Tube, 304L sst, 1.875" O.D. x 0.012" wall x 15.33" long

Ribs, 304L sst, 0.0355" thick, elliptically contoured center to shape the vacuum chamber tube

Assembly fixture to form the tube with ribs to the ultimate elliptical shape.

Hydrostatic chamber to externally pressurize the vacuum test chamber.

All chambers were assembled according to the chamber assembly procedure by H. Morales, dated 10-16-87.

II. One - Atmosphere pressure test (non-brazed ribs)

Initial chamber deflection tests were performed by blanking one end of the chamber and evacuating the test chamber through the other end to approximately 10^{-3} T (1 atmosphere).

Chamber deflection was measured at various intervals along the length, with the greatest measured deflection, at 1 atmosphere, of 0.0027".

III. One - Atmosphere pressure test (brazed ribs)

Tests performed as in II.

Measured chamber deflection was approximately 0.004" at 1 atmosphere.

IV. One - Atmosphere pressure test (brazed ribs and welded end components)

Setup and test:

A blank elliptically contoured end piece, recessed approximately 1/4" into the test chamber was welded on one end. The other end of the vacuum test chamber was welded to a dual purpose 8" conflat flange. The flange incorporated provisions for either internal evacuation of the vacuum test chamber or for attachment to the hydrostatic chamber to externally pressurize the test chamber.

The vacuum test chamber was evacuated to approximately 10^{-3} T (1 atmosphere), and measured chamber deflection was approximately 0.004".

V. Two - Atmosphere pressure test (brazed rib and welded end components)

The vacuum test chamber was prepared as in V, but installed into the hydrostatic chamber and pressurized with nitrogen gas to approximately 30 psi (>2 atm.).

An indicator was designed and fabricated to check the internal deflection of the test chamber as the externally applied pressure was increased to 30 psi (2 atm), the measured deflection was 0.007".

VI. Collapse Test (brazed ribs and welded ends)

The vacuum test chamber was prepared as in V, installed into the hydrostatic chamber, and pressurized with water.

Deflection of the vacuum test chamber, measured to approximately 70 psi (> 4 atm), indicated a deflection 0.017".

Ultimate chamber collapse occured at approximately 150 psi (> 10 atm.).

STANFORD SYNCHROTRON RADIATION LABORATORY

ENGINEERING NOTE

CODE	SERIAL	PAGE
		1 OF

AUTHOR	DEPARTMENT	LOCATION	DATE
H. Morales / T. Martinez	SSRL Injector	SSRL	10-16-87

PROGRAM — PROJECT — JOB: Collapse Test, Brazed Rib Vacuum chamber, .012" wall thickness.

TITLE: Summary Results, w/ + w/o brazed ribs

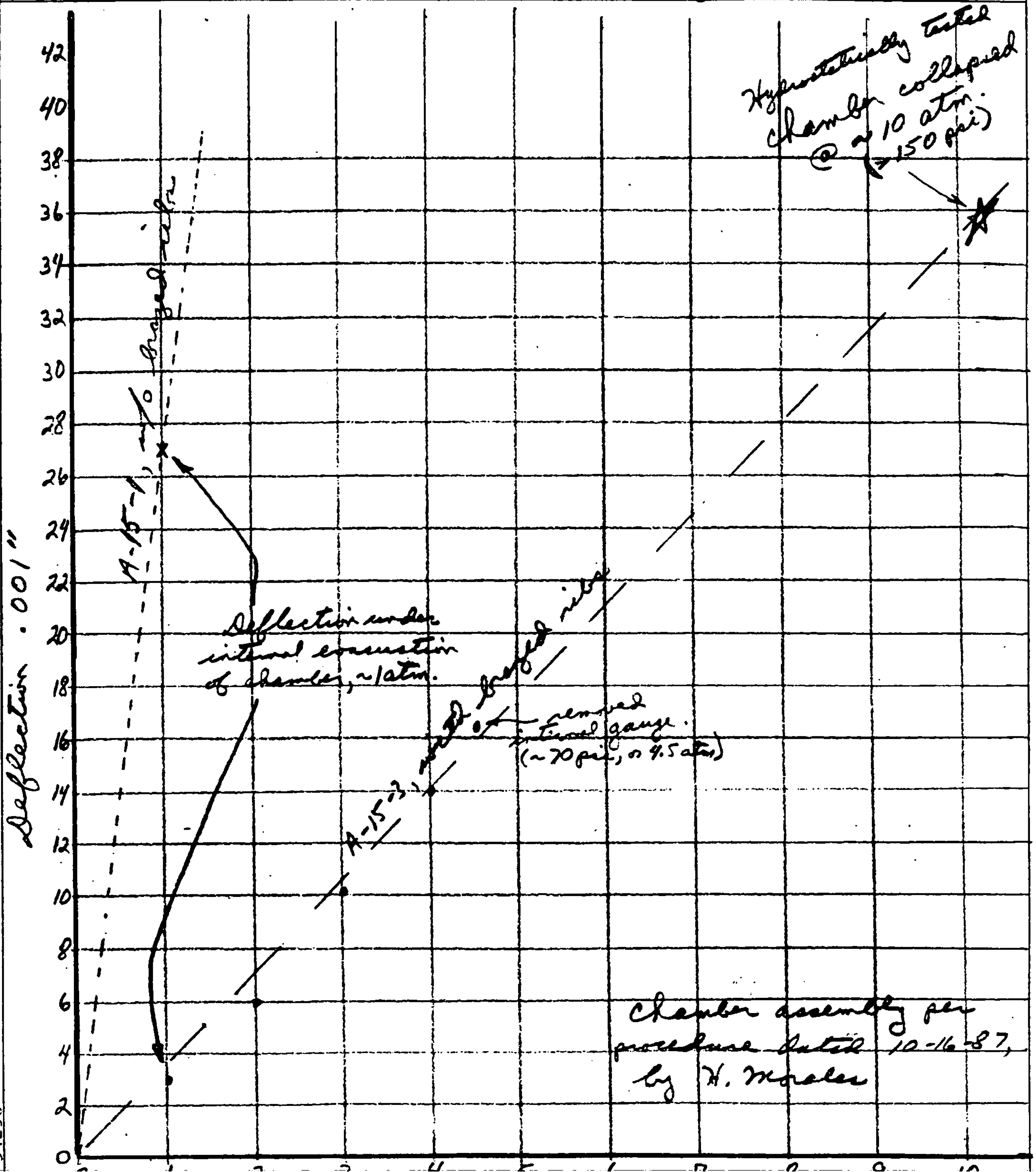

54250

INSTRUMENTATION AND CONTROLS

7 Instrumentation and Controls

Chapter 7

Instrumentation and Controls

7 Instrumentation and Controls

The controls of the booster synchrotron components are mostly incorporated into the hardware. The accelerating system, for example, will have an internal feedback system to keep the RF parameters constant at the desired values. During the energy ramping process the quadrupole power supply amplitudes and phases will be controlled by a small computer to assure proper tracking with the bending magnet current and field. Similarly the beam current or the beam position will be recorded and displayed during acceleration. In this way it is possible to operate the booster synchrotron independent from the storage ring control computer which will be important during initial debugging. A separate control console with a microcomputer will be available to operate the injector independent from the SPEAR control system. On the other hand the booster components are ready to be controlled by any other computer and therefore can be also connected to the main SPEAR control system whenever this becomes desirable.

Due to the variation of the main dipole field at injection an injection timing trigger with a precision of about 1 μ is required to keep the energy of the beam at ejection to SPEAR within tight tolerances. This trigger is to be locked to the main dipole field variation and is used to trigger the gun, linac and the injection septum and kicker. This timing trigger is derived from a pick up coil and a permally strip to give a signal when the magnetic field is reverted. A special delay unit will be also triggered from this timing signal to later produce the trigger for the ejection septum and kicker magnets.

For particle beam monitoring a current monitor will be installed to measure the beam intensity. Beam position monitors will detect the beam orbit and provide the signals to correct it. During particle acceleration in the booster it will be desirable to control the beam orbit to adjust for slight variations in the magnetic fields of the individual magnets. Trim magnets as part of the quadrupoles or bending magnets will be used in conjunction with the beam position monitors to dynamically control the beam orbit when needed.

The magnet current during acceleration will be computer controlled and a feedback system which monitors the betatron oscillation frequency will be used to keep the betatron tunes of the synchrotron constant during energy ramping.

The controls for the RF system will be similar to those developed for the storage rings PEP and SPEAR.

The linac controls contain mostly a timing system, as well as a phase and amplitude detection system which provide the signals for the purpose of phasing the klystrons. The timing system makes use of a signal from the master oscillator set precisely to a harmonic of the revolution frequency of the beam in the storage ring. From these signals the timing for the phasing of the linac RF, the synchrotron RF and for the chopper cavity are derived. A set of beam monitors, bending magnets and slits will be provided to control the beam energy and the beam energy spread before it is injected into the synchrotron.

For beam monitoring a DC current transformer will be used as well as beam position monitors to control the beam orbit. The magnet current during acceleration will be computer controlled and a feedback system which monitors the betatron oscillation will be used to keep the betatron tunes of the synchrotron constant during energy ramping. The controls for the RF system will be equal to the SPEAR storage ring system with the additional capability to change the klystron drive as required by the beam energy during acceleration. The linac controls contain mostly a timing system and a phase and amplitude detection system, which provides the signals for the purpose of phasing the klystrons. The booster timing system will tie into the SPEAR timing system to allow the filling of any arbitrary bunch pattern in the SPEAR storage ring.

RF

8 RF - System

Chapter 8

RF - System

8 RF - System

To accelerate the electrons from the preinjector energy to the final storage ring operating energy, a 358 MHz RF system will be used. This system makes use of a 5-cell cavity which has been used in SPEAR and has been secured from SLAC surplus. One such cavity is sufficient to accelerate the electrons up to 3 GeV.

If the RF-system were operated just like in a 3 GeV storage ring at a constant RF-voltage level the system would require a RF-power of 150 kW of which about 135 kW are losses in the cavity walls. These losses can be greatly reduced if the RF-voltage is modulated during the accelerating process to the minimum values needed by the particles at any time. This modulation can be easily achieved by control of the klystron drive. At the highest energy of 3 GeV, however, the klystron power must reach a maximum instantaneous power of 150 kW to generate a sufficiently large accelerating voltage in the cavities to overcome the synchrotron radiation losses. This power rating is less than that for the klystrons presently used in SPEAR. To simplify maintenance it is proposed to use the same klystrons as for the SPEAR storage ring although they are, at 500 kW, overrated. The relative small cost difference between a 150 kW and 500 kW klystron makes this decision simple.

The low level electronics and power supplies will be of the same design as for the SPEAR or PEP RF-systems. No new development is necessary.

The choice of the accelerating system is mainly determined by the available surplus accelerating cavity from SPEAR. This cavity operates at a frequency of 358 MHz, has a shunt impedance of 30 MOhm and can absorb in its cooling system an average power of about 100 kWatt. The cavity consists of five cells coupled together in π mode by two slots in the common wall between the cells. The construction material is Aluminum 6061. A layer of Titanium Nitride deposited on the surface of the cavity serves to prohibit field breakdown by multipactoring. A water cooled loop in the center cavity is used to couple the RF power from the klystron into the cavity.

The cavities are equipped with a movable tuner and a sampling loop. The tuner is used to compensate for the thermal expansion of the cavity which causes a change of the resonance frequency. The field amplitudes are monitored by the sampling loop and the signal is compared with a reference signal to set the desired RF Voltage in the cavity. The resulting difference signal is applied to a variable attenuator in the drive line to the klystron. The whole system is similar to the SPEAR or PEP control system and could also be equal to the system used for the storage ring.

The accelerating system of a synchrotron, in addition to providing the accelerating field U_{accel} to raise the electron energy from 120 MeV to 3.0 GeV, also compensates for the loss of energy due to synchrotron radiation U_{rad} and the energy lost due to the excitation of parasitic modes U_{pm}.

The energy balance can be written like:

$$U_{tot} = U_{accel} + U_{rad} + U_{pm}, \qquad \text{where}$$
$$U_{accel} = (E - E_0) / (T_c * f_{rev})$$

where E = 3.0 GeV, E_0 the linac energy, T_c is the ramping time of the synchrotron and f_{rev} is the particle revolution time in the synchrotron.

For this synchrotron we have at 3 GeV:

$$\begin{aligned} f_{rev} &= 2974\ kHz \\ T_c &= 0.10\ sec \\ U_{rad} &= 1\ MeV \\ U_{accel} &= 10.0\ keV \\ U_{pm} &= 0.4\ keV \\ U_{tot} &= 1.01\ MeV \end{aligned}$$

Here we have assumed that the maximum cycling rate for the synchrotron is 10 Hz.

The parasitic mode parameter for the SPEAR cavity K_{pm} is 1.5 V/pCb and the number of electrons per bunch is at most $2{*}10^9$ in maximum of 8 bunches. The parasitic mode losses in the SPEAR cavity, U_{pm}, therefore, is no more than 0.4 keV. The required accelerating voltage, even for a fast cycling booster at 10 pps and the maximum expected beam loading, is negligible compared to the synchrotron radiation losses. The RF power, therefore, is mainly applied to replace the synchrotron radiation energy loss.

The RF parameters of the injector synchrotron are:

Frequency	358	MHz
Harmonic Number	120	
No. of Klystrons	1	
No. of Cavities	1	
Cavity shunt impedance	30.0	MOhm
Max. Cavity Power	130.0	kWatt
Avg. Cavity Power	35.0	kWatt
Max. Cavity Voltage	2.0	MVolt
Max. Beam Power	4.0	kWatt

During each accelerating cycle, the electron energy raises from 120 MeV to 3.0 GeV and the synchrotron radiation energy loss per turn increases from 1 eV to 900 keV. Therefore, to minimize power consumption and to avoid beam instability the RF power will be modulated from 5 kW to 135 kW as shown in Figure 8-1. This modulation must be split into two regimes: one for energies from 100 MeV to 1.3 GeV and the other for 1.3 GeV to 3 GeV. During the first step, the RF power is kept at about 5 kW which is the minimum stable output power for the klystron. The RF voltage in the cavity is, in this case, 387 kV and provides an energy acceptance of 1.6% at injection and of 0.5% at 1.3 GeV. During the second step the energy acceptance is kept at a minimum 0.5% and the resulting RF power and RF voltage in the cavity are shown in Figure 8-1 and 8-2. This kind of modulation of the RF power can be achieved by controlling the drive power to the klystron. Of course more energy acceptance can be obtained should that be desirable for some reason, by raising the RF power up to the maximum level of 100 kW as limited by the cavity cooling capacity.

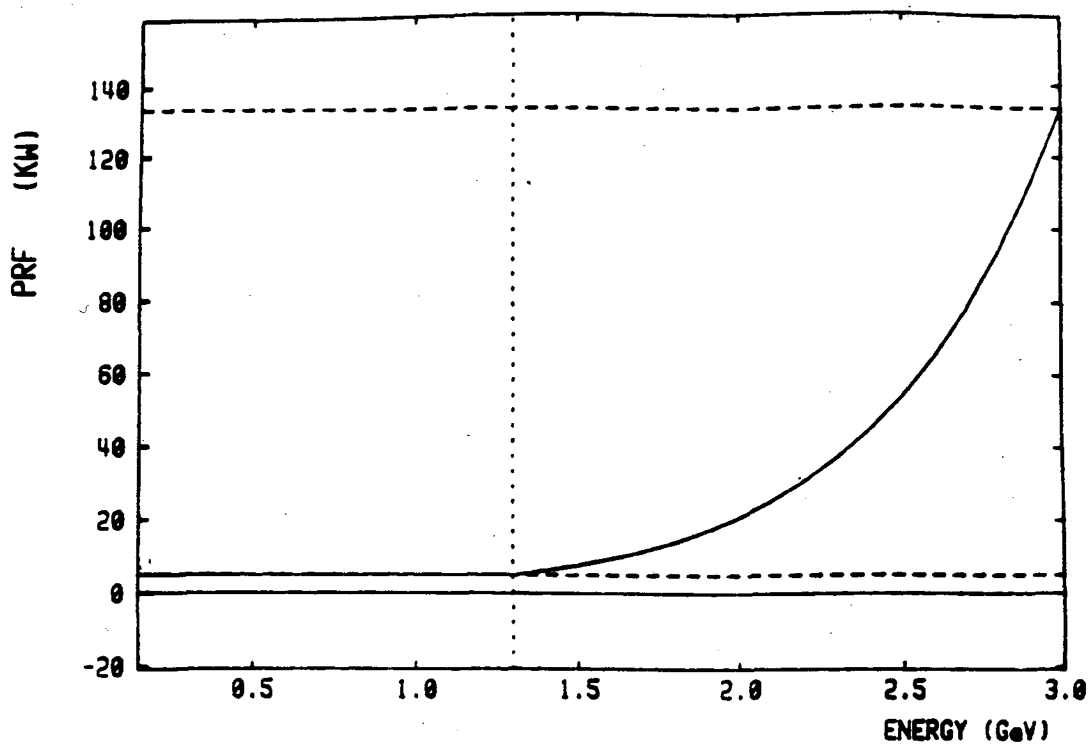

Fig. 8-1: The Cavity RF Power Variation with Beam Energy

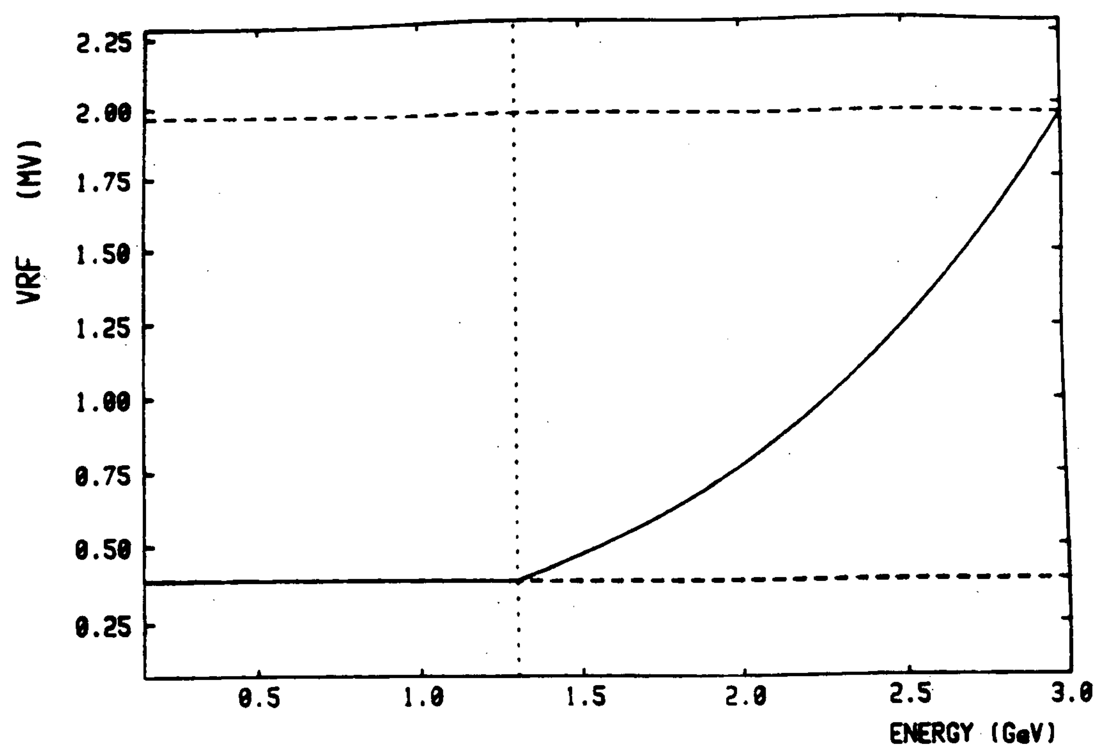

Fig. 8-2: Variation of the Cavity Voltage with Beam Energy

BEAM
TRANSFER LINES

9 Beam Transfer Lines

Chapter 9

Beam Transfer Lines

9 Beam Transfer Lines

The proposed SPEAR injection system involves a series of injections and ejections processes in and out of the booster and finally into the SPEAR storage ring. The injection and ejection at the booster is relatively simple since no accumulation is attempted and therefore both injection and ejection is performed during one revolution only. As a consequence only one kicker magnet and one septum magnet is needed for injection and the same for ejection. Obviously the design of these pulsed magnets is much simpler for the low injection energy of 120 to 150 MeV compared to the ejection energy of 3.0 GeV.

Both Injection at 120 MeV and Ejection at 3.0 GeV will take place in the east straight sections of the booster. The ejection will utilize a vertically deflecting Lambertson septum which deflects the beam upwards from the booster ring plane. Another vertical bending magnet further downstream deflects the beam again into a horizontal plane at the same elevation as the existing SPEAR beam line. This simplifies the connection to that beam line.

The injection into the booster will be effected by a horizontally deflecting septum magnet.

In both cases a full aperture kicker magnet will be used to deflect the beam either onto the ideal orbit of the booster ring during injection or for ejection into the aperture of the Lambertson septum. The schematic layout of both the injection and the ejection systems is shown in Figure 9-1.

9.1 Injection from the Linac to the Booster

The electron beam from the preinjector linear accelerator is guided through a simple transport line to the injection point in the booster lattice. The septum magnet is strong enough to accomodate a large deflection angle such that the incoming beam need not pass through a ring magnet. The magnet parameters for the injection magnets are compiled in Table 9-1.

Table 9-1: Parameters of the Injection Magnets

Magnet:	Septum	Kicker
Number of Magnets	1	1
Max. Beam Energy (MeV)	150	150
Magnet Field (Gauss)	4560	458
Deflection Angle (mrad)	136	5.5
Length of Magnet (m)	0.25	0.6
Aperture Width (mm)	60.0	60.0
Aperture Height (mm)	15.0	15.0
Magnet Type	pulsed	pulsed
Max. Pulse Length (msec)	10.0	-
Max. Fall Time ($1.0e^{-9}$ sec)	-	≤ 300

9.2 Ejection from the Booster Synchrotron

After acceleration of the particles to the storage ring energy an ejection process is triggered for the transfer of the beam to SPEAR. A fast full aperture kicker magnet in the booster synchrotron will deflect the beam into the magnetic aperture of a Lambertson septum magnet to finally deflect the beam vertically out and away from the booster components into a beam transport system. Because of the high beam energy it will not be possible like in the injection path to totally avoid an interference with a quadrupole downstream of the septum magnet. The septum magnet therefore will be adjusted to deflect the beam such as to aim to an area of the quadrupole which is unobstructed by steel and coils but inside the return yoke of the magnet. No other magnets interfere with the ejected beam.

The parameters of the ejection magnets are compiled in Table 9-2,

Table 9-2: Parameters of the Ejection Magnets

Magnet:	Septum	Kicker
Number of Magnets	1	1
Max. Beam Energy (GeV)	3.0	3.0
Magnet Field (kGauss)	4.6	0.550
Deflection Angle (mrad)	63	5.5
Length of Magnet (m)	1.6	1.0
Aperture Width (mm)	60.0	60.0
Aperture Height (mm)	15.0	15.0
Magnet Type	pulsed	pulsed
Max. Pulse Length (msec)	10.0	-
Max. Rise Time ($1.0e^{-9}$ sec)	-	300

9.3 Beam Transport to SPEAR

The beam ejected from the booster synchrotron enters a short beam transport system leading into the nearby existing electron injection transport line. Where both beam lines merge a bending magnet will deflect the booster beam onto the existing path of the injection line. If no other modifications were contemplated this beam would then enter the SPEAR storage ring at the now existing entry point through existing injection components. Some existing pulsed magnets, however, would limit the injection energy to 2.3 GeV and therefore need to be replaced. With more powerful components. A layout of this beam transport system is shown in Fig. 9-1.

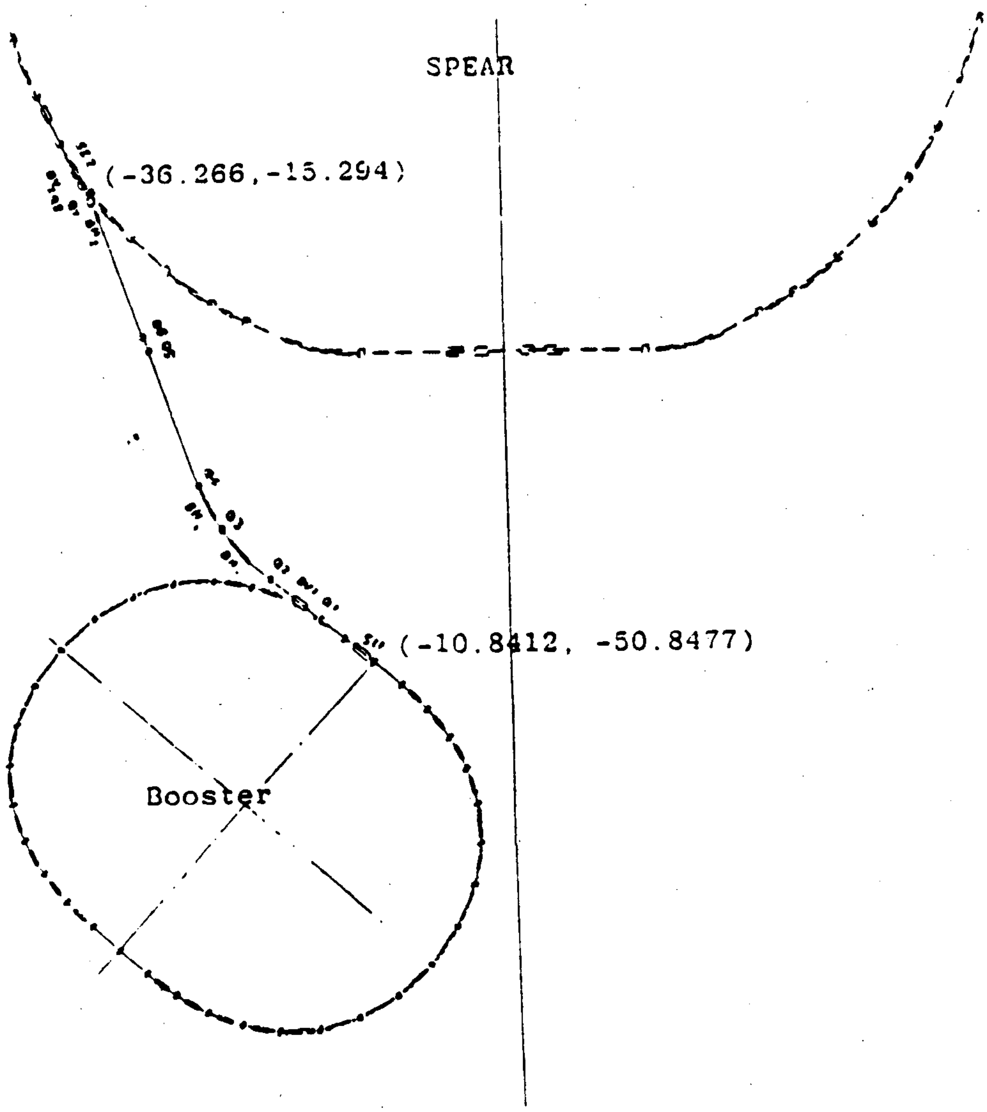

Figure 9-1: Beam Transport Line from the Booster to SPEAR Tunnel

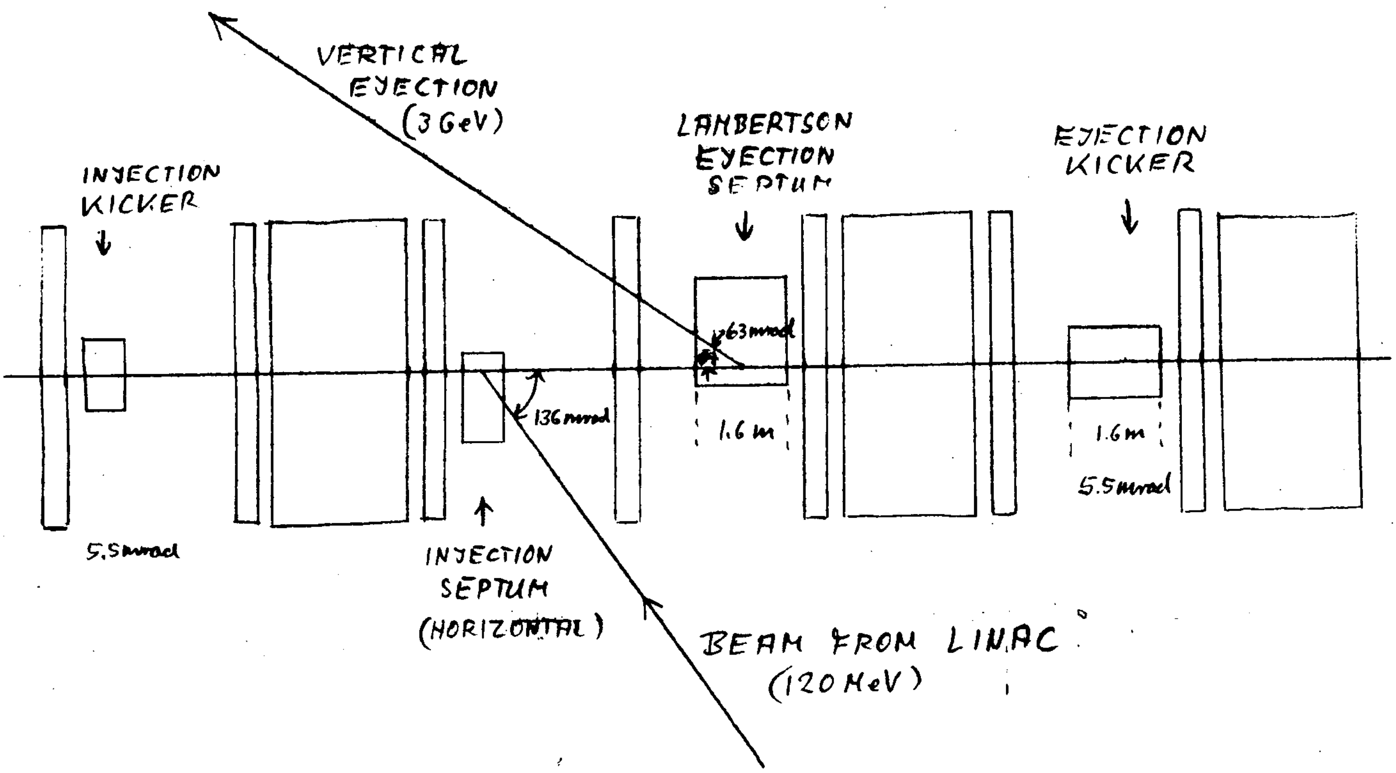

Figure 9-2: Booster Injection/Ejection

EQUIPMENT
SHELTERS

10 Equipment Shelters

Chapter 10

Equipment Shelters

10 Equipment Shelters

10.1 Shielding and Shelters

The linac preinjector and the synchrotron must be housed in a radiation safe shelter. The accelerators will be housed in an above-ground concrete tunnel, with 2 feet thick wall and 1 foot thick roof of blocks to protect the outside world from radiation. The inside dimensions of the ring tunnel will be 7 feet high and 8 feet wide with a 5.5 feet aisle for easy access to the ring (Figure 10-1). There will be three access ways into the ring. One can be used for component installation, while another access through the linac tunnel serves as an escape way for emergencies.

Most of the ring shielding walls and roof will be constructed of poured reinforced concrete blocks.

All shielding shelters will be constructed on a flat 6" concrete ring surface poured in the SLAC research yard next to the SPEAR storage ring (Figure 1-1). It is planned to keep the present electron beam line which crosses the synchrotron tunnel operational at least until the synchrotron is commissioned. This is possible since the existing injection line is on a higher elevation than the booster synchrotron beam lines by about 2.5 feet. The existing electron beam transport line, therefore, is no more than a small beam pipe just underneath the shielding roof where it crosses the ring tunnel.

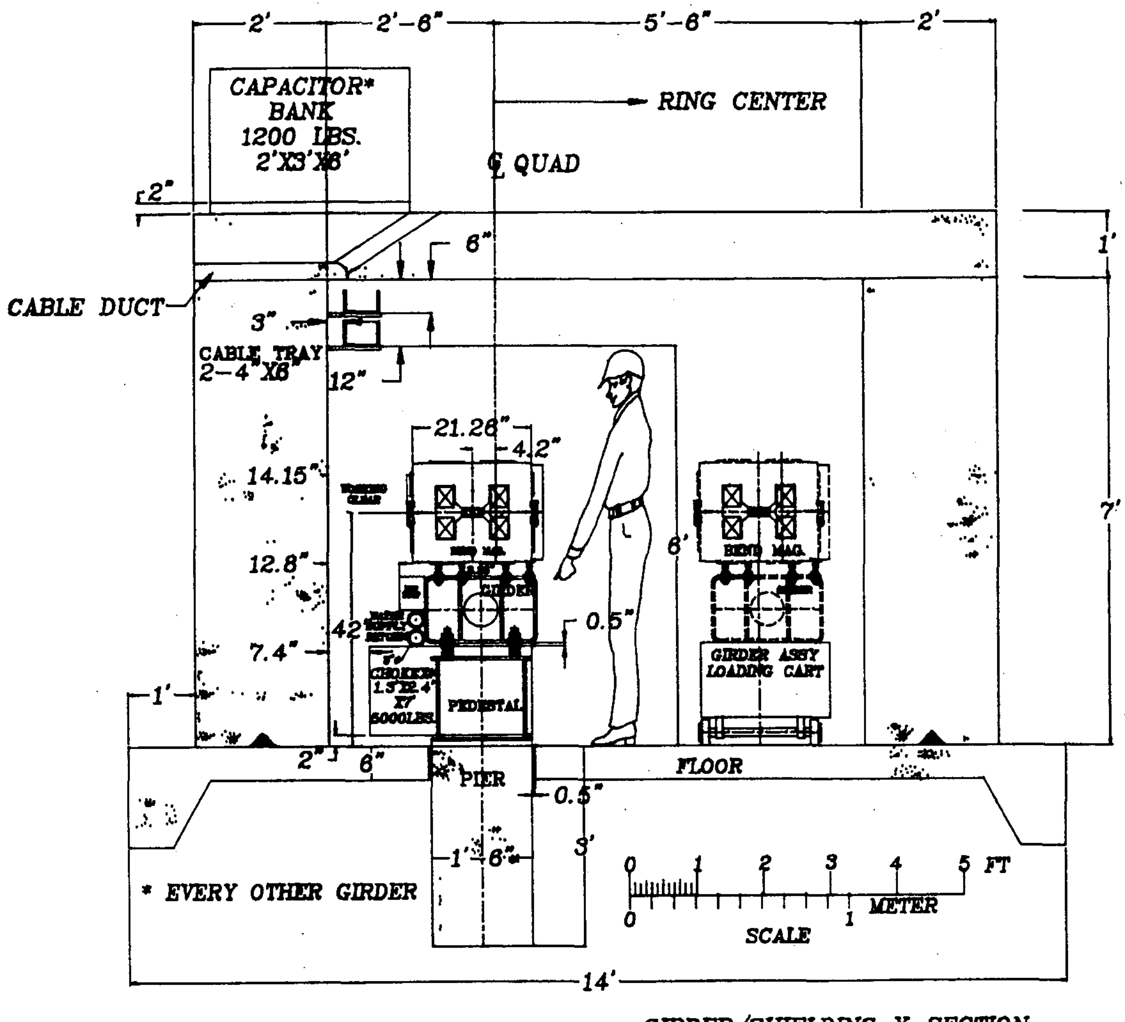

Fig. 10-1: Ring Shielding Cross Section

10.2 Shelters

The injector shelter will be constructed on an existing flat asphalt surface and will span the east and west ring shielding straight sections. The east and west straight sections contain respectively the injection and ejection and RF cavity systems. The shelter will also span the existing spear ejection beam line 17. The center of the shelter will contain the linac preinjector linac klystron and modulators, the synchrotron klystron, the magnet power supplies and some local electronics.

The shelter will be 75 x 130 feet with an eave height of apporximately 22 feet. The floor of the shelter will be at an elevation of + 9.2" from SPEAR movement 18 in the beamline Y. This is level with the floor of building 101 and 5" above the ESA protruding floor slab. The remainder of the existing asphalt yard varies from + 2" to + 9" within. The injector ring area is necessitating minimal site work. The shelter proposed layout is shown is Figure 10-1 and in the next figure (Figure 10-2).

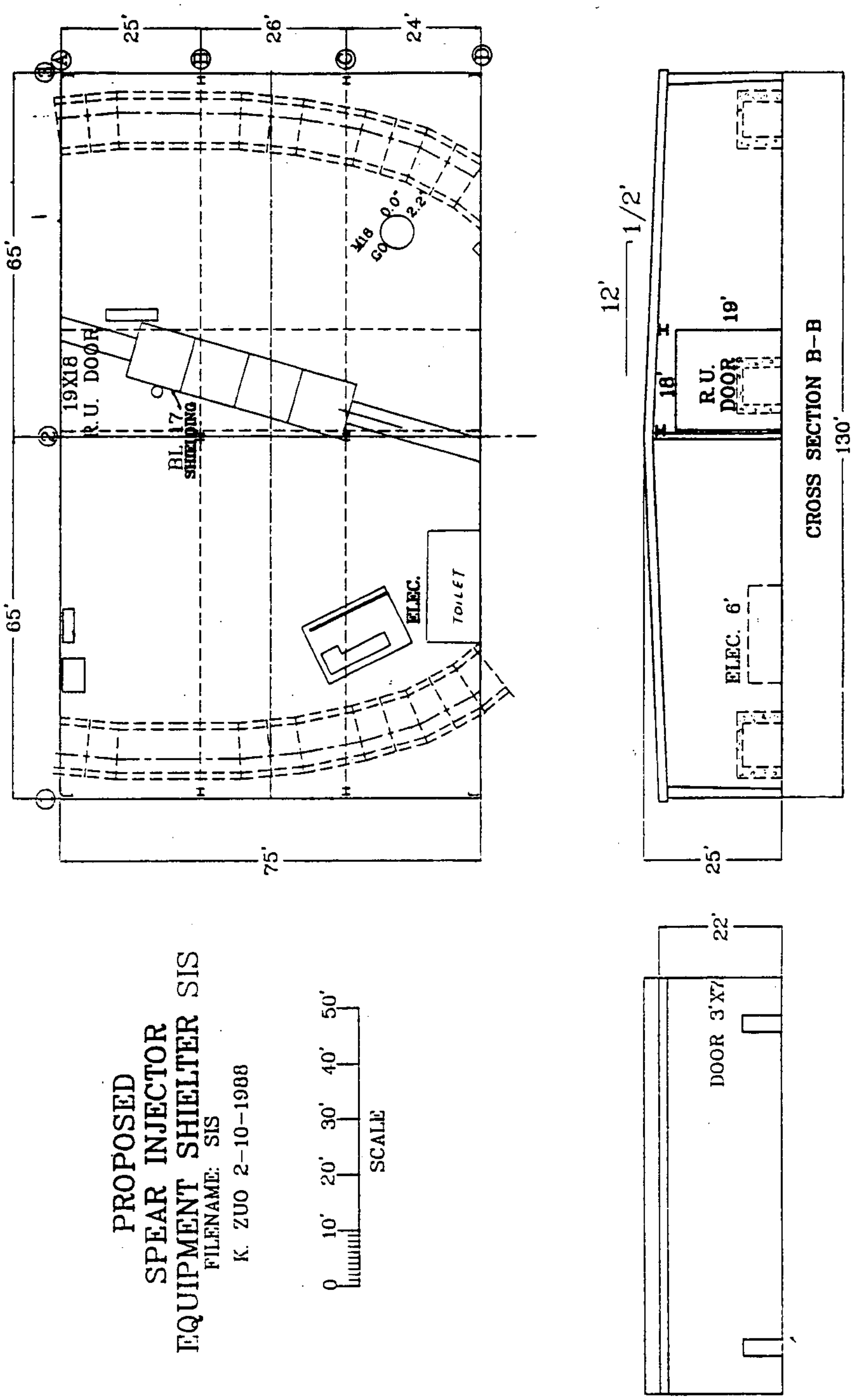

Fig. 10-2: Proposed SPEAR Injector Equipment Shelters, SIS

UTILITIES

11 Utilities

Chapter 11

Utilities

11 Utilities

11.1 Electrical

The synchrotron will require electrical as well as mechanical utilities. An overview of existing and planned utilities is shown in Figure 26. The maximum total electrical power requirement at 3 GeV is about 1 MVA, although less than half of that will be needed on average during operation. From that about 250 kW is needed for the RF system and 450 kW is needed for magnet power systems. The remaining power is for miscellaneous components including house power.

A 3 phase, 4 wire, 12.5 kV power source will be extended from an existing high voltage box located in the north-western corner of the north research year, about 30 feet away from the booster ring tunnel (Figure 26). New transformers and switch gear located next to the western booster shielding, outside the ring tunnel, are used to reduce this voltage level to 480 V and 120/208 V for general power distribution systems, as well as to special voltage levels for large power supplies. Switch gear, AC cabling, and metering are required for these systems. In particular, a 15 kV fast vacuum breaker is needed for the power supply transformer systems.

AC receptacles (120/208 V) and lighting are required for both the equipment shelter and ring tunnel. In addition, two 480 V welding outlets will be installed in the shelter. Communication and fire alarm systems will be extended from the existing SPEAR/SSRL system.

11.2 Mechanical - LCW

The system consists of;

- Six inch stainless steel headers from End Station A.
- A metering station at the connection point measuring and recording flow and temperature.
- A pressure reducing station to control system pressure.
- A flanged take-down piece over the beam line.
- Four inch stainless steel sub headers to both sides of the equipment shelter.
- Two inch copper power supply sub headers inside the equipment shelter complete with header valves and a further pressure reducing station.
- Isolation, header, and flushing valves as appropiate.

1 - A self-contained temperature controlled system to provide temperature controlled LCW to both the Ring Cavity Cooling Water Circuit and the Gun Cooling Water Circuit. The combined capacity of these two circuits is 60 gpm, differential pressure at the loads of less than or equal to 70 psi, LCW supply temperature to the loads of 92 degrees F plus or minus 1/2 degree F. Maximum pressure at any point in the system will be 100 psig. The heat sink for the primary side of the heat exchanger will be Cooling Tower Water (CTW). The distribution system for the LCW will be 3 inch and smaller copper piping to the Cavity and Gun loads. The CTW transmission lines will be Steel.

2 - High (200 psig) pressure 2 inch diameter supply and return headers will encircle the ring providing Magnet Cooling Water. These headers will be in the housing with valves every 20 feet to connect to hoses. The headers will be made of copper. The differential pressure between the supply and return header will be less than or equal to 130 psi. The total flow in this subsystem will be 80 gpm. Temperature will be held within 12 degrees F of setpoint. Setpoint is assumed to be at least 85 degrees F.

3 - Low (100 psig) pressure LCW will be circulated in 3 inch copper headers to provide cooling to both the magnet power supplies and the accelerator sections. Total flow will be 70 gpm, the differential pressure

between supply and return headers will be less than 50 psi. Temperature will be held within 12 degrees F of setpoint (assumed to be at least 85 degrees F).

15 Summary of Parameters

Chapter 15

Summary of Parameters

A summary of general parameters of the ring and the lattice functions are given in Table 15-1:

Table 15-1

Synchrotron Parameter

Energy	3.0	GeV
Circumference	100.339	m
Cycling Rate	2	Hz
Revolution		
Frequency	2987.79	kHz
Time	335	nsec
Lattice	FODO	
Cell length	5.5744	m
Beam Emittance	.478	$mm * mrad$
Energy Spread	0.092	%
Energy Loss/Turn	0.896	MeV
Tunes: ν_x	5.250	
ν_y	3.170	
Lattice Functions		
β_{xmax}	13.0	m
β_{ymax}	15.4	m
η_{xmax}	1.57	m
Natural Chromaticity		
ξ_x	-6.38	
ξ_y	-5.09	
RF frequency	358.53	MHz
Harmonic number	120	
Momentum Comp. Factor	0.05404	
Transverse damping time	2.241	msec
Vacuum chamber aperture		
x:(quad) (diameter)	50	mm
y:(bend) (height)	32	mm
Acceptance x:	69.4	mm * mrad
y:	22.4	mm * mrad

A more detailed compilation of the injector lattice and its parameters is attached in Appendix A.

A Appendix

Chapter A

Appendix

A: Appendix

A.1: Lattice Details

```
THIS VERSION OF PATRICIA ALLOWS :
                                A MAXIMUM OF  1000 ELEMENTS PER SUPERPERIOD
                                A MAXIMUM OF   200 DIFFERENT ELEMENTS AND
                                A MAXIMUM OF   300 MULTIPOLE MAGNETS PER SUPERPERIOD
*****************************************************************************************************************

                         INPUT-DATA FOR THE PROGRAM  PATRICIA

*****************************************************************************************************************

        3 GEV Booster,  C = 133 meter, (DECEMBER 29, 1987)

*****************************************************************************************************************

$PARAM
ENERGY  =   3.000000000000000     ,
EN0     =   2.000000000000000     ,
DEN     =  0.5000000000000000     ,
CHROMX  =  0.0000000000000000E+00,
CHROMY  =  0.0000000000000000E+00,
HARM    =         160,
NSUP    =           2,
SYM     = T,
DELMAX  =   3.000000000000000     ,
NHAR    =         200,
RFV     =  0.0000000000000000E+00,
TQU     =  2.7000000000000000E-03,
TRACE   = F,
BETX0   =   1.000000000000000     ,
ALX0    =  0.0000000000000000E+00,
ETAX0   =  0.0000000000000000E+00,
ETXP0   =  0.0000000000000000E+00,
BETY0   =   1.000000000000000     ,
ALY0    =  0.0000000000000000E+00,
ETAY0   =  0.0000000000000000E+00,
ETYP0   =  0.0000000000000000E+00,
PETROS  =  0.0000000000000000E+00,
PROTON  = F
$END
$TRP
TURNS   =        1000,
TRACK   = T,
TRSYN   = F,
OFFEN   = F,
DAMP    = F,
JPRINT  =           1,
PLOTS   =   4.000000000000000     ,
SPECT   = T,
SCALEB  =  0.0000000000000000E+00,
DYNAP   = T
$END
         1   1   1   1   1   1   1   0   0   0   0   0   0   0   0   0
       -47.62800  47.62800   0.00000  46.11700   6.00000
                 0    0 0           0.0000000D+00        0.0000000D+00  0.0  0.0   0.00000
       STRT      1    0 0           0.0000000D+00        0.0000000D+00  0.0  0.0   0.00000
         DR      1    0 0           0.0000000D+00        0.0000000D+00  0.0  0.0   0.00000
         L0      1    0 0           0.1625000D+00        0.0000000D+00  0.0  0.0   0.00000
         LB      1    0 0           0.2350000D+01        0.0000000D+00  0.0  0.0   0.00000
          B      2    0 1           0.2351275D+01       -0.1197495D+02 30.0 15.0   0.00000
        QDH      3    0 0           0.1500000D+00        0.1345690D+01 30.0 15.0   0.00000
        QFH      3    0 0           0.1900000D+00       -0.1299656D+01 30.0 15.0   0.00000
         SF      4    0 0           0.0000000D+00        0.0000000D+00  0.0  0.0   0.00000
         SD      4    0 0           0.0000000D+00        0.0000000D+00  0.0  0.0   0.00000
        SF1      4    0 0           0.0000000D+00        0.0000000D+00  0.0  0.0   0.00000
        END      0    0 0           0.0000000D+00        0.0000000D+00  0.0  0.0   0.00000
       STRT
         1   0   0   0   0   0   0   0   0   0   0   0   0   0   0   0   0   0   0   0
        QDH  L0  DR  L0   B  L0  L0 QFH
         1   1   1   1   1   1   1   1   0   0   0   0   0   0   0   0   0   0   0   0
        QFH  L0  SF  L0   B  L0  L0 QDH QDH  L0  SD  L0   B  L0  L0 QFH
         1   1   1   1   1   1   1   1   1   1   1   1   1   1   1   1   0   0   0   0
        QFH  L0  SF  L0   B  L0  L0 QDH QDH  L0  SD  L0   B  L0  L0 QFH
         1   1   1   1   1   1   1   1   1   1   1   1   1   1   1   1   0   0   0   0
        QFH  L0  SF  L0   B  L0  L0 QDH QDH  L0  SD  L0   B  L0  L0 QFH
```

```
   1    1    1    1    1    1    1    1    1    1    1    1    1    1    1    1    0    0    0    0
 QFH   LO   LO   LB   LO   LO  QDH  QDH   LO   DR   LO    B   LO   LO  QFH
   1    1    1    1    1    1    1    1    1    1    1    1    1    1    1    0    0    0    0    0
 QFH   LO   LO   LB   LO   LO  QDH
   1    1    1    1    1    1    1    0    0    0    0    0    0    0    0    0    0    0    0    0
   0.00000   0.00000   0.00000   0.00000   0.00000   0.00000   0.00000   0.00000
   0.00000
------------------------------------------------------------------REAL-TIME SO FAR =        2. SEC
```

*** PROGRAM P A T R I C I A 85.5 *** 12-MAR-88 09:12:03

3 GEV Booster, C = 133 meter, (DECEMBER 29, 1987)

** KW(1)= 1

LATTICE-PARAMETER UNITS: RHO(M),K(1/M**2),SM(1/M**2),FDRIF(M),LENGTH(M),LTOT(M)

NR	TYP	RHO-K-SM	GRADIENT	FDRIF	LENGTH	LTOT
1	STRT	0.0000000	0.0000000	0.00000	0.00000	0.00000
2	QDH	1.3456904	0.0000000	0.00000	0.15000	0.15000
3	LO	0.0000000	0.0000000	0.00000	0.16250	0.31250
4	DR	0.0000000	0.0000000	0.00000	0.00000	0.31250
5	LO	0.0000000	0.0000000	0.00000	0.16250	0.47500
6	B	-11.9749460	0.0000000	0.00000	2.35128	2.82628
7	LO	0.0000000	0.0000000	0.00000	0.16250	2.98878
8	LO	0.0000000	0.0000000	0.00000	0.16250	3.15128
9	QFH	-1.2996556	0.0000000	0.00000	0.19000	3.34128
10	QFH	-1.2996556	0.0000000	0.00000	0.19000	3.53128
11	LO	0.0000000	0.0000000	0.00000	0.16250	3.69378
12	SF	0.0000000	0.0000000	0.00000	0.00000	3.69378
13	LO	0.0000000	0.0000000	0.00000	0.16250	3.85628
14	B	-11.9749460	0.0000000	0.00000	2.35128	6.20755
15	LO	0.0000000	0.0000000	0.00000	0.16250	6.37005
16	LO	0.0000000	0.0000000	0.00000	0.16250	6.53255
17	QDH	1.3456904	0.0000000	0.00000	0.15000	6.68255
18	QDH	1.3456904	0.0000000	0.00000	0.15000	6.83255
19	LO	0.0000000	0.0000000	0.00000	0.16250	6.99505
20	SD	0.0000000	0.0000000	0.00000	0.00000	6.99505
21	LO	0.0000000	0.0000000	0.00000	0.16250	7.15755
22	B	-11.9749460	0.0000000	0.00000	2.35128	9.50883
23	LO	0.0000000	0.0000000	0.00000	0.16250	9.67133
24	LO	0.0000000	0.0000000	0.00000	0.16250	9.83383
25	QFH	-1.2996556	0.0000000	0.00000	0.19000	10.02383
26	QFH	-1.2996556	0.0000000	0.00000	0.19000	10.21383
27	LO	0.0000000	0.0000000	0.00000	0.16250	10.37633
28	SF	0.0000000	0.0000000	0.00000	0.00000	10.37633
29	LO	0.0000000	0.0000000	0.00000	0.16250	10.53883
30	B	-11.9749460	0.0000000	0.00000	2.35128	12.89010
31	LO	0.0000000	0.0000000	0.00000	0.16250	13.05260
32	LO	0.0000000	0.0000000	0.00000	0.16250	13.21510
33	QDH	1.3456904	0.0000000	0.00000	0.15000	13.36510
34	QDH	1.3456904	0.0000000	0.00000	0.15000	13.51510
35	LO	0.0000000	0.0000000	0.00000	0.16250	13.67760
36	SD	0.0000000	0.0000000	0.00000	0.00000	13.67760
37	LO	0.0000000	0.0000000	0.00000	0.16250	13.84010
38	B	-11.9749460	0.0000000	0.00000	2.35128	16.19138
39	LO	0.0000000	0.0000000	0.00000	0.16250	16.35388
40	LO	0.0000000	0.0000000	0.00000	0.16250	16.51638
41	QFH	-1.2996556	0.0000000	0.00000	0.19000	16.70638
42	QFH	-1.2996556	0.0000000	0.00000	0.19000	16.89638
43	LO	0.0000000	0.0000000	0.00000	0.16250	17.05888
44	SF	0.0000000	0.0000000	0.00000	0.00000	17.05888
45	LO	0.0000000	0.0000000	0.00000	0.16250	17.22138
46	B	-11.9749460	0.0000000	0.00000	2.35128	19.57265
47	LO	0.0000000	0.0000000	0.00000	0.16250	19.73515
48	LO	0.0000000	0.0000000	0.00000	0.16250	19.89765
49	QDH	1.3456904	0.0000000	0.00000	0.15000	20.04765
50	QDH	1.3456904	0.0000000	0.00000	0.15000	20.19765
51	LO	0.0000000	0.0000000	0.00000	0.16250	20.36015
52	SD	0.0000000	0.0000000	0.00000	0.00000	20.36015
53	LO	0.0000000	0.0000000	0.00000	0.16250	20.52265
54	B	-11.9749460	0.0000000	0.00000	2.35128	22.87393
55	LO	0.0000000	0.0000000	0.00000	0.16250	23.03643
56	LO	0.0000000	0.0000000	0.00000	0.16250	23.19893
57	QFH	-1.2996556	0.0000000	0.00000	0.19000	23.38893
58	QFH	-1.2996556	0.0000000	0.00000	0.19000	23.57893
59	LO	0.0000000	0.0000000	0.00000	0.16250	23.74143
60	LO	0.0000000	0.0000000	0.00000	0.16250	23.90393
61	LB	0.0000000	0.0000000	0.00000	2.35000	26.25393
62	LO	0.0000000	0.0000000	0.00000	0.16250	26.41643
63	LO	0.0000000	0.0000000	0.00000	0.16250	26.57893
64	QDH	1.3456904	0.0000000	0.00000	0.15000	26.72893
65	QDH	1.3456904	0.0000000	0.00000	0.15000	26.87893
66	LO	0.0000000	0.0000000	0.00000	0.16250	27.04143
67	DR	0.0000000	0.0000000	0.00000	0.00000	27.04143
68	LO	0.0000000	0.0000000	0.00000	0.16250	27.20393
69	B	-11.9749460	0.0000000	0.00000	2.35128	29.55520
70	LO	0.0000000	0.0000000	0.00000	0.16250	29.71770

71	LO	0.0000000	0.0000000	0.00000	0.16250	29.88020
72	QFH	-1.2996556	0.0000000	0.00000	0.19000	30.07020
73	QFH	-1.2996556	0.0000000	0.00000	0.19000	30.26020
74	LO	0.0000000	0.0000000	0.00000	0.16250	30.42270
75	LO	0.0000000	0.0000000	0.00000	0.16250	30.58520
76	LB	0.0000000	0.0000000	0.00000	2.35000	32.93520
77	LO	0.0000000	0.0000000	0.00000	0.16250	33.09770
78	LO	0.0000000	0.0000000	0.00000	0.16250	33.26020
79	QDH	1.3456904	0.0000000	0.00000	0.15000	33.41020

REAL-TIME SO FAR = 3. SEC

TRANSFORMATION MATRICES

MATRIX-X

0.70710958	1.02874762	0.11335524
-0.48602401	0.70710958	0.18810231
0.00000000	0.00000000	1.00000000

MATRIX-Y

0.85264340	6.48609089	0.00000000
-0.04208995	0.85264340	0.00000000
0.00000000	0.00000000	1.00000000

DP/P = 0.00000E+00

PERIODIC LATTICE FUNCTIONS

BETA-X =	1.45487 M	ALPHA-X =	0.00000
BETY-Y =	12.41373 M	ALPHA-Y =	0.00000
ETA-X =	0.38702 M	ETAP-X =	0.00000 RAD
ETA-Y =	0.00000 M	ETAP-Y =	0.00000 RAD

REAL-TIME SO FAR = 4. SEC

M I T T E L W E R T E
****
DP/P = 0.00000E+00

*** PROGRAM P A T R I C I A 85.5 ***

KW(2) = 1

DEFINITION: <FUNCT> = INTEGRAL OF FUNCT ALONG NSUP SUPERPERIODS DIVIDED BY TOTAL INTEGRATION LENGTH
CHROMATIC TERMS (SEE H.WIEDEMANN DESY H5/71-10)

ELECTRON STORAGE RING PARAMETERS

CIRCUMFERENCE (M)	133.64081	REVOLUTIONFREQUENCY (KHZ)	2243.27
RF-FREQUENCY (MHZ)	358.92330	HARMONIC NUMBER	160
MOMENTUM COMPACTION FACTOR	0.0334862	NAT.EMITTANCE(HORIZ)(RAD*M)	2.104E-08 * E(GEV))**2
ENERGYSPREAD (%)	0.0244191 * E(GEV)	TRANSITION ENERGY	5.46471
DAMPING PARTITION NUMBERS JS=	2.059		
JX=	0.941		
JY=	1.000		

RADIATION AND OTHER INTEGRALS (SEE R.H.HELM ET AL. SLAC-PUB-1193 AND H.WIEDEMANN PEP-NOTE 39 :)

<K*BETAX> =	-0.77960E+00	<-K*BETAY> =	0.55716E+00
<DX/R>+<DDX/R>*DP/P =	0.33486E-01	<BETAX =	5.1838 M
<1/R**2> =	0.39262E-02	<BETAY> =	6.4816 M
<1/R**3> =	0.32786E-03	<GAMAX> =	0.7621 1/M
<(GAMMAX*DX**2+BETAX*DPX**2+2*ALPHAX*DPX*DX)/R**3> =	0.52837E-04	<GAMAY> =	0.5572 1/M
<(GAMMAY*DY**2+BETAY*DPY**2+2*ALPHAY*DPY*DY)/R**3> =	0.00000E+00	<ETAX> =	0.6680 M
<2*K**2*DX**2>/<1/R**2> =	0.64769E+02	<ETAXP**2> =	0.37891E-01
<DX*(ISEC/R**3-2*K/R)> =	0.23352E-03	<ETAYP**2> =	0.00000E+00
<DY*(ISEC/R**3+2*K/R)> =	0.00000E+00	<(ETAX/R)**2> =	0.23689E-02
		<(ETAY/R)**2> =	0.00000E+00

MOMENTUM (GEV/C)	3.000	2.000	2.500	3.000	3.500	4.000	4.500	5.000	5.500
ENERGYLOSS/TURN (MEV)	0.598	0.118	0.289	0.598	1.109	1.891	3.029	4.617	6.760
RF-PHASE (DEGREE)	32.921	27.620	30.522	32.921	34.941	36.279	37.411	38.370	39.325
RF-VOLTAGE (MVOLT)	1.101	0.255	0.568	1.101	1.935	3.196	4.986	7.438	10.667
SYNCHR.FREQUENCY (KC)	36.358	22.015	28.984	36.358	44.105	52.573	61.453	70.744	80.236
SYNCHROTRON TUNE (1/1000)	16.208	9.814	12.921	16.208	19.661	23.436	27.395	31.536	35.767
QUANTUMLIFETIME (HOURS)	0.004	0.015	0.008	0.004	0.003	0.003	0.003	0.003	0.003
SYNCH-DAMP-TIME (MSEC)	2.170	7.325	3.751	2.170	1.367	0.916	0.643	0.469	0.352
BET-DAMP-TIME-HOR (MSEC)	4.753	16.040	8.213	4.753	2.993	2.005	1.408	1.027	0.771
BET-DAMP-TIME-VER (MSEC)	4.470	15.086	7.724	4.470	2.815	1.886	1.324	0.966	0.725
NAT.EMITTANCE (RAD*M)	1.89E-07	8.42E-08	1.32E-07	1.89E-07	2.58E-07	3.37E-07	4.26E-07	5.26E-07	6.37E-07
BUNCHLENGTH (MM)	32.193	35.444	33.652	32.193	30.961	29.685	28.570	27.575	26.744
BUNCHLENGTH (PSEC)	107.383	118.230	112.251	107.383	103.276	99.018	95.298	91.981	89.209
ENERGYSPREAD (PERCENT)	0.073	0.049	0.061	0.073	0.085	0.098	0.110	0.122	0.134

RING ACCEPTANCE FOR A MONOCHROMATIC BEAM IN MM*MRAD (DP/P = 0.000000)

EPSX-MAX =	74.02	LIMITED IN MAGNET	QFH AT J =	25	HALF APERTURE	30.00 MM
EPSY-MAX =	18.12	LIMITED IN MAGNET	QDH AT J =	79	HALF APERTURE	15.00 MM

REAL-TIME SO FAR = 10. SEC

REAL-TIME SO FAR = 10. SEC

B E A M - D Y N A M I C S - P A R A M E T E R

****

*** PROGRAM P A T R I C I A 85.5 ***

KW(3)= 1

DP/P = 0.00000E+00

UNITS OF BETA,ETA AND LENGTH ARE METERS;BSC IS FOR 10 SIGMA-TOT; PARAMETERS AT THE END OF ELEMENTS

MAGNET	J	BETAX	ALFAX	BSCX(MM)	ETAX	DNUEX	BETAY	ALFAY	BSCY(MM)	ETAY	DNUEY	TOT-L
STRT	1	1.45487	0.00000	5.96582	0.38702	0.00000	12.41373	0.00000	10.84186	0.00000	0.00000	0.0000
QDH	2	1.51499	−0.40483	6.08074	0.39290	0.01619	12.04344	2.44364	10.67893	0.00000	0.00194	0.1500
LO	3	1.66685	−0.52967	6.35594	0.40566	0.03249	11.26454	2.34958	10.32783	0.00000	0.00416	0.3125
DR	4	1.66685	−0.52967	6.35594	0.40566	0.03249	11.26454	2.34958	10.32783	0.00000	0.00416	0.3125
LO	5	1.85928	−0.65451	6.67881	0.41841	0.04720	10.51621	2.25551	9.97889	0.00000	0.00654	0.4750
B	6	8.98083	−2.33527	14.37041	0.82390	0.14407	3.10973	0.89447	5.42643	0.00000	0.07398	2.8263
LO	7	9.75877	−2.45204	15.00510	0.86701	0.14683	2.83432	0.80041	5.18056	0.00000	0.08269	2.9888
LO	8	10.57465	−2.56881	15.64339	0.91012	0.14937	2.58947	0.70634	4.95174	0.00000	0.09225	3.1513
QFH	9	11.05767	0.06652	16.02233	0.93886	0.15215	2.45721	0.00059	4.82363	0.00000	0.10434	3.3413
QFH	10	10.52566	2.68957	15.65654	0.92373	0.15493	2.58900	−0.70504	4.95130	0.00000	0.11643	3.5313
LO	11	9.67221	2.56245	15.02931	0.89208	0.15749	2.83341	−0.79901	5.17973	0.00000	0.12599	3.6938
SF	12	9.67221	2.56245	15.02931	0.89208	0.15749	2.83341	−0.79901	5.17973	0.00000	0.12599	3.6938
LO	13	8.86007	2.43533	14.40566	0.86042	0.16029	3.10836	−0.89297	5.42523	0.00000	0.13471	3.8563
B	14	1.63207	0.59914	7.17412	0.61895	0.26558	10.50445	−2.25259	9.97331	0.00000	0.20220	6.2076
LO	15	1.45934	0.46383	6.93465	0.61734	0.28237	11.25181	−2.34656	10.32200	0.00000	0.20458	6.3701
LO	16	1.33058	0.32852	6.74862	0.61572	0.30097	12.02971	−2.44052	10.67284	0.00000	0.20680	6.5326
QDH	17	1.28965	−0.05286	6.72981	0.62356	0.31933	12.39948	0.00030	10.83563	0.00000	0.20875	6.6826
QDH	18	1.36294	−0.44070	6.96481	0.65033	0.33747	12.02953	2.44110	10.67276	0.00000	0.21069	6.8326
LO	19	1.52931	−0.58308	7.38240	0.68983	0.35542	11.25145	2.34709	10.32183	0.00000	0.21292	6.9951
SD	20	1.52931	−0.58308	7.38240	0.68983	0.35542	11.25145	2.34709	10.32183	0.00000	0.21292	6.9951
LO	21	1.74195	−0.72547	7.84441	0.72932	0.37129	10.50392	2.25309	9.97306	0.00000	0.21530	7.1576
B	22	9.78236	−2.65007	17.55404	1.51321	0.46703	3.10684	0.89290	5.42390	0.00000	0.28281	9.5088
LO	23	10.66529	−2.78334	18.33695	1.58172	0.46956	2.83192	0.79890	5.17837	0.00000	0.29153	9.6713
LO	24	11.59153	−2.91661	19.12243	1.65023	0.47189	2.58756	0.70489	4.94991	0.00000	0.30109	9.8338
QFH	25	12.15925	−0.02453	19.58969	1.69114	0.47442	2.45577	−0.00044	4.82221	0.00000	0.31319	10.0238
QFH	26	11.60959	2.87209	19.14433	1.65302	0.47694	2.58790	−0.70585	4.95024	0.00000	0.32530	10.2138
LO	27	10.69720	2.74263	18.37727	1.58687	0.47926	2.83259	−0.79993	5.17898	0.00000	0.33485	10.3763
SF	28	10.69720	2.74263	18.37727	1.58687	0.47926	2.83259	−0.79993	5.17898	0.00000	0.33485	10.3763
LO	29	9.82688	2.61318	17.61276	1.52072	0.48179	3.10786	−0.89401	5.42479	0.00000	0.34357	10.5388
B	30	1.82572	0.74588	8.15092	0.77052	0.57477	10.51260	−2.25524	9.97717	0.00000	0.41105	12.8901
LO	31	1.60581	0.60736	7.69871	0.73332	0.58990	11.26084	−2.34932	10.32614	0.00000	0.41342	13.0526
LO	32	1.43093	0.46884	7.28725	0.69611	0.60699	12.03966	−2.44339	10.67725	0.00000	0.41565	13.2151
QDH	33	1.35056	0.07235	7.05855	0.67216	0.62428	12.40999	−0.00053	10.84022	0.00000	0.41759	13.3651
QDH	34	1.38664	−0.31530	7.08879	0.66861	0.64185	12.03997	2.44240	10.67739	0.00000	0.41953	13.5151
LO	35	1.51005	−0.44413	7.28705	0.67572	0.65976	11.26147	2.34839	10.32642	0.00000	0.42175	13.6776
SD	36	1.51005	−0.44413	7.28705	0.67572	0.65976	11.26147	2.34839	10.32642	0.00000	0.42175	13.6776
LO	37	1.67533	−0.57297	7.53324	0.68283	0.67605	10.51351	2.25438	9.97761	0.00000	0.42413	13.8401
B	38	8.56456	−2.31927	14.69972	1.00204	0.78183	3.11049	0.89413	5.42709	0.00000	0.49157	16.1914
LO	39	9.33799	−2.44030	15.32211	1.03891	0.78472	2.83518	0.80012	5.18134	0.00000	0.50028	16.3539
LO	40	10.15075	−2.56134	15.94815	1.07578	0.78738	2.59041	0.70611	4.95264	0.00000	0.50983	16.5164
QFH	41	10.65152	−0.03296	16.30583	1.09342	0.79026	2.45828	0.00017	4.82468	0.00000	0.52192	16.7064
QFH	42	10.17502	2.50151	15.90562	1.05995	0.79314	2.59028	−0.70575	4.95252	0.00000	0.53401	16.8964
LO	43	9.38087	2.38561	15.24380	1.00975	0.79579	2.83492	−0.79973	5.18111	0.00000	0.54356	17.0589
SF	44	9.38087	2.38561	15.24380	1.00975	0.79579	2.83492	−0.79973	5.18111	0.00000	0.54356	17.0589
LO	45	8.62438	2.26970	14.58567	0.95956	0.79867	3.11010	−0.89371	5.42675	0.00000	0.55227	17.2214

MAGNET	J	BETAX	ALFAX	BSCX(MM)	ETAX	DNUEX	BETAY	ALFAY	BSCY(MM)	ETAY	DNUEY	TOT-L
B	46	1.78789	0.60041	6.68617	0.44955	0.90008	10.51020	-2.25356	9.97604	0.00000	0.61973	19.5727
LO	47	1.61285	0.47675	6.35950	0.42948	0.91533	11.25788	-2.34754	10.32478	0.00000	0.62211	19.7352
LO	48	1.47800	0.35310	6.08160	0.40941	0.93211	12.03610	-2.44152	10.67568	0.00000	0.62433	19.8977
QDH	49	1.43242	-0.04616	5.96538	0.39701	0.94863	12.40598	0.00061	10.83847	0.00000	0.62627	20.0477
QDH	50	1.50626	-0.45107	6.08021	0.39665	0.96500	12.03574	2.44268	10.67552	0.00000	0.62822	20.1977
LO	51	1.67395	-0.58090	6.35663	0.40276	0.98131	11.25716	2.34862	10.32445	0.00000	0.63044	20.3602
SD	52	1.67395	-0.58090	6.35663	0.40276	0.98131	11.25716	2.34862	10.32445	0.00000	0.63044	20.3602
LO	53	1.88384	-0.71073	6.68188	0.40886	0.99590	10.50914	2.25456	9.97553	0.00000	0.63282	20.5227
B	54	9.42982	-2.45723	14.36372	0.71888	1.08940	3.10704	0.89356	5.42408	0.00000	0.70031	22.8739
LO	55	10.24813	-2.57851	14.99034	0.75549	1.09203	2.83192	0.79950	5.17837	0.00000	0.70903	23.0364
LO	56	11.10585	-2.69979	15.62032	0.79210	1.09446	2.58737	0.70544	4.94973	0.00000	0.71859	23.1989
QFH	57	11.61355	0.06963	15.98990	0.81606	1.09710	2.45536	0.00015	4.82181	0.00000	0.73070	23.3889
QFH	58	11.05457	2.82619	15.61602	0.80188	1.09975	2.58725	-0.70512	4.94962	0.00000	0.74280	23.5789
LO	59	10.15752	2.69408	14.98242	0.77351	1.10219	2.83169	-0.79916	5.17816	0.00000	0.75236	23.7414
LO	60	9.30342	2.56197	14.35219	0.74514	1.10485	3.10670	-0.89319	5.42378	0.00000	0.76108	23.9039
LB	61	1.75196	0.65142	6.26059	0.33482	1.20373	10.50047	-2.25309	9.97142	0.00000	0.82857	26.2539
LO	62	1.56172	0.51930	5.88352	0.30645	1.21939	11.24801	-2.34713	10.32025	0.00000	0.83095	26.4164
LO	63	1.41441	0.38719	5.56202	0.27808	1.23683	12.02611	-2.44117	10.67124	0.00000	0.83318	26.5789
QDH	64	1.35763	-0.00485	5.40623	0.25598	1.25418	12.39618	-0.00108	10.83419	0.00000	0.83512	26.7289
QDH	65	1.41738	-0.39749	5.47505	0.24164	1.27151	12.02674	2.43914	10.67152	0.00000	0.83707	26.8789
LO	66	1.56814	-0.53025	5.70440	0.23015	1.28889	11.24928	2.34524	10.32083	0.00000	0.83929	27.0414
DR	67	1.56814	-0.53025	5.70440	0.23015	1.28889	11.24928	2.34524	10.32083	0.00000	0.83929	27.0414
LO	68	1.76205	-0.66301	5.99462	0.21865	1.30447	10.50233	2.25135	9.97230	0.00000	0.84167	27.2039
B	69	9.19234	-2.45638	13.35182	0.27929	1.40304	3.10979	0.89271	5.42648	0.00000	0.90915	29.5552
LO	70	10.01087	-2.58073	13.94233	0.29914	1.40574	2.83492	0.79881	5.18111	0.00000	0.91787	29.7177
LO	71	10.86981	-2.70507	14.53663	0.31899	1.40822	2.59056	0.70491	4.95279	0.00000	0.92742	29.8802
QFH	72	11.39102	0.00490	14.89062	0.33456	1.41091	2.45888	-0.00105	4.82527	0.00000	0.93951	30.0702
QFH	73	10.86621	2.71396	14.55298	0.33450	1.41361	2.59139	-0.70721	4.95357	0.00000	0.95159	30.2602
LO	74	10.00450	2.58886	13.97243	0.32771	1.41609	2.83652	-0.80129	5.18257	0.00000	0.96114	30.4227
LO	75	9.18345	2.46375	13.39565	0.32092	1.41879	3.11222	-0.89536	5.42860	0.00000	0.96984	30.5852
LB	76	1.85543	0.65455	6.14816	0.22271	1.51518	10.51737	-2.25577	9.97944	0.00000	1.03721	32.9352
LO	77	1.66303	0.52945	5.83064	0.21591	1.52993	11.26578	-2.34984	10.32840	0.00000	1.03959	33.0977
LO	78	1.51128	0.40435	5.56486	0.20912	1.54627	12.04476	-2.44391	10.67952	0.00000	1.04181	33.2602
QDH	79	1.45124	0.00000	5.45535	0.20600	1.56250	12.41510	0.00000	10.84245	0.00000	1.04375	33.4102

****

TUNES NUEX = 6.25000 NUEY = 4.17500 DP/P = 0.00000E+00

****

REAL-TIME SO FAR = 12. SEC.

3 GEV Booster, C = 133 meter, (DECEMBER 29, 1987)

**** MULTIPOLE-STRUCTURE IN ONE HALF-SUPERPERIOD ****

	J	MULTIPOLE	<BETX(M)>	<BETY(M)>	<PHIX>	<PHIY>	<ETAX(M)>	SM(1/M**2)
1. MULTIPOLE AT: J =	12	SF	9.672	2.833	0.157	0.126	0.892	-0.84893
2. MULTIPOLE AT: J =	20	SD	1.529	11.251	0.355	0.213	0.690	1.35678
3. MULTIPOLE AT: J =	28	SF	10.697	2.833	0.479	0.335	1.587	-0.84893
4. MULTIPOLE AT: J =	36	SD	1.510	11.261	0.660	0.422	0.676	1.35678
5. MULTIPOLE AT: J =	44	SF	9.381	2.835	0.796	0.544	1.010	-0.84893
6. MULTIPOLE AT: J =	52	SD	1.674	11.257	0.981	0.630	0.403	1.35678

TOTAL NUMBER OF MULTIPOLES IN STORAGE RING: 24

	WITHOUT SEXTUPOLES		WITH SPEC.SEXTUPOLES		WITH ALL SEXTUPOLES		CHROMATICITY WANTED	
CHROMATICITY IN X =	-8.291	*	-8.291	*	0.000	*	0.000	*
CHROMATICITY IN Y =	-5.925	*	-5.925	*	0.000	*	0.000	*

TOTAL CORRECTED CHROMATICITY

POSITIVE SEXTUPOLES: DCHX = -1.18746 DCHY = 8.59653
NEGATIVE SEXTUPOLES: DCHX = 9.47832 DCHY = -2.67120

REAL-TIME SO FAR = 13. SEC

BETA(DP/P)/BETA(DP/P=0) AT THE REF.POINT : (J=1) 12 SEXTUPOLES PER SUPERPERIOD *** PROGRAM P A T R I C I A 85.5 ***

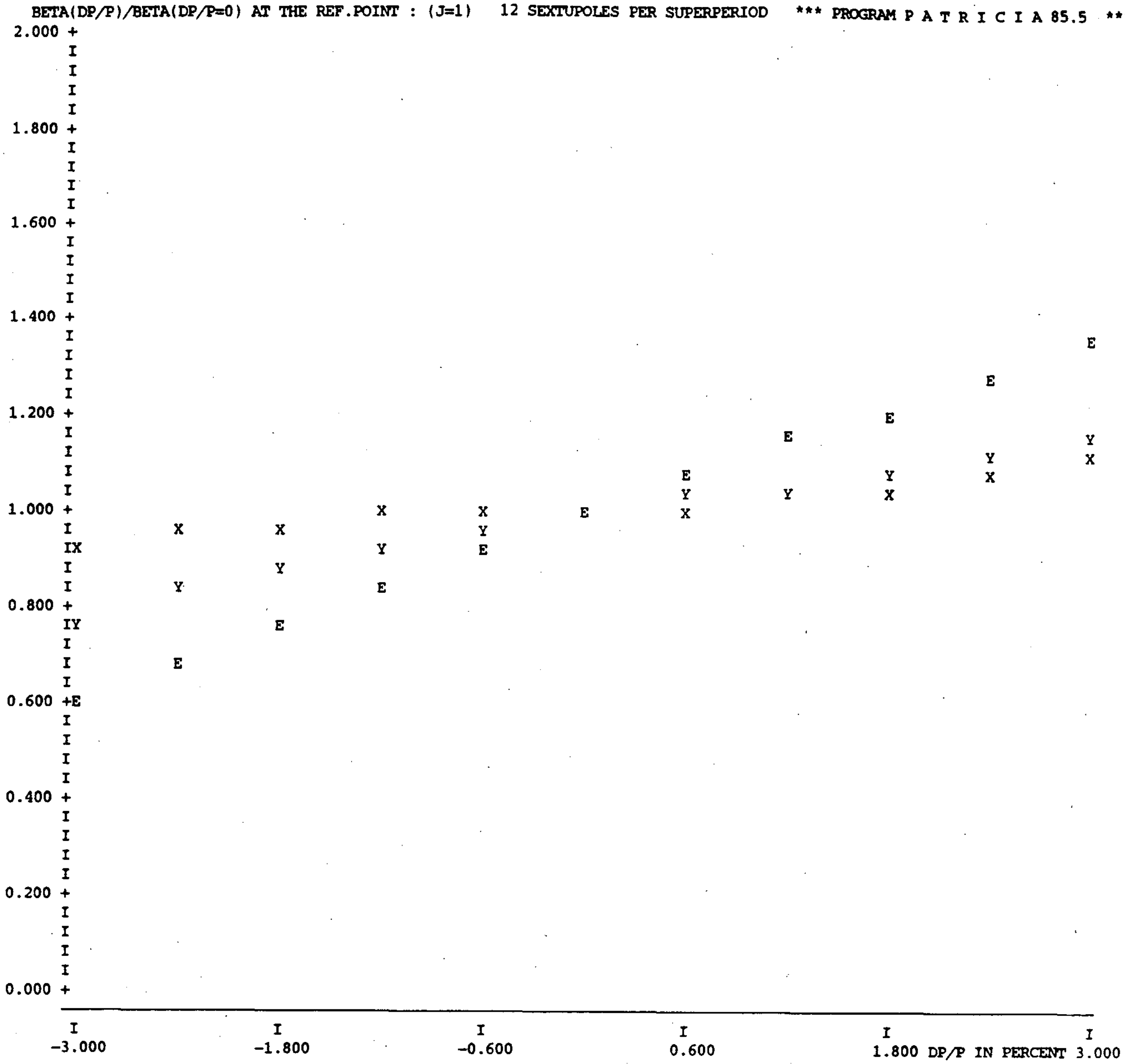

BETX0	1.3654	1.3948	1.4165	1.4321	1.4439	1.4549	1.4684	1.4881	1.5180	1.5630	1.6301
BETY0	9.6547	10.4440	11.0786	11.5960	12.0311	12.4137	12.7682	13.1138	13.4658	13.8369	14.2385
ETAX0	0.2399	0.2690	0.2987	0.3285	0.3580	0.3870	0.4154	0.4432	0.4706	0.4979	0.5255
ETAY0	0.0000	0.0000	0.0000	0.0000	0.0000	0.0000	0.0000	0.0000	0.0000	0.0000	0.0000

NONINTEGRAL PART OF THE TUNE VS. MOMENTUM   12 MULTIPOLES PER SUPERPERIOD   *** PROGRAM P A T R I C I A 85.5 ***

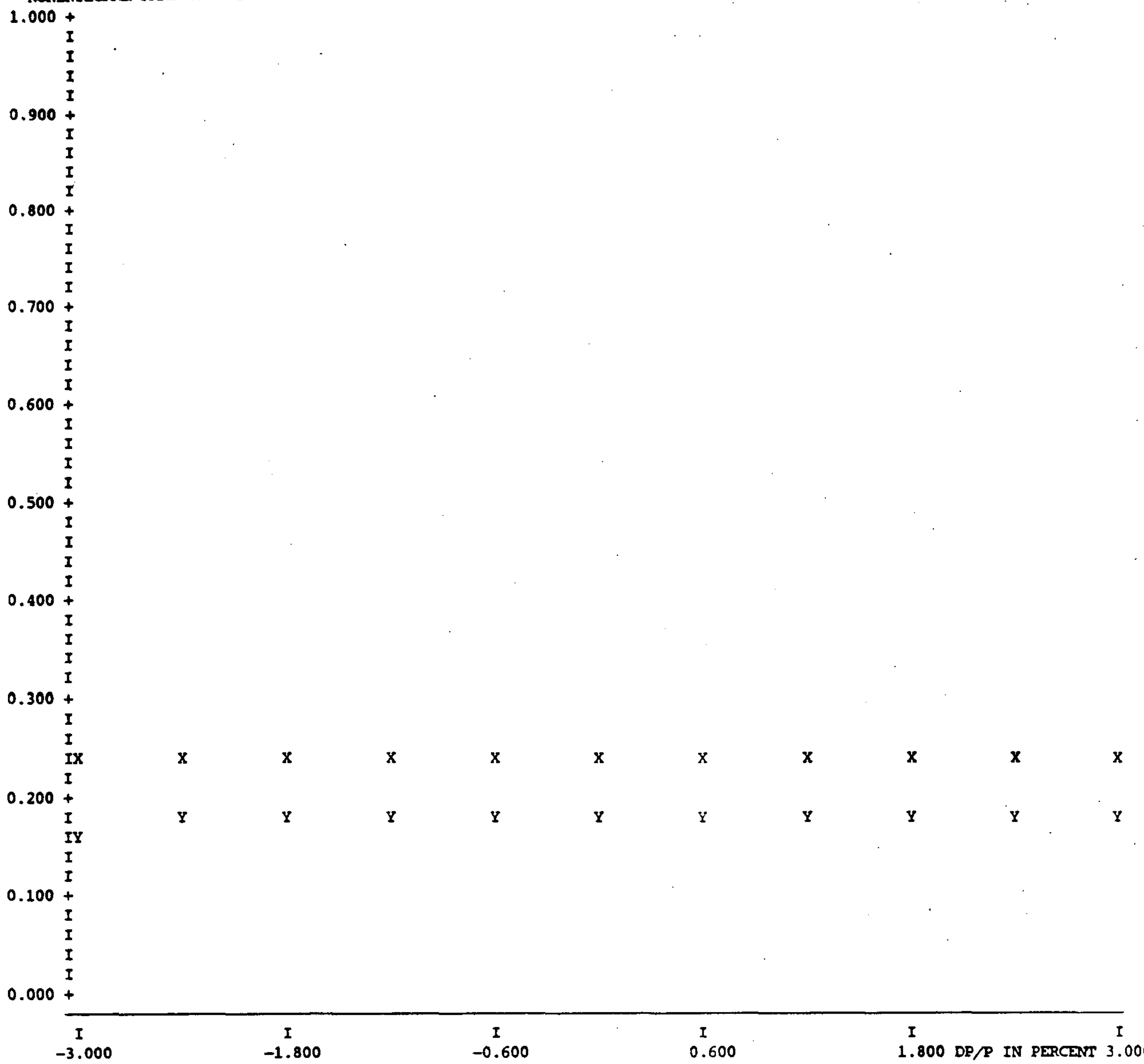

NUEX	0.2466	0.2477	0.2487	0.2495	0.2499	0.2500	0.2498	0.2491	0.2481	0.2462	0.2431
NUEY	0.1659	0.1704	0.1729	0.1743	0.1749	0.1750	0.1749	0.1747	0.1744	0.1740	0.1736

REAL-TIME SO FAR = 192. SEC

REAL-TIME SO FAR = 192. SEC

*** BEAM DYNAMICS PARAMETER AVERAGED OVER MAGNET*** KW(7)= 1

J	MAGNET	<BETAX>	<BETAY>	<PHIX>	<PHIY>	<ETA>	<ETAP>	FMST	FL(M)
1	STRT	1.45487	12.41373	0.00000	0.00000	0.38702	0.00000	0.00000	0.00000
2	QDH	1.47483	12.28980	0.00815	0.00097	0.38898	0.03916	1.34569	0.15000
3	LO	1.58754	11.65144	0.02447	0.00304	0.39928	0.07852	0.00000	0.16250
4	DR	1.66685	11.26454	0.03249	0.00416	0.40566	0.07852	0.00000	0.00000
5	LO	1.75968	10.88783	0.03998	0.00534	0.41204	0.07852	0.00000	0.16250
6	B	4.75970	6.27961	0.10825	0.03346	0.58454	0.17245	-11.97495	2.35128
7	LO	9.36664	2.96948	0.14547	0.07827	0.84545	0.26528	0.00000	0.16250
8	LO	10.16355	2.70935	0.14812	0.08740	0.88856	0.26528	0.00000	0.16250
9	QFH	10.89987	2.50106	0.15077	0.09824	0.92812	0.15128	-1.29966	0.19000
10	QFH	10.87499	2.50083	0.15353	0.11044	0.93495	-0.07965	-1.29966	0.19000
11	LO	10.09549	2.70866	0.15619	0.12128	0.90790	-0.19478	0.00000	0.16250
12	SF	9.67221	2.83341	0.15749	0.12599	0.89208	-0.19478	-0.84893	0.00000
13	LO	9.26270	2.96834	0.15887	0.13042	0.87625	-0.19478	0.00000	0.16250
14	B	4.52465	6.27360	0.19821	0.17526	0.70345	-0.10270	-11.97495	2.35128
15	LO	1.54204	10.87559	0.27382	0.20341	0.61814	-0.00996	0.00000	0.16250
16	LO	1.39130	11.63822	0.29153	0.20571	0.61653	-0.00996	0.00000	0.16250
17	QDH	1.30060	12.27574	0.31010	0.20778	0.61808	0.05229	1.34569	0.15000
18	QDH	1.31662	12.27565	0.32848	0.20972	0.63534	0.17847	1.34569	0.15000
19	LO	1.44227	11.63795	0.34661	0.21179	0.67008	0.24305	0.00000	0.16250
20	SD	1.52931	11.25145	0.35542	0.21292	0.68983	0.24305	1.35678	0.00000
21	LO	1.63177	10.87514	0.36353	0.21409	0.70957	0.24305	0.00000	0.16250
22	B	5.00600	6.27235	0.43277	0.24224	1.08626	0.33339	-11.97495	2.35128
23	LO	10.22021	2.96684	0.46832	0.28710	1.54747	0.42159	0.00000	0.16250
24	LO	11.12480	2.70720	0.47074	0.29624	1.61597	0.42159	0.00000	0.16250
25	QFH	11.96726	2.49940	0.47316	0.30709	1.67725	0.21534	-1.29966	0.19000
26	QFH	11.97644	2.49957	0.47567	0.31930	1.67865	-0.20063	-1.29966	0.19000
27	LO	11.14989	2.70770	0.47809	0.33015	1.61995	-0.40710	0.00000	0.16250
28	SF	10.69720	2.83259	0.47926	0.33485	1.58687	-0.40710	-0.84893	0.00000
29	LO	10.25853	2.96768	0.48051	0.33928	1.55379	-0.40710	0.00000	0.16250
30	B	5.09266	6.27679	0.51538	0.38412	1.11069	-0.31906	-11.97495	2.35128
31	LO	1.71201	10.88417	0.58217	0.41225	0.75192	-0.22896	0.00000	0.16250
32	LO	1.51462	11.64770	0.59828	0.41455	0.71471	-0.22896	0.00000	0.16250
33	QDH	1.38086	12.28602	0.61555	0.41662	0.68241	-0.15969	1.34569	0.15000
34	QDH	1.35893	12.28618	0.63311	0.41856	0.66870	-0.02367	1.34569	0.15000
35	LO	1.44486	11.64817	0.65094	0.42063	0.67216	0.04376	0.00000	0.16250
36	SD	1.51005	11.26147	0.65976	0.42175	0.67572	0.04376	1.35678	0.00000
37	LO	1.58920	10.88494	0.66805	0.42293	0.67927	0.04376	0.00000	0.16250
38	B	4.43384	6.27895	0.74323	0.45105	0.80653	0.13576	-11.97495	2.35128
39	LO	8.94799	2.97029	0.78329	0.49586	1.02048	0.22689	0.00000	0.16250
40	LO	9.74109	2.71025	0.78607	0.50499	1.05735	0.22689	0.00000	0.16250
41	QFH	10.48146	2.50206	0.78883	0.51582	1.08886	0.09281	-1.29966	0.19000
42	QFH	10.49378	2.50200	0.79169	0.52802	1.08091	-0.17614	-1.29966	0.19000
43	LO	9.77481	2.71006	0.79445	0.53886	1.03485	-0.30890	0.00000	0.16250
44	SF	9.38087	2.83492	0.79579	0.54356	1.00975	-0.30890	-0.84893	0.00000
45	LO	8.99948	2.96997	0.79721	0.54798	0.98465	-0.30890	0.00000	0.16250
46	B	4.55028	6.27726	0.83616	0.59280	0.66821	-0.21690	-11.97495	2.35128
47	LO	1.69702	10.88150	0.90758	0.62093	0.43952	-0.12351	0.00000	0.16250
48	LO	1.54207	11.64445	0.92360	0.62323	0.41945	-0.12351	0.00000	0.16250
49	QDH	1.44524	12.28222	0.94033	0.62530	0.40220	-0.08271	1.34569	0.15000
50	QDH	1.45923	12.28204	0.95689	0.62724	0.39583	-0.00237	1.34569	0.15000
51	LO	1.58659	11.64390	0.97330	0.62931	0.39970	0.03757	0.00000	0.16250
52	SD	1.67395	11.25716	0.98131	0.63044	0.40276	0.03757	1.35678	0.00000
53	LO	1.77538	10.88060	0.98875	0.63161	0.40581	0.03757	0.00000	0.16250
54	B	4.97065	6.27475	1.05509	0.65975	0.52707	0.13185	-11.97495	2.35128
55	LO	9.83569	2.96693	1.09074	0.70460	0.73719	0.22528	0.00000	0.16250
56	LO	10.67370	2.70709	1.09326	0.71374	0.77379	0.22528	0.00000	0.16250
57	QFH	11.44767	2.49910	1.09579	0.72459	0.80724	0.12611	-1.29966	0.19000
58	QFH	11.42162	2.49904	1.09841	0.73680	0.81215	-0.07462	-1.29966	0.19000
59	LO	10.60247	2.70692	1.10095	0.74765	0.78769	-0.17460	0.00000	0.16250
60	LO	9.72689	2.96665	1.10350	0.75679	0.75932	-0.17460	0.00000	0.16250
61	LB	4.77939	6.27096	1.14068	0.80163	0.53998	-0.17460	0.00000	2.35000
62	LO	1.65326	10.87169	1.21141	0.82978	0.32064	-0.17460	0.00000	0.16250
63	LO	1.48449	11.63451	1.22797	0.83208	0.29226	-0.17460	0.00000	0.16250
64	QDH	1.37624	12.27227	1.24544	0.83415	0.26636	-0.14735	1.34569	0.15000
65	QDH	1.37771	12.27259	1.26291	0.83609	0.24818	-0.09555	1.34569	0.15000
66	LO	1.48917	11.63546	1.28035	0.83817	0.23590	-0.07074	0.00000	0.16250
67	DR	1.56814	11.24928	1.28889	0.83929	0.23015	-0.07074	0.00000	0.00000
68	LO	1.66150	10.87326	1.29683	0.84047	0.22440	-0.07074	0.00000	0.16250
69	B	4.77260	6.27364	1.36720	0.86861	0.21115	0.02579	-11.97495	2.35128
70	LO	9.59824	2.96981	1.40441	0.91344	0.28921	0.12215	0.00000	0.16250
71	LO	10.43698	2.71020	1.40699	0.92257	0.30906	0.12215	0.00000	0.16250
72	QFH	11.21650	2.50244	1.40958	0.93341	0.32806	0.08196	-1.29966	0.19000
73	QFH	11.21467	2.50284	1.41225	0.94560	0.33584	-0.00033	-1.29966	0.19000
74	LO	10.43196	2.71140	1.41483	0.95643	0.33110	-0.04179	0.00000	0.16250
75	LO	9.59058	2.97182	1.41742	0.96556	0.32431	-0.04179	0.00000	0.16250
76	LB	4.81083	6.28197	1.45426	1.01032	0.27181	-0.04179	0.00000	2.35000
77	LO	1.75584	10.88902	1.52242	1.03841	0.21931	-0.04179	0.00000	0.16250

78	LO	1.58377	11.65272	1.53797	1.04071	0.21252	−0.04179	0.00000	0.16250
79	QDH	1.47117	12.29115	1.55433	1.04278	0.20704	−0.02084	1.34569	0.15000

BETA VARIATION WITH MOMENTUM : (DBETA/BETA)/(DP/P) VS. PHASE

*** PROGRAM P A T R I C I A 85.5 ***

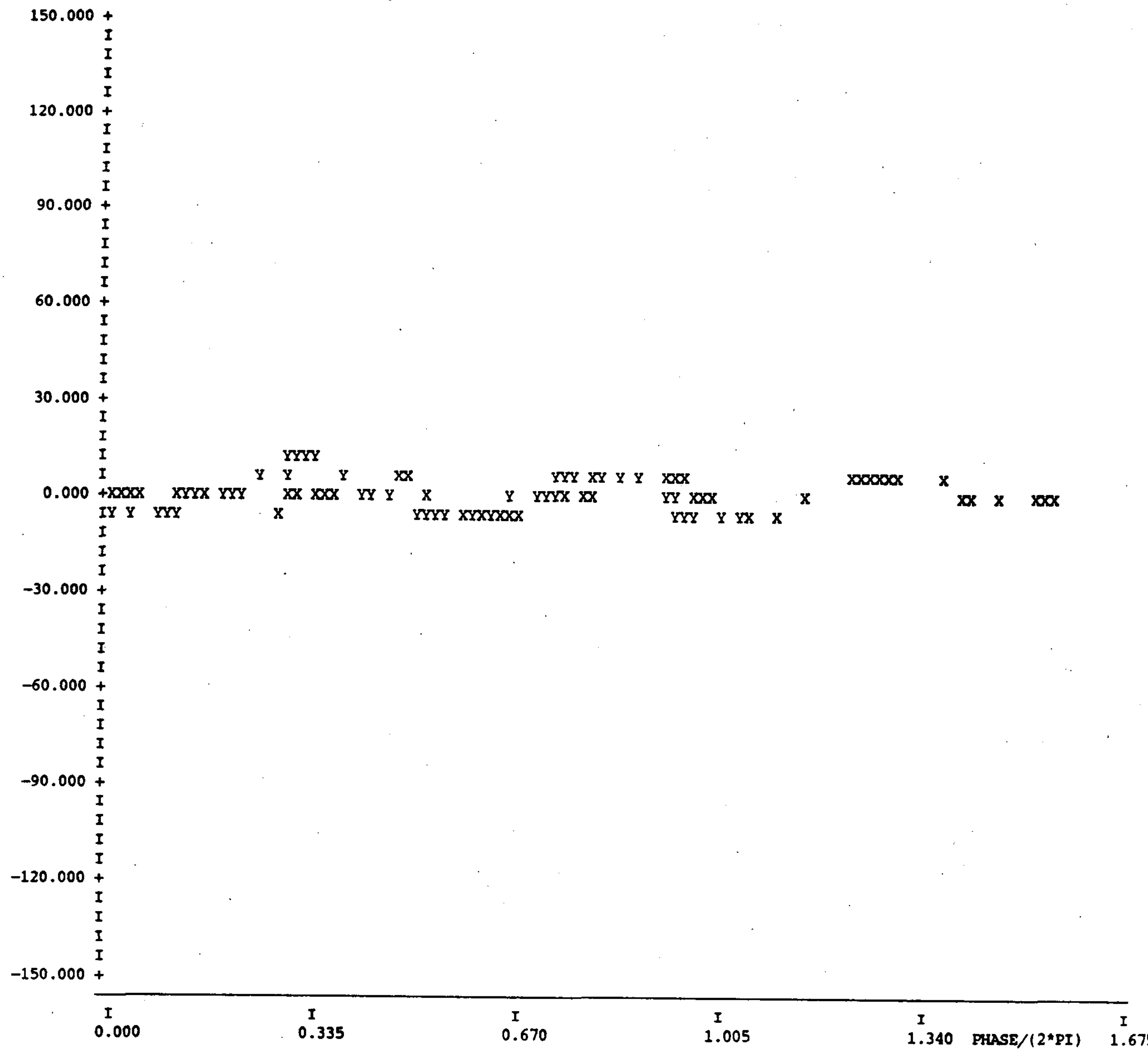

ETA-VARIATION WITH MOMENTUM (LINEAR TERM IN DP/P)VS PHASE *** PROGRAM P A T R I C I A 85.5 ***

*** MOMENTUM COMPACTION FACTOR: AC = 3.34862E-02 + 1.72481E-03*(DP/P) ***

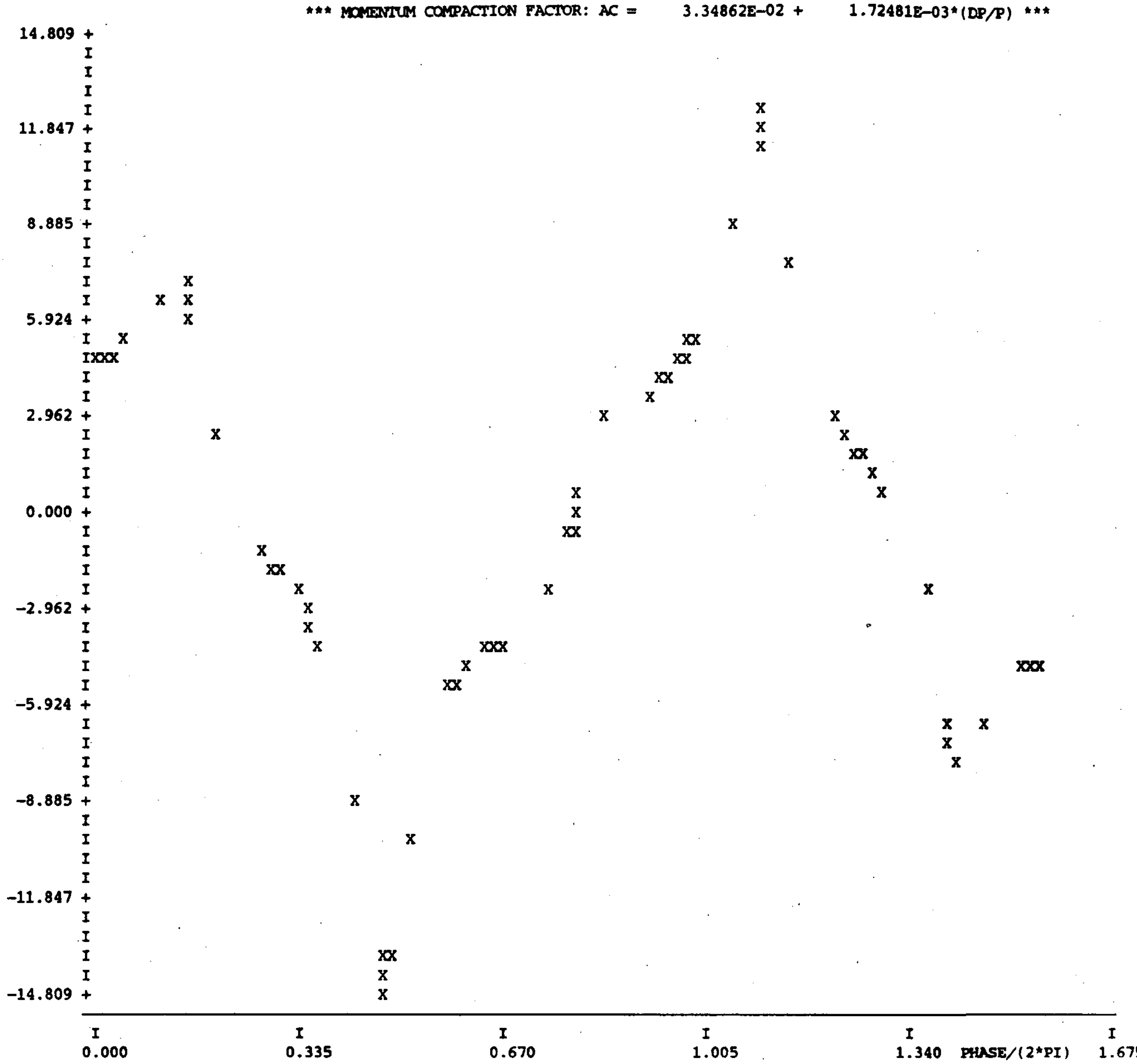

REAL-TIME SO FAR = 221. SEC
REAL-TIME SO FAR = 221. SEC
REAL-TIME SO FAR = 221. SEC

3 GEV Booster, C = 133 meter, (DECEMBER 29, 1987)

**** D Y N A M I C - A P E R T U R E (at J = 1) ****

AMPLITUDES IN SIGMA. (1000 TURNS ; DP/P= 0.00000 % ; SIGMAX= 0.52490 MM SIGMAY= 1.08419 MM)

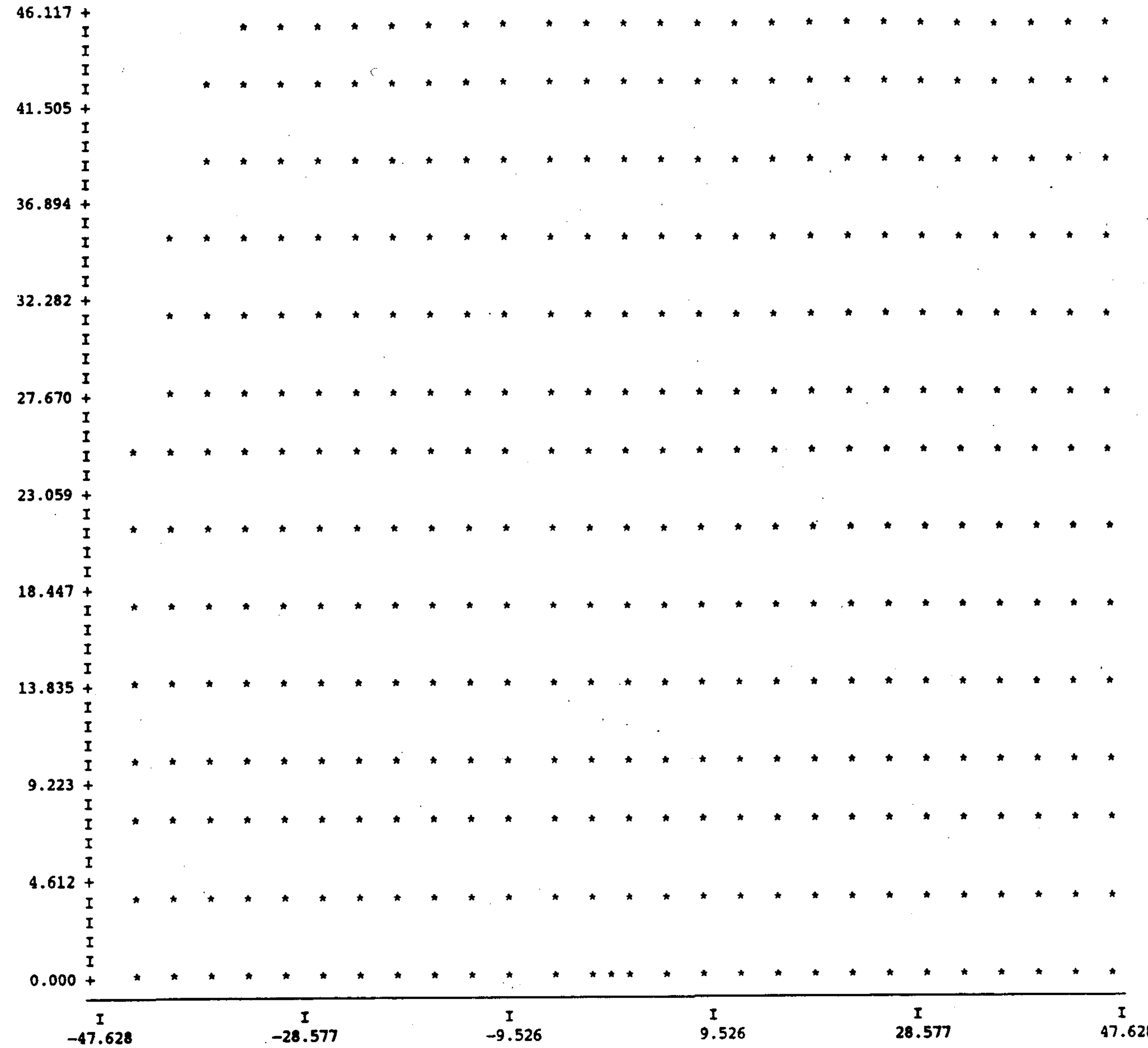

*** PROGRAM P A T R I C I A 85.5 *** 12-MAR-88 09:41:45

3 GEV Booster, C = 133 meter, (DECEMBER 29, 1987)

**** D Y N A M I C - A P E R T U R E (at J = 1) ****

AMPLITUDES IN MM . (1000 TURNS ; DP/P= 0.00000 % ; SIGMAX= 0.52490 MM SIGMAY= 1.08419 MM)

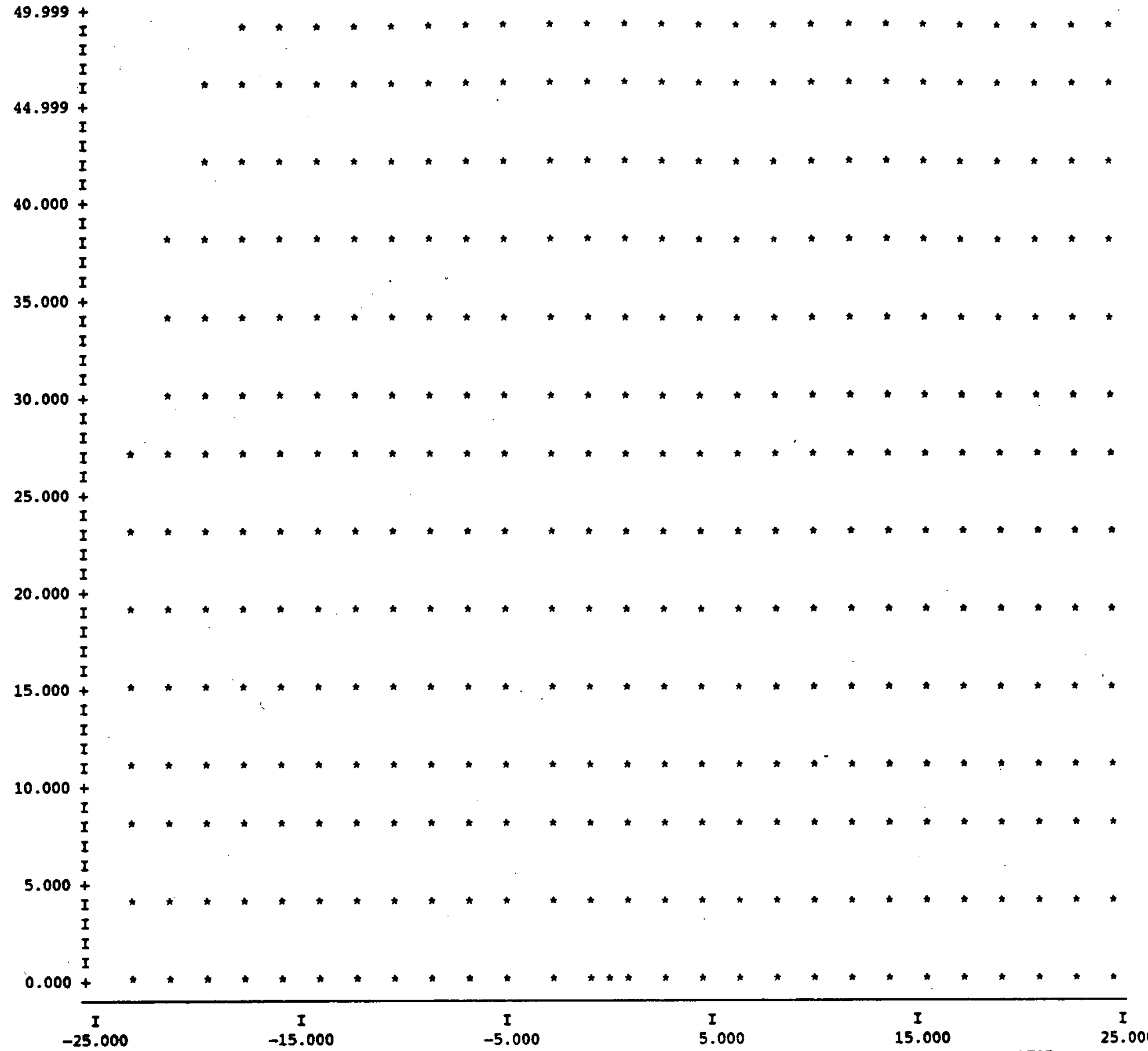

REAL-TIME SO FAR = 1785. SEC

A.2: Geometry of the Booster Ring

5 GeV BOOSTER RING FOR SPEAR (Version Dec 9) "MAD" VERSION: 2.03 RUN: 3/12/88 09:12:22

SURVEY OF BEAM LINE "RING"

ELEMENT			SEQUENCE		POSITIONS			ANGLES		
POS. NO.	ELEMENT NAME	OCC. NO.	SUM(L) [M]	ARC [M]	X [M]	Y [M]	Z [M]	PHI [RAD]	THETA [RAD]	PSI [RAD]
BEGIN	RING	1	0.000000	0.000000	0.000000	0.000000	0.000000	0.000000	0.000000	0.000000
1	QDH	1	0.150000	0.150000	0.000000	0.150000	0.000000	0.000000	0.000000	0.000000
2	L1	1	0.475000	0.475000	0.000000	0.475000	0.000000	0.000000	0.000000	0.000000
3	B	1	2.826275	2.826275	−0.230095	2.811196	0.000000	0.196350	0.000000	0.000000
4	L1	2	3.151275	3.151275	−0.293500	3.129951	0.000000	0.196350	0.000000	0.000000
5	QFH	1	3.341275	3.341275	−0.330567	3.316301	0.000000	0.196350	0.000000	0.000000
6	QFH	2	3.531275	3.531275	−0.367634	3.502650	0.000000	0.196350	0.000000	0.000000
7	L1	3	3.856275	3.856275	−0.431038	3.821405	0.000000	0.196350	0.000000	0.000000
8	B	2	6.207550	6.207550	−1.112482	6.067822	0.000000	0.392699	0.000000	0.000000
9	L1	4	6.532550	6.532550	−1.236854	6.368083	0.000000	0.392699	0.000000	0.000000
10	QDH	2	6.682550	6.682550	−1.294256	6.506665	0.000000	0.392699	0.000000	0.000000
11	QDH	3	6.832550	6.832550	−1.351659	6.645247	0.000000	0.392699	0.000000	0.000000
12	L1	5	7.157550	7.157550	−1.476031	6.945508	0.000000	0.392699	0.000000	0.000000
13	B	3	9.508826	9.508826	−2.582635	9.015818	0.000000	0.589049	0.000000	0.000000
14	L1	6	9.833826	9.833826	−2.763195	9.286046	0.000000	0.589049	0.000000	0.000000
15	QFH	3	10.023826	10.023826	−2.868753	9.444025	0.000000	0.589049	0.000000	0.000000
16	QFH	4	10.213826	10.213826	−2.974312	9.602004	0.000000	0.589049	0.000000	0.000000
17	L1	7	10.538826	10.538826	−3.154872	9.872232	0.000000	0.589049	0.000000	0.000000
18	B	4	12.890101	12.890101	−4.644110	11.686874	0.000000	0.785398	0.000000	0.000000
19	L1	8	13.215101	13.215101	−4.873920	11.916684	0.000000	0.785398	0.000000	0.000000
20	QDH	4	13.365101	13.365101	−4.979986	12.022750	0.000000	0.785398	0.000000	0.000000
21	QDH	5	13.515101	13.515101	−5.086052	12.128816	0.000000	0.785398	0.000000	0.000000
22	L1	9	13.840101	13.840101	−5.315862	12.358625	0.000000	0.785398	0.000000	0.000000
23	B	5	16.191376	16.191376	−7.130504	13.847864	0.000000	0.981748	0.000000	0.000000
24	L1	10	16.516376	16.516376	−7.400731	14.028424	0.000000	0.981748	0.000000	0.000000
25	QFH	5	16.706376	16.706376	−7.558710	14.133982	0.000000	0.981748	0.000000	0.000000
26	QFH	6	16.896376	16.896376	−7.716690	14.239541	0.000000	0.981748	0.000000	0.000000
27	L1	11	17.221376	17.221376	−7.986917	14.420101	0.000000	0.981748	0.000000	0.000000
28	B	6	19.572651	19.572651	−10.057227	15.526705	0.000000	1.178097	0.000000	0.000000
29	L1	12	19.897651	19.897651	−10.357488	15.651077	0.000000	1.178097	0.000000	0.000000
30	QDH	6	20.047651	20.047651	−10.496070	15.708479	0.000000	1.178097	0.000000	0.000000
31	QDH	7	20.197651	20.197651	−10.634652	15.765882	0.000000	1.178097	0.000000	0.000000
32	L1	13	20.522651	20.522651	−10.934913	15.890254	0.000000	1.178097	0.000000	0.000000
33	B	7	22.873927	22.873927	−13.181330	16.571697	0.000000	1.374447	0.000000	0.000000
34	L1	14	23.198927	23.198927	−13.500086	16.635102	0.000000	1.374447	0.000000	0.000000
35	QFH	7	23.388927	23.388927	−13.686435	16.672169	0.000000	1.374447	0.000000	0.000000
36	QFH	8	23.578927	23.578927	−13.872784	16.709236	0.000000	1.374447	0.000000	0.000000
37	L1	15	23.903927	23.903927	−14.191539	16.772641	0.000000	1.374447	0.000000	0.000000
38	LB	1	26.253927	26.253927	−16.496385	17.231103	0.000000	1.374447	0.000000	0.000000
39	L1	16	26.578927	26.578927	−16.815140	17.294507	0.000000	1.374447	0.000000	0.000000
40	QDH	8	26.728927	26.728927	−16.962258	17.323771	0.000000	1.374447	0.000000	0.000000
41	QDH	9	26.878927	26.878927	−17.109375	17.353034	0.000000	1.374447	0.000000	0.000000
42	L1	17	27.203927	27.203927	−17.428131	17.416439	0.000000	1.374447	0.000000	0.000000
43	B	8	29.555202	29.555202	−19.764327	17.646534	0.000000	1.570796	0.000000	0.000000
44	L1	18	29.880202	29.880202	−20.089327	17.646534	0.000000	1.570796	0.000000	0.000000
45	QFH	9	30.070202	30.070202	−20.279327	17.646534	0.000000	1.570796	0.000000	0.000000
46	QFH	10	30.260202	30.260202	−20.469327	17.646534	0.000000	1.570796	0.000000	0.000000
47	L1	19	30.585202	30.585202	−20.794327	17.646534	0.000000	1.570796	0.000000	0.000000
48	LB	2	32.935202	32.935202	−23.144327	17.646534	0.000000	1.570796	0.000000	0.000000
49	L1	20	33.260202	33.260202	−23.469327	17.646534	0.000000	1.570796	0.000000	0.000000

POS. NO.	ELEMENT NAME	ELEMENT OCC. NO.	SEQUENCE SUM(L) [M]	SEQUENCE ARC [M]	POSITIONS X [M]	POSITIONS Y [M]	POSITIONS Z [M]	ANGLES PHI [RAD]	ANGLES THETA [RAD]	ANGLES PSI [RAD]
50	QDH	10	33.410202	33.410202	-23.619327	17.646534	0.000000	1.570796	0.000000	0.000000
51	QDH	11	33.560202	33.560202	-23.769327	17.646534	0.000000	1.570796	0.000000	0.000000
52	L1	21	33.885202	33.885202	-24.094327	17.646534	0.000000	1.570796	0.000000	0.000000
53	LB	3	36.235202	36.235202	-26.444327	17.646534	0.000000	1.570796	0.000000	0.000000
54	L1	22	36.560202	36.560202	-26.769327	17.646534	0.000000	1.570796	0.000000	0.000000
55	QFH	11	36.750202	36.750202	-26.959327	17.646534	0.000000	1.570796	0.000000	0.000000
56	QFH	12	36.940202	36.940202	-27.149327	17.646534	0.000000	1.570796	0.000000	0.000000
57	L1	23	37.265202	37.265202	-27.474327	17.646534	0.000000	1.570796	0.000000	0.000000
58	B	9	39.616477	39.616477	-29.810523	17.416439	0.000000	1.767146	0.000000	0.000000
59	L1	24	39.941477	39.941477	-30.129278	17.353035	0.000000	1.767146	0.000000	0.000000
60	QDH	12	40.091477	40.091477	-30.276396	17.323771	0.000000	1.767146	0.000000	0.000000
61	QDH	13	40.241477	40.241477	-30.423514	17.294508	0.000000	1.767146	0.000000	0.000000
62	L1	25	40.566477	40.566477	-30.742269	17.231103	0.000000	1.767146	0.000000	0.000000
63	LB	4	42.916477	42.916477	-33.047114	16.772641	0.000000	1.767146	0.000000	0.000000
64	L1	26	43.241477	43.241477	-33.365870	16.709237	0.000000	1.767146	0.000000	0.000000
65	QFH	13	43.431477	43.431477	-33.552219	16.672170	0.000000	1.767146	0.000000	0.000000
66	QFH	14	43.621477	43.621477	-33.738568	16.635102	0.000000	1.767146	0.000000	0.000000
67	L1	27	43.946477	43.946477	-34.057323	16.571698	0.000000	1.767146	0.000000	0.000000
68	B	10	46.297752	46.297752	-36.303741	15.890255	0.000000	1.963495	0.000000	0.000000
69	L1	28	46.622752	46.622752	-36.604002	15.765883	0.000000	1.963495	0.000000	0.000000
70	QDH	14	46.772752	46.772752	-36.742583	15.708480	0.000000	1.963495	0.000000	0.000000
71	QDH	15	46.922752	46.922752	-36.881165	15.651078	0.000000	1.963495	0.000000	0.000000
72	L1	29	47.247752	47.247752	-37.181426	15.526706	0.000000	1.963495	0.000000	0.000000
73	B	11	49.599027	49.599027	-39.251736	14.420102	0.000000	2.159845	0.000000	0.000000
74	L1	30	49.924027	49.924027	-39.521964	14.239541	0.000000	2.159845	0.000000	0.000000
75	QFH	15	50.114027	50.114027	-39.679943	14.133983	0.000000	2.159845	0.000000	0.000000
76	QFH	16	50.304027	50.304027	-39.837923	14.028425	0.000000	2.159845	0.000000	0.000000
77	L1	31	50.629027	50.629027	-40.108150	13.847865	0.000000	2.159845	0.000000	0.000000
78	B	12	52.980303	52.980303	-41.922792	12.358626	0.000000	2.356194	0.000000	0.000000
79	L1	32	53.305303	53.305303	-42.152602	12.128817	0.000000	2.356194	0.000000	0.000000
80	QDH	16	53.455303	53.455303	-42.258668	12.022751	0.000000	2.356194	0.000000	0.000000
81	QDH	17	53.605303	53.605303	-42.364734	11.916685	0.000000	2.356194	0.000000	0.000000
82	L1	33	53.930303	53.930303	-42.594544	11.686875	0.000000	2.356194	0.000000	0.000000
83	B	13	56.281578	56.281578	-44.083782	9.872233	0.000000	2.552544	0.000000	0.000000
84	L1	34	56.606578	56.606578	-44.264342	9.602005	0.000000	2.552544	0.000000	0.000000
85	QFH	17	56.796578	56.796578	-44.369901	9.444026	0.000000	2.552544	0.000000	0.000000
86	QFH	18	56.986578	56.986578	-44.475459	9.286047	0.000000	2.552544	0.000000	0.000000
87	L1	35	57.311578	57.311578	-44.656019	9.015819	0.000000	2.552544	0.000000	0.000000
88	B	14	59.662853	59.662853	-45.762623	6.945509	0.000000	2.748894	0.000000	0.000000
89	L1	36	59.987853	59.987853	-45.886995	6.645248	0.000000	2.748894	0.000000	0.000000
90	QDH	18	60.137853	60.137853	-45.944398	6.506666	0.000000	2.748894	0.000000	0.000000
91	QDH	19	60.287853	60.287853	-46.001801	6.368084	0.000000	2.748894	0.000000	0.000000
92	L1	37	60.612853	60.612853	-46.126173	6.067824	0.000000	2.748894	0.000000	0.000000
93	B	15	62.964128	62.964128	-46.807616	3.821406	0.000000	2.945243	0.000000	0.000000
94	L1	38	63.289128	63.289128	-46.871020	3.502651	0.000000	2.945243	0.000000	0.000000
95	QFH	19	63.479128	63.479128	-46.908088	3.316302	0.000000	2.945243	0.000000	0.000000
96	QFH	20	63.669128	63.669128	-46.945155	3.129953	0.000000	2.945243	0.000000	0.000000
97	L1	39	63.994128	63.994128	-47.008559	2.811197	0.000000	2.945243	0.000000	0.000000
98	B	16	66.345404	66.345404	-47.238654	0.475001	0.000000	3.141593	0.000000	0.000000
99	L1	40	66.670404	66.670404	-47.238654	0.150001	0.000000	3.141593	0.000000	0.000000

POS. NO.	ELEMENT NAME	OCC. NO.	SUM(L) [M]	ARC [M]	X [M]	Y [M]	Z [M]	PHI [RAD]	THETA [RAD]	PSI [RAD]
100	QDH	20	66.820404	66.820404	-47.238655	0.000001	0.000000	3.141593	0.000000	0.000000
101	QDH	21	66.970404	66.970404	-47.238655	-0.149999	0.000000	3.141593	0.000000	0.000000
102	L1	41	67.295404	67.295404	-47.238655	-0.474999	0.000000	3.141593	0.000000	0.000000
103	B	17	69.646679	69.646679	-47.008559	-2.811195	0.000000	3.337942	0.000000	0.000000
104	L1	42	69.971679	69.971679	-46.945155	-3.129950	0.000000	3.337942	0.000000	0.000000
105	QFH	21	70.161679	70.161679	-46.908088	-3.316299	0.000000	3.337942	0.000000	0.000000
106	QFH	22	70.351679	70.351679	-46.871021	-3.502649	0.000000	3.337942	0.000000	0.000000
107	L1	43	70.676679	70.676679	-46.807616	-3.821404	0.000000	3.337942	0.000000	0.000000
108	B	18	73.027954	73.027954	-46.126173	-6.067821	0.000000	3.534292	0.000000	0.000000
109	L1	44	73.352954	73.352954	-46.001801	-6.368082	0.000000	3.534292	0.000000	0.000000
110	QDH	22	73.502954	73.502954	-45.944399	-6.506664	0.000000	3.534292	0.000000	0.000000
111	QDH	23	73.652954	73.652954	-45.886996	-6.645246	0.000000	3.534292	0.000000	0.000000
112	L1	45	73.977954	73.977954	-45.762624	-6.945507	0.000000	3.534292	0.000000	0.000000
113	B	19	76.329229	76.329229	-44.656020	-9.015817	0.000000	3.730641	0.000000	0.000000
114	L1	46	76.654229	76.654229	-44.475460	-9.286045	0.000000	3.730641	0.000000	0.000000
115	QFH	23	76.844229	76.844229	-44.369902	-9.444024	0.000000	3.730641	0.000000	0.000000
116	QFH	24	77.034229	77.034229	-44.264343	-9.602003	0.000000	3.730641	0.000000	0.000000
117	L1	47	77.359229	77.359229	-44.083783	-9.872231	0.000000	3.730641	0.000000	0.000000
118	B	20	79.710504	79.710504	-42.594545	-11.686873	0.000000	3.926991	0.000000	0.000000
119	L1	48	80.035504	80.035504	-42.364735	-11.916683	0.000000	3.926991	0.000000	0.000000
120	QDH	24	80.185504	80.185504	-42.258669	-12.022749	0.000000	3.926991	0.000000	0.000000
121	QDH	25	80.335504	80.335504	-42.152603	-12.128815	0.000000	3.926991	0.000000	0.000000
122	L1	49	80.660504	80.660504	-41.922794	-12.358624	0.000000	3.926991	0.000000	0.000000
123	B	21	83.011780	83.011780	-40.108152	-13.847863	0.000000	4.123340	0.000000	0.000000
124	L1	50	83.336780	83.336780	-39.837924	-14.028423	0.000000	4.123340	0.000000	0.000000
125	QFH	25	83.526780	83.526780	-39.679945	-14.133981	0.000000	4.123340	0.000000	0.000000
126	QFH	26	83.716780	83.716780	-39.521966	-14.239540	0.000000	4.123340	0.000000	0.000000
127	L1	51	84.041780	84.041780	-39.251738	-14.420100	0.000000	4.123340	0.000000	0.000000
128	B	22	86.393055	86.393055	-37.181428	-15.526704	0.000000	4.319690	0.000000	0.000000
129	L1	52	86.718055	86.718055	-36.881167	-15.651076	0.000000	4.319690	0.000000	0.000000
130	QDH	26	86.868055	86.868055	-36.742585	-15.708479	0.000000	4.319690	0.000000	0.000000
131	QDH	27	87.018055	87.018055	-36.604003	-15.765881	0.000000	4.319690	0.000000	0.000000
132	L1	53	87.343055	87.343055	-36.303742	-15.890253	0.000000	4.319690	0.000000	0.000000
133	B	23	89.694330	89.694330	-34.057325	-16.571697	0.000000	4.516039	0.000000	0.000000
134	L1	54	90.019330	90.019330	-33.738570	-16.635101	0.000000	4.516039	0.000000	0.000000
135	QFH	27	90.209330	90.209330	-33.552221	-16.672168	0.000000	4.516039	0.000000	0.000000
136	QFH	28	90.399330	90.399330	-33.365871	-16.709236	0.000000	4.516039	0.000000	0.000000
137	L1	55	90.724330	90.724330	-33.047116	-16.772640	0.000000	4.516039	0.000000	0.000000
138	LB	5	93.074330	93.074330	-30.742271	-17.231102	0.000000	4.516039	0.000000	0.000000
139	L1	56	93.399330	93.399330	-30.423516	-17.294507	0.000000	4.516039	0.000000	0.000000
140	QDH	28	93.549330	93.549330	-30.276398	-17.323770	0.000000	4.516039	0.000000	0.000000
141	QDH	29	93.699330	93.699330	-30.129280	-17.353034	0.000000	4.516039	0.000000	0.000000
142	L1	57	94.024330	94.024330	-29.810525	-17.416438	0.000000	4.516039	0.000000	0.000000
143	B	24	96.375605	96.375605	-27.474329	-17.646534	0.000000	4.712389	0.000000	0.000000
144	L1	58	96.700605	96.700605	-27.149329	-17.646534	0.000000	4.712389	0.000000	0.000000
145	QFH	29	96.890605	96.890605	-26.959329	-17.646534	0.000000	4.712389	0.000000	0.000000
146	QFH	30	97.080605	97.080605	-26.769329	-17.646534	0.000000	4.712389	0.000000	0.000000
147	L1	59	97.405605	97.405605	-26.444329	-17.646534	0.000000	4.712389	0.000000	0.000000
148	LB	6	99.755605	99.755605	-24.094329	-17.646534	0.000000	4.712389	0.000000	0.000000
149	L1	60	100.080605	100.080605	-23.769329	-17.646534	0.000000	4.712389	0.000000	0.000000

POS. NO.	ELEMENT NAME	OCC. NO.	SUM(L) [M]	ARC [M]	X [M]	Y [M]	Z [M]	PHI [RAD]	THETA [RAD]	PSI [RAD]
150	QDH	30	100.230605	100.230605	-23.619329	-17.646534	0.000000	4.712389	0.000000	0.000000
151	QDH	31	100.380605	100.380605	-23.469329	-17.646534	0.000000	4.712389	0.000000	0.000000
152	L1	61	100.705605	100.705605	-23.144329	-17.646534	0.000000	4.712389	0.000000	0.000000
153	LB	7	103.055605	103.055605	-20.794329	-17.646534	0.000000	4.712389	0.000000	0.000000
154	L1	62	103.380605	103.380605	-20.469329	-17.646534	0.000000	4.712389	0.000000	0.000000
155	QFH	31	103.570605	103.570605	-20.279329	-17.646534	0.000000	4.712389	0.000000	0.000000
156	QFH	32	103.760605	103.760605	-20.089329	-17.646534	0.000000	4.712389	0.000000	0.000000
157	L1	63	104.085605	104.085605	-19.764329	-17.646534	0.000000	4.712389	0.000000	0.000000
158	B	25	106.436880	106.436880	-17.428133	-17.416439	0.000000	4.908738	0.000000	0.000000
159	L1	64	106.761880	106.761880	-17.109377	-17.353035	0.000000	4.908738	0.000000	0.000000
160	QDH	32	106.911880	106.911880	-16.962259	-17.323771	0.000000	4.908738	0.000000	0.000000
161	QDH	33	107.061880	107.061880	-16.815142	-17.294508	0.000000	4.908738	0.000000	0.000000
162	L1	65	107.386880	107.386880	-16.496386	-17.231104	0.000000	4.908738	0.000000	0.000000
163	LB	8	109.736880	109.736880	-14.191541	-16.772642	0.000000	4.908738	0.000000	0.000000
164	L1	66	110.061880	110.061880	-13.872786	-16.709237	0.000000	4.908738	0.000000	0.000000
165	QFH	33	110.251880	110.251880	-13.686437	-16.672170	0.000000	4.908738	0.000000	0.000000
166	QFH	34	110.441880	110.441880	-13.500087	-16.635103	0.000000	4.908738	0.000000	0.000000
167	L1	67	110.766880	110.766880	-13.181332	-16.571699	0.000000	4.908738	0.000000	0.000000
168	B	26	113.118156	113.118156	-10.934915	-15.890255	0.000000	5.105088	0.000000	0.000000
169	L1	68	113.443156	113.443156	-10.634654	-15.765883	0.000000	5.105088	0.000000	0.000000
170	QDH	34	113.593156	113.593156	-10.496072	-15.708481	0.000000	5.105088	0.000000	0.000000
171	QDH	35	113.743156	113.743156	-10.357490	-15.651078	0.000000	5.105088	0.000000	0.000000
172	L1	69	114.068156	114.068156	-10.057229	-15.526706	0.000000	5.105088	0.000000	0.000000
173	B	27	116.419431	116.419431	-7.986919	-14.420103	0.000000	5.301438	0.000000	0.000000
174	L1	70	116.744431	116.744431	-7.716691	-14.239542	0.000000	5.301438	0.000000	0.000000
175	QFH	35	116.934431	116.934431	-7.558712	-14.133984	0.000000	5.301438	0.000000	0.000000
176	QFH	36	117.124431	117.124431	-7.400733	-14.028426	0.000000	5.301438	0.000000	0.000000
177	L1	71	117.449431	117.449431	-7.130505	-13.847865	0.000000	5.301438	0.000000	0.000000
178	B	28	119.800706	119.800706	-5.315863	-12.358627	0.000000	5.497787	0.000000	0.000000
179	L1	72	120.125706	120.125706	-5.086053	-12.128818	0.000000	5.497787	0.000000	0.000000
180	QDH	36	120.275706	120.275706	-4.979987	-12.022752	0.000000	5.497787	0.000000	0.000000
181	QDH	37	120.425706	120.425706	-4.873921	-11.916686	0.000000	5.497787	0.000000	0.000000
182	L1	73	120.750706	120.750706	-4.644111	-11.686876	0.000000	5.497787	0.000000	0.000000
183	B	29	123.101981	123.101981	-3.154873	-9.872234	0.000000	5.694137	0.000000	0.000000
184	L1	74	123.426981	123.426981	-2.974313	-9.602006	0.000000	5.694137	0.000000	0.000000
185	QFH	37	123.616981	123.616981	-2.868754	-9.444027	0.000000	5.694137	0.000000	0.000000
186	QFH	38	123.806981	123.806981	-2.763196	-9.286048	0.000000	5.694137	0.000000	0.000000
187	L1	75	124.131981	124.131981	-2.582636	-9.015820	0.000000	5.694137	0.000000	0.000000
188	B	30	126.483257	126.483257	-1.476032	-6.945510	0.000000	5.890486	0.000000	0.000000
189	L1	76	126.808257	126.808257	-1.351659	-6.645250	0.000000	5.890486	0.000000	0.000000
190	QDH	38	126.958257	126.958257	-1.294257	-6.506668	0.000000	5.890486	0.000000	0.000000
191	QDH	39	127.108257	127.108257	-1.236854	-6.368086	0.000000	5.890486	0.000000	0.000000
192	L1	77	127.433257	127.433257	-1.112482	-6.067825	0.000000	5.890486	0.000000	0.000000
193	B	31	129.784532	129.784532	-0.431039	-3.821407	0.000000	6.086836	0.000000	0.000000
194	L1	78	130.109532	130.109532	-0.367634	-3.502652	0.000000	6.086836	0.000000	0.000000
195	QFH	39	130.299532	130.299532	-0.330567	-3.316303	0.000000	6.086836	0.000000	0.000000
196	QFH	40	130.489532	130.489532	-0.293500	-3.129954	0.000000	6.086836	0.000000	0.000000
197	L1	79	130.814532	130.814532	-0.230096	-2.811199	0.000000	6.086836	0.000000	0.000000
198	B	32	133.165807	133.165807	0.000000	-0.475003	0.000000	6.283185	0.000000	0.000000
199	L1	80	133.490807	133.490807	0.000000	-0.150003	0.000000	6.283185	0.000000	0.000000

POS. NO.	ELEMENT NAME	OCC. NO.	SUM(L) [M]	ARC [M]	X [M]	Y [M]	Z [M]	PHI [RAD]	THETA [RAD]	PSI [RAD]
200	QDH	40	133.640807	133.640807	0.000000	-0.000003	0.000000	6.283185	0.000000	0.000000
END	RING	1	133.640807	133.640807	0.000000	-0.000003	0.000000	6.283185	0.000000	0.000000

TOTAL LENGTH =	133.640807	ARC LENGTH =	133.640807		
ERROR(X) =	-0.127887E-12	ERROR(Y) =	-0.253151E-05	ERROR(Z) =	0.000000E+00
ERROR(PHI) =	-0.107180E-06	ERROR(THETA) =	0.000000E+00	ERROR(PSI) =	0.000000E+00